The Thesis Committee for Stephen Andrew Bryant
Certifies that this is the approved version of the following thesis:

Simulating Refracturing Treatments that Employ Diverting Agents on Horizontal Wells

APPROVED BY
SUPERVISING COMMITTEE:

Supervisor:

Mukul M. Sharma

Jon E. Olson

Simulating Refracturing Treatments that Employ Diverting Agents on Horizontal Wells

by

Stephen Andrew Bryant, B.S.M.E.

Thesis

Presented to the Faculty of the Graduate School of

The University of Texas at Austin

in Partial Fulfillment

of the Requirements

for the Degree of

Master of Science in Engineering

The University of Texas at Austin

August 2013

Acknowledgements

I am very grateful to the participating companies of the Hydraulic Fracturing and Sand Control consortium who financially supported this research.

I would like to express my sincere gratitude to Dr. Mukul M. Sharma for the essential guidance and support he provided during the project. I am also very appreciative of the comments and time provided by Dr. Jon E. Olson. I am very thankful for the significant amount of tips, time and UTWID knowledge supplied by my colleague Jongsoo Hwang. I would also like to thank Jin Lee for administrative support that helped keep me organized and improved my experience in the department.

Last, I am deeply thankful for the constant support and encouragement from my parents Randy and Sandra Bryant.

Abstract

Simulating Refracturing Treatments that Employ Diverting Agents on Horizontal Wells

Stephen Andrew Bryant, M.S.E.

The University of Texas at Austin, 2013

Supervisor: Mukul M. Sharma

The use of hydraulic fracturing has increased rapidly and is now a necessary technique for the development of shale oil and gas resources. However, production rates from these plays typically exhibit high levels of decline. After one year, rates often decrease by over fifty percent. Refracturing – the process of hydraulically fracturing a well that has previously been fractured – is a proposed technique designed to offset these high decline rates and provide a sustainable increase in production. Benefits from refracturing can occur due to a variety of reasons, including the extension of fracture length, the increase in fracture conductivity or the reorientation of the fracture into new areas of the reservoir.

In this thesis, the simulation of refracturing treatments on horizontal wells with the use of a diverting agent is described. Diverting agents are used to distribute flow more evenly along the wellbore and to replace the use of costly downhole equipment employed to isolate sections of the wellbore.

When diverting agent is deposited, a cake forms with an associated permeability. Flow is diverted from the fractures with high amounts of diverting agent because the larger cake results in a greater resistance to flow. The diverting agent cake breaks down with time at reservoir temperature so that production is uninhibited. Two different models are used to account for the application of diverting agent. One assumes the diverting agent cake forms in the perforation tunnel and the other assumes it forms in the fracture. The propagation of competing fractures is calculated using a computer code developed at the University of Texas called UTWID.

In both models, the simulations showed successful diversion of flow. Previously understimulated fractures – that is, shorter fractures or fractures that would grow less preferentially under normal fracturing treatments – grew at a faster pace after pumping of the diverting agent. A sensitivity analysis was conducted on several of the key refracturing design parameters, and the interdependence of the parameters was demonstrated. The simulations support the concept that diverting agents can be used to more evenly stimulate the entire length of the lateral.

Table of Contents

List of Tables x

List of Figures xi

Chapter 1: Introduction 1

Impact of Hydraulic Fracturing 1

Motivation for Refracturing 2

Research Objectives 4

Chapter 2: Background 6

History 6

Methods and Mechanisms 7

Contacting New Parts of the Reservoir 7

Enhancing Fracture Conductivity 18

Proppant Degradation 18

Preventing Proppant Embedment 22

Diversion Methods 23

Candidate Selection 29

Candidate Selection Study by the Gas Research Institute 30

Other Candidate Selection Methods 34

Field Studies of Refracturing Treatments on Horizontal Wells with the Use of Diversion 36

Restimulation of Wells using Biodegradable Particulates as Temporary Diverting Agents 36

Barnett Shale Refracture Stimulations Using a Novel Diversion Technique 38

Restimulation of Unconventional Reservoirs: When Are Refracs Beneficial? 39

Barnett Shale Horizontal Restimulations - A Case Study of 13 Wells 40

Chapter 3: Model Formulation 43
Summary of UTWID 43
Assumptions....43
UTWID Features....44
Fracture Propagation....44
Thermoelastic Stresses....46
Particle Plugging....47
Flow Resistance / Pressure Drop Calculations 51
Modifications to UTWID to Accommodate Application of Diverting Agent....59
Diverting Agent Plugging in the Perforation Tunnel....62
Diverting Agent Plugging in the Fracture....65
Nomenclature....70
Chapter 4: Refracture Simulation Results and Discussion for Diverting Agent that Plugs in the Fracture 74
Scenario I – Baseline Case....74
Scenario II – One Fracture with Reduced Length 80
Scenario III – Mix of Frac Lengths....85
Scenario IV – Sensitivity to the Diverting Agent Cake Permeability 90
Scenario V – Sensitivity to Pumped Diverting Agent Volume Fraction 96
Scenario VI – Sensitivity to Pumping Rate of Injected Fluid....100
Scenario VII – Sensitivity to Rock Fracture Propagation Pressure 106
Chapter 5: Refrac Simulation Results and Discussion for Diverting Agent that Plugs in the Perforation Tunnel....112
Scenario I – Baseline Case....112
Scenario II – One Fracture with Reduced Length 118
Scenario III – Mix of Frac Lengths....123
Scenario IV – Diverting Agent Stage Duration 128
Scenario V – Addition of a Second Diverting Agent Stage....131

Scenario VI – Sensitivity to Diverting Agent Cake Permeability 134
Scenario VII – Sensitivity to Volume Fraction of Diverting Agent 139
Scenario VIII – Importance of Tuning Parameters for Successful Diversion 142
Scenario IX – Sensitivity to Pumping Rates 144
Scenario X – Sensitivity to Fracture Propagation Pressure 147
Chapter 6: Summary and Conclusions 152
Plugging in the Fracture 152
Plugging in the Perforations 154
Future Work 156
References 158

List of Tables

Table 3-1 – A typical pumping schedule used in simulations 61
Table 4-1 – Selection of Input Parameters 75
Table 4-2 – Refrac Pumping Schedule 76
Table 5-1 – Selection of Input Parameters 113

List of Figures

Figure 1-1 – Actual versus forecasted carbon dioxide emissions in the U.S., compiled from the EIA (Carey, 2012) 2
Figure 1-2 – Averaged production curves of unconventional wells by basin; high decline rates are seen (Baihly et al., 2010). 3
Figure 1-3 – Example of a horizontal well successfully refractured (Potapenko et al., 2009) 4
Figure 2-1 – Successful refracturing attempt from 1953; refrac resulted in sustained production increase and jump in estimated ultimate recovery (Sallee and Rugg, 1953) 6
Figure 2-2 – Sustained production gains from refracturing treatments attributed to an increase in fracture half length due to better proppant transport capabilities in the fracturing fluid (Shaefer, 2006). 8
Figure 2-3 – Log of radioactive tracer along wellbore. The tracer indicates that the refracture delivered proppant to previously bypassed zones in the top portion of the wellbore (Fisher 1995) 11
Figure 2-4 – Production in the well from figure 3, before and after the recompletion. The refrac doubled the stabilized gas rate (Fisher 1995). 12
Figure 2-5 – fracture comparison spacing using a reservoir simulator. The formation is a 400 nd shale gas reservoir with an initial pressure of 3,000 psi. In the left image, fractures are spaced at 1,000 ft intervals and in the right image, fractures are spaced at 250 ft intervals (Waters et al., 2009). 14
Figure 2-6 – radioactive tracer log that shows the presence of proppant from both the original fracturing treatment and the subsequent refracturing treatment. Prior to the refracturing treatment, new perforations were shot; during the refracturing treatment, ball sealers were used to divert flow to other perforations. The log clearly shows that the refracture resulted in greater coverage along the length of the lateral (Vincent, 2010a; adapted from Lantz and Greene, 2007) 14
Figure 2-7 – Wellbore schematic of a typical well from the refracturing program described by Lantz and Greene. The hydra-jetted perforations are the new perforations added for the refracturing treatment (Lantz and Greene, 2007). 15
Figure 2-8 – Production rates of the well from Figure 2-6. Oil production saw a sustained increase after the refrac (adapted from Lantz and Greene, 2007) 15
Figure 2-9 – The refracture reorients in a new direction inside the stress-reversal region, before returning to the orientation of the initial fracture (Roussel and Sharma, 2010). 17

Figure 2-10 – Evidence of fracture reorientation. (a) is a mapview of microseismic events during a refracture; reorientation of the refrac to a North-South orientation is seen. (b) displays the same event, but at a later time; the fracture reorients back to the initial direction, orthogonal to the wellbore. 17
Figure 2-11 – Reduction in fracture conductivity over time for five different properties (McDaniel, 1986). ISB, HSB, and ISC are different types of ceramic proppant. 19
Figure 2-12 – Images of proppant diagensis captured using electron microscopy and energy dispersive X-ray (Rayson and Weaver, 2012). (a) ceramic proppant after exposure to 10,000-psi closure stress and 275 F for 140 hr in 2% KCl water. The debris is not thought to be crushed proppant; (b) a ceramic proppant grain embedded in Ohio sandstone after exposure to 10,000-psi closure stress at 250 F for 140 hr in 2% KCl solution under static flow condition; chemical makeup differs between proppant, precipitate, and core surface (c) and (d) closeup view of proppant from (b) showing an aluminosilicate crystal growing on the surface of the ceramic proppant 21
Figure 2-13 – Proppant embedment reduces fracture width (Terracina et al., 2010) 23
Figure 2-14 – An illustration of the limited entry technique for diverting treatment fluids. The method limits the number of perforations in a zone in order to use the increased friction forces in the perforations as a means to govern flow through a zone and accomplish diversion (Lagrone and Rasmussen, 1963). 26
Figure 2-15 – Ball sealers are designed to seat on perforations (Wang et al., 2011) 26
Figure 2-16 – (a) Initial configuration of perforation holes before an erosion test; (b) eroded perforations caused by pumping 250,000 lbm of sand 27
Figure 2-17 – A depiction of Biovert, Halliburton's diverting agent product. Different sized particles are injected simultaneously to enhance the plug. (Halliburton) 28
Figure 2-18 – Microseismic events during a refrac treatment before application of diverting agent (Stage 1) and afterwards (Stage 2). Diversion is clearly seen (Potapenko et al., 2009). 29
Figure 2-19 – Monthly production for wells refractured with diverting agent. Production rates after the refracture reached 55% and 70% of the initial rates (Allison et al., 2011). 37
Figure 2-20 – Treatment schedule for the refracturing of Well A with the use of a diverting agent (Allison et al., 2011). 38
Figure 2-21 – Monthly production figures of two horizontal wells restimulated with the use of a diverting agent (Potapenko et al., 2009). 39
Figure 2-22 – (a) shows cumulative oil production of a well that was initially fractured using sand and subsequently refractured using ceramic proppant. Results

from (b) were mixed, with some refracs a success and some had little effect. Green symbols represent refracs, and yellow symbols denote dates when pumping equipment was run/rerun (Vincent, 2010b). 40
Figure 2-23 – Normalized graph of production rate for 13 wells from date of refracturing treatment. The refrac resulted in sustained increases in production and EUR gains (Craig et al. 2012)..... 41
Figure 3-1 – Thermal front with elliptical geometry in the presence of a two-wing fracture (The University of Texas, 2009) 47
Figure 3-2 – Map view of the fluid fronts due to elliptical flow geometry (The University of Texas, 2009) 54
Figure 3-3 – Diagram of five fractures along a wellbore. The cumulative amount of friction exerted on a fluid particle increases as it moves away from the heel. 60
Figure 3-4 – Diagram of diverting agent plugging for one of the two models used. In this model, the agent is assumed to plug in the perforation tunnel, beginning at the face of the fracture and proppant..... 64
Figure 3-5 – Resistors configured in a parallel configuration. The total resistance due to diverting agent is calculated by combining the resistance from each perforation into a system of parallel resistors. 64
Figure 3-6 – (a) cross sectional view of the fracture with diverting agent inside. (b) Side view of diverting agent cake deposited adjacent to proppant. Note that the diverting agent particles are larger than the proppant..... 69
Figure 3-7 – Side view of the fracture including the wellbore. The diverting agent cake surrounds the well. 69
Figure 4-1 – Scenario I: Baseline case without the use of diverting agent. All fractures are identical, except for their positions along the wellbore and consequently their frictional pressure drop. Select properties are given in Table 4-1 77
Figure 4-2 – Scenario I: The baseline case with the standard diverting agent stage included. All fractures are identical, except for their positions along the wellbore. The fractures closest to the heel initially grow the fastest due to less friction, but also take more diverting agent and as a result become plugged. Successful diversion is seen. 79
Figure 4-3 – Scenario II, Case A without diverting agent. All fractures are identical except fracture L1 begins the treatment with a shorter fracture length..... 81
Figure 4-4 – Scenario II, Case A with diverting agent. All fractures are identical except fracture L1 begins the treatment with a shorter fracture length..... 82
Figure 4-5 – Scenario II, Case B without diverting agent. All of the fractures are identical, except fracture L4 begins the treatment with a shorter fracture length... 83

Figure 4-6 – Scenario II, Case B with diverting agent. All fractures are identical, except fracture L4 begins the treatment with a shorter fracture length.....84
Figure 4-7 – Scenario III, Case A without diverting agent. The fractures begin the treatment with a mix of fracture lengths.....86
Figure 4-8 - Scenario III, Case A with diverting agent. The fractures begin the treatment with a mix of fracture lengths.....87
Figure 4-9 - Scenario III, Case B without diverting agent. The fractures begin the treatment with a different mix of fracture lengths than those in Case A.....88
Figure 4-10 - Scenario III, Case B with diverting agent. The fractures begin the treatment with a different mix of fracture lengths than those in Case A.....89
Figure 4-11 – Scenario IV, Case A. The fracture system is the same as in Scenario III Case B, except the permeability of the diverting agent cake is reduced to 100 mD. 92
Figure 4-12 - Scenario IV, Case B. The fracture system is the same as in Scenario III Case B, except the permeability of the diverting agent cake is reduced to 50 mD. ..93
Figure 4-13 - Scenario IV, Case C. The fracture system is the same as in Scenario III Case B, except the permeability of the diverting agent cake is increased to 100 D. .94
Figure 4-14 - Scenario IV, Case D. The fracture system is the same as in Scenario III Case B, except the permeability of the diverting agent cake is increased to 5E3D. ..95
Figure 4-15 - Scenario V, Case A. The fracture system is identical to Scenario III, Case B, except the volume fraction of diverting agent is reduced to 1E-5.....98
Figure 4-16 - Scenario V, Case B. The fracture system is identical to Scenario III, Case B, except the volume fraction of diverting agent is increased to 1E-2. 99
Figure 4-17 – Scenario VI, Case A. Fracture system is identical to Scenario III, Case B, except the pump rate of the injected fluid is increased to 56 bpm.....103
Figure 4-18 - Scenario VI, Case B. Fracture system is identical to Scenario III, Case B, except the pump rate of the injected fluid is increased to 83 bpm.....104
Figure 4-19 - Scenario VI, Case C. Fracture system is identical to Scenario III, Case B, except the pump rate of the injected fluid is decreased to 28 bpm.....105
Figure 4-20 – Scenario VII, Case A with no diverting agent. All fractures are equal, except fractures L1 and L4 have lower fracture propagation pressures 108
Figure 4-21 – Scenario VII, Case A with diverting agent. All fractures are equal, except fractures L1 and L4 have lower fracture propagation pressures 109
Figure 4-22 – Scenario VII, Case B without diverting agent. All fractures are equal, except fractures L2, L3, and L4 have a lower fracture propagation pressure.....110
Figure 4-23 – Scenario VII, Case B with diverting agent. All fractures are equal, except fractures L2, L3, and L4 have a lower fracture propagation pressure.....111
Figure 5-1 – Scenario I: Baseline case without the use of diverting agent. All fractures are identical, except their position along the wellbore and consequently their frictional pressure drop. Select properties are given in Table 4-1. 115

Figure 5-2 – Scenario I: Baseline case with the standard diverting agent stage included. All fractures are identical, except their position along the wellbore. The fractures closest to the heel initially grow the fastest due to less friction, but also take more diverting agent. 116
Figure 5-3 – Zoomed in flow rate plot for Scenario I with diverting agent. The diverting agent acts as a feedback mechanism to equalize flow between the fractures. 117
Figure 5-4 – Scenario II, Case A without diverting agent. All fractures are identical except fracture L3 begins the treatment with a shorter fracture length 119
Figure 5-5 – Scenario II, Case A with diverting agent. All fractures are identical except fracture L3 begins the treatment with a shorter fracture length 120
Figure 5-6 – Scenario II, Case B without diverting agent. All of the fractures are identical, except fracture L1 begins the treatment with a shorter fracture length . 121
Figure 5-7 – Scenario II, Case B with diverting agent. All fractures are identical, except fracture L4 begins the treatment with a shorter fracture length 122
Figure 5-8 – Scenario III, Case A without diverting agent. The fractures begin the treatment with a mix of fracture lengths 124
Figure 5-9 - Scenario III, Case A with diverting agent. The fractures begin the treatment with a mix of fracture lengths 125
Figure 5-10 - Scenario III, Case B without diverting agent. The fractures begin the treatment with a different mix of fracture lengths than those in Case A 126
Figure 5-11 - Scenario III, Case B with diverting agent. The fractures begin the treatment with a different mix of fracture lengths than those in Case A 127
Figure 5-12 – Scenario IV, Case A. The fracture system is the same as in Scenario III Case A, except the duration of the diverting agent stage is reduced from 29 minutes to 2.9 minutes. The reduced length results in a permanent disparity in flow rates between the fractures after the diverting agent stage 129
Figure 5-13 - Scenario IV, Case B. The fracture system is the same as in Scenario III Case B, except the duration of the diverting agent stage is reduced from 29 minutes to 2.9 minutes. The reduced length results in a permanent disparity in flow rates between the fractures after the diverting agent stage 130
Figure 5-14 - Scenario V, Case A. The fracture system is the same as in Scenario IV Case A, except a second diverting agent stage is added from minute 274 to 288. The second stage equalizes growth and flow rates between the fractures, leading to more similar fracture lengths 132
Figure 5-15 - Scenario V – Case B. The fracture system is the same as in Scenario IV Case B, except a second diverting agent stage is added from minute 274 to 288. The second stage equalizes growth and flow rates between the fractures, leading to more similar fracture lengths 133

Figure 5-16 – Scenario VI – Case A. Fracture system is identical to Scenario V, Case A, except the permeability of the diverting agent cake is changed from 1 Darcy to 10 Darcies 136
Figure 5-17 - Scenario VI – Case B. Fracture system is identical to Scenario V, Case A, except the diverting agent cake is increased from 1 Darcy to 100 Darcies 137
Figure 5-18 - Scenario VI – Case C. Fracture system is identical to Scenario V, Case A, except the permeability of the diverting agent cake is decreased from 1 Darcy to 100 mD 138
Figure 5-19 – Scenario VII – Case A. Fracture system is identical to Scenario V, Case A, except the volume fraction of the injected diverting agent is decreased from 5E-5 to 5E-6. 140
Figure 5-20 – Scenario VII – Case B with diverting agent. Fracture system is identical to Scenario V, Case A, except the volume fraction of the injected diverting agent is increased from 5E-5 to 1E-4. 141
Figure 5-21 - Scenario VIII with diverting agent. Fracture system is identical to Scenario V, Case A, except the permeability of the diverting agent cake is reduced from 1 Darcy to 100 mD and the volume fraction of the injected diverting agent is reduced from 5E-5 to 5E-6. 143
Figure 5-22 - Scenario IX, Case A with diverting agent. Fracture system is identical to Scenario V, Case A, except the pumping rate is increased from 56 bpm to 69 bpm. 145
Figure 5-23 - Scenario IX, Case B with diverting agent. Fracture system is identical to Scenario V, Case A, except the pumping rate is decreased from 56 bpm to 28 bpm. 146
Figure 5-24 - Scenario X, Case A without diverting agent. Fracture system is identical to Scenario V, Case A, except the fracture propagation pressure is decreased for fractures L3 and L5. 148
Figure 5-25 - Scenario X, Case A with diverting agent. Fracture system is identical to Scenario V, Case A, except the fracture propagation pressure is decreased for fractures L3 and L5. 149
Figure 5-26 - Scenario X, Case B without diverting agent. Fracture system is identical to Scenario V, Case B, except the fracture propagation pressure is decreased for fractures L2 and L4. 150
Figure 5-27 - Scenario X, Case B with diverting agent. Fracture system is identical to Scenario V, Case A, except the fracture propagation pressure is decreased for fractures L2 and L4. 151

Chapter 1: Introduction

IMPACT OF HYDRAULIC FRACTURING

The impact of hydraulic fracturing on the U.S. and international energy sector has been immense. A report from the U.S. Energy Information Administration (EIA, 2013a) details the production and reserve increases caused by the exploitation of shale gas and oil that was made possible by modern hydraulic fracturing and horizontal drilling techniques. After shale gas became a commercial reality in the Barnett Shale in 2000, production of shale gas in the United States rose from 0.3 trillion cubic feet in 2000 to 9.6 trillion cubic feet in 2012. As a result, forty percent of U.S. dry natural gas production now comes from shale gas. U.S. production of tight oil (that is, oil produced from low permeability rock including shale) jumped almost tenfold in twelve years from an average of 0.2 million barrels per day in 2000 to an average of 1.9 million barrels per day in 2012.

The EIA report's estimates on technically recoverable shale gas and oil resources are equally significant. Technically recoverable resources indicate the amount of a resource that can technically be produced, but the production of which is not necessarily justified given current economic conditions. The global estimates are 7,298 tcf for shale gas and 345 billion barrels for crude oil. By including these figures, estimates for the amount of total worldwide technically recoverable gas and oil increased by 47% and 11%, respectively.

Prices for natural gas fell steeply in response to the large increase in production and reserves in the U.S. market. The Henry Hub Spot Price dropped from a peak of $13.42/MBtu in October of 2005 to a nadir of $1.95/MBtu in April of 2012 (EIA, 2013d). Natural gas consumers have moved to take advantage of the lowered prices. Electricity

power generating companies, for instance, began using more natural gas at the expense of coal. From 2000 to 2010, the use of natural gas for energy generation increased by 76%, whereas the use of coal declined by 22% (EIA, 2013b). Since coal produces almost twice as much carbon dioxide as does natural gas for the same amount of energy generated (EIA, 2013c), the shift to natural gas has greatly reduced greenhouse gas emissions (see Figure 1-1). Total CO_2 emissions from energy in 2012 were at the lowest levels since 1994 – having dropped 733 million metric tons, or 12%, from 2007 to 2012 (EIA, 2013b).

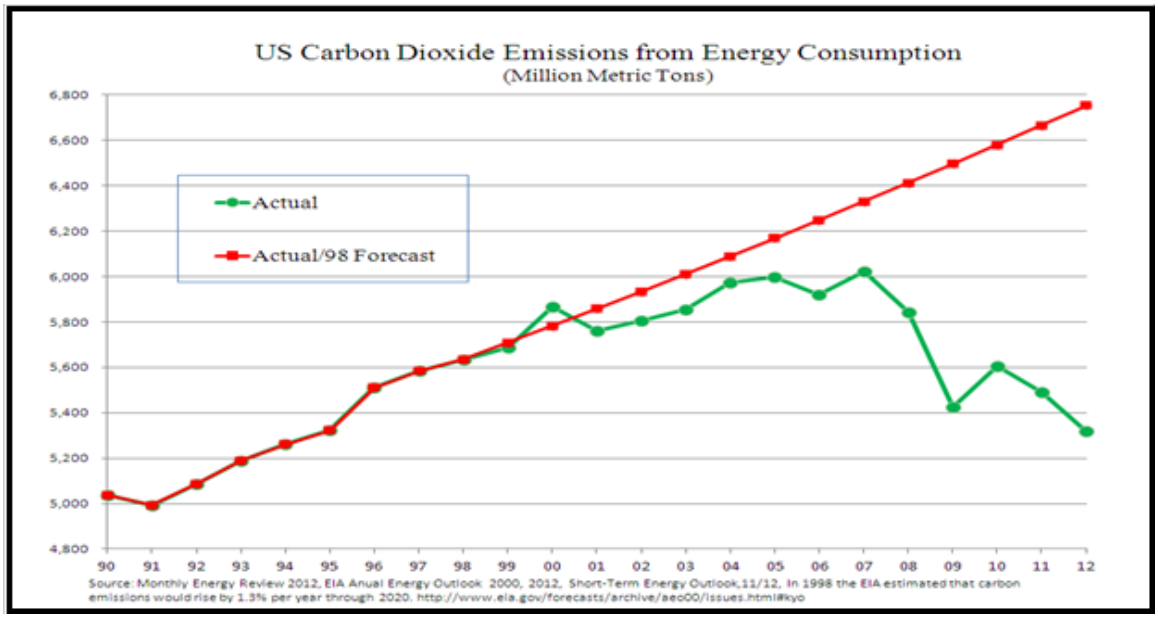

Figure 1-1 – Actual versus forecasted carbon dioxide emissions in the U.S., compiled from the EIA (Carey, 2012)

MOTIVATION FOR REFRACTURING

Refracturing – the process of hydraulically fracturing a well that has previously been fractured – may be able to further increase the production of shale gas and oil. Unconventional wells in tight formations often see very high decline rates. Baihly et al.

(2010) compiled an average production decline curve by basin that can be seen in Figure 1-2. In the best scenarios wells are producing at 50% of the peak rate after one year, and most often rates are much lower.

In many instances, refracturing has been able to offset these high decline rates, sustain production gains, and grow reserves in a cost efficient manner. These benefits have been well documented in published case histories (Potapenko et al., 2009; Vincent, 2010a; Vincent, 2010b; Craig et al., 2012; Allison et al., 2011; Green and Seanard, 2006; Reeves and Wolhart, 2001). In some cases, wells showed clear economic gains. Figure 1-3 shows a horizontal well in the Barnett that displayed a sustained production increase after a successful refracturing treatment.

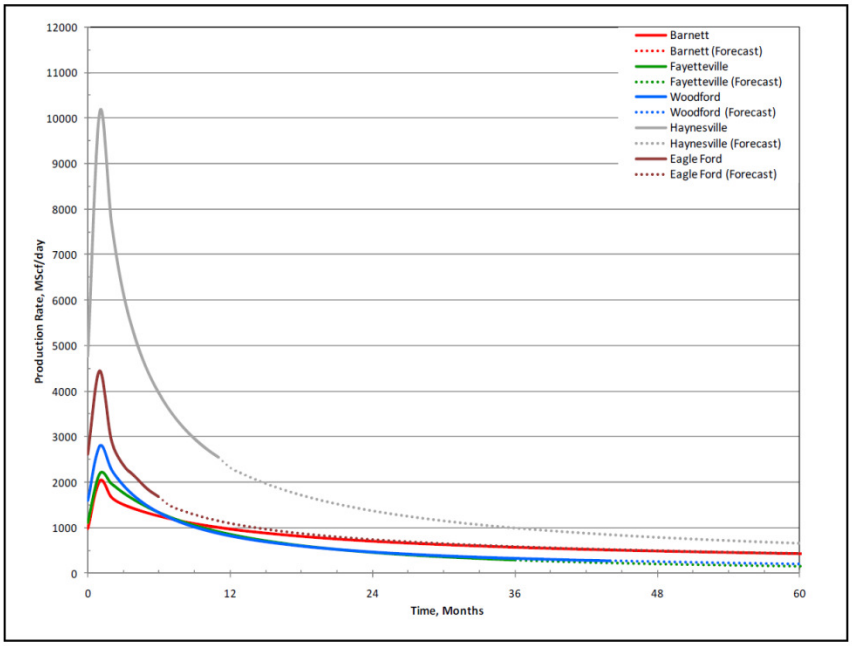

Figure 1-2 – Averaged production curves of unconventional wells by basin; high decline rates are seen (Baihly et al., 2010).

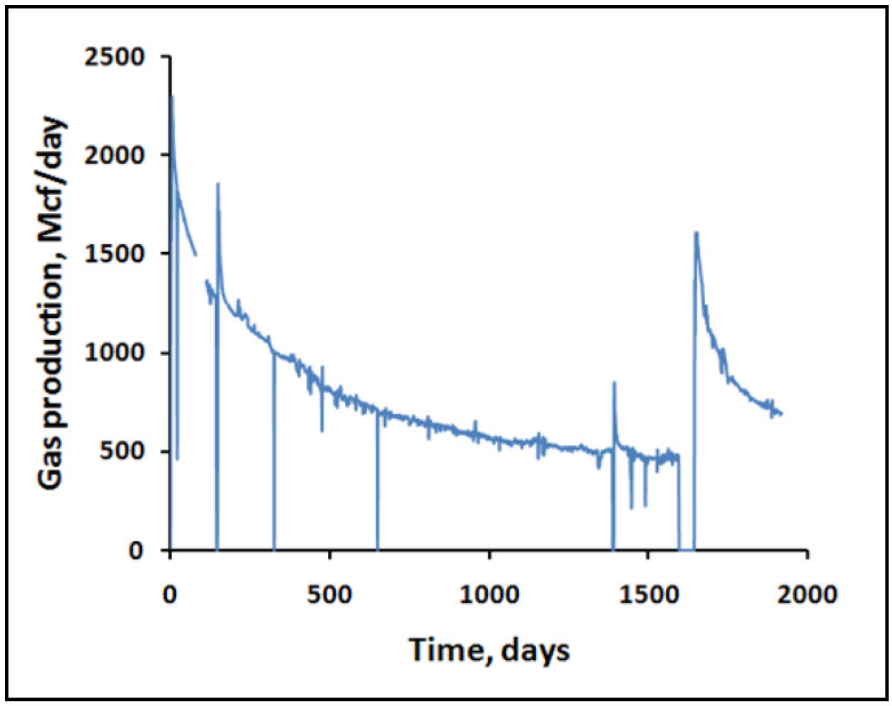

Figure 1-3 – Example of a horizontal well successfully refractured (Potapenko et al., 2009)

RESEARCH OBJECTIVES

Refracturing treatments can be performed in a number of ways, and a variety of mechanisms have been proposed to explain the resulting production increases. Refracturing criteria such as proppant type, fluid type, elapsed time since original completion, pumping rate and diversion technique can all be tailored to counteract specific problems thought to occur in a well. While successes have occurred in refracturing treatments, so too have failures, and in some cases wells have actually been damaged by a refrac. The keys to optimizing refracturing operations are an understanding of the mechanisms that lead to success and an effective method for choosing the wells best suited for the treatment.

The objective of the research described in this thesis is to understand and optimize the use of diverting agents in a refracturing operation on a horizontal well through

computer modeling. Diverting agents are employed in refrac jobs to accomplish diversion of the fracturing fluid and to ensure that the treatment covers the entire targeted portion of the wellbore. The fractures are assumed to grow only along the direction in which they are oriented. By modeling fracture growth under the influence of diverting agents, diverting agent volume, timing, and permeability can be tailored to optimize the success of a refrac.

Chapter 2: Background

HISTORY

Refracturing, a hydraulic fracturing treatment on a well that has been previously hydraulically fractured, has been in use since the advent of fracturing (Conway et al., 1985). In a compilation of past refracturing treatments, Vincent (2010a) noted a successful case described in a paper from 1953 when hydraulic fracturing was a recently commercialized treatment. After a second hydraulic fracture job in an oil producing well in Texas, production increased by 103%, and the estimated ultimate recovery (EUR) increased by about 15% (Sallee and Rugg, 1953). The cost of the second treatment was recovered within 60 days (see Figure 2-1).

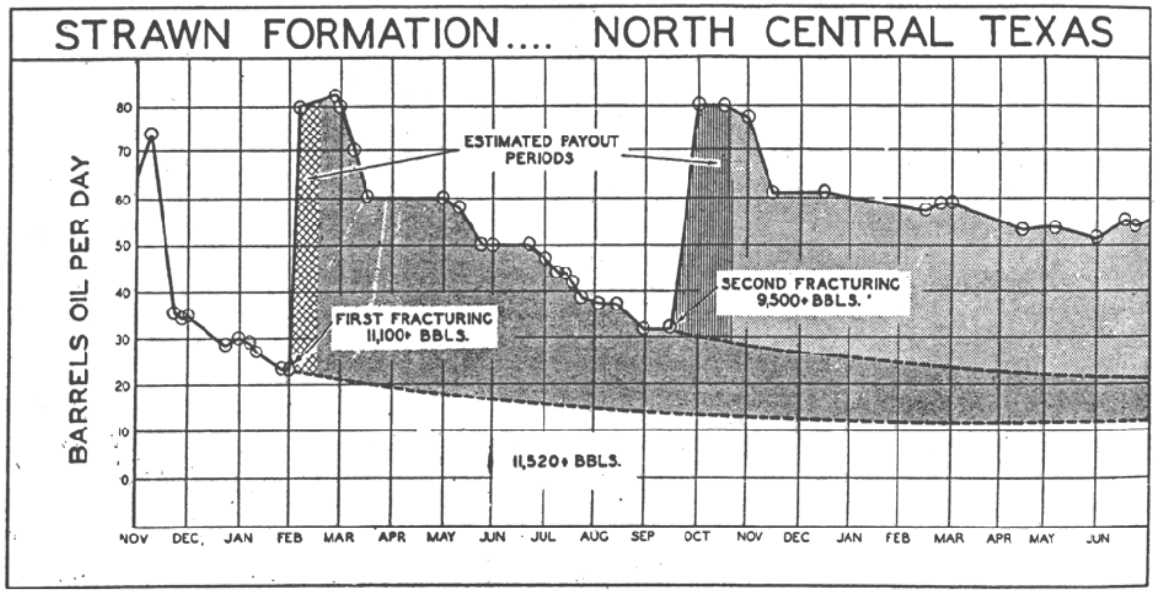

Figure 2-1 – Successful refracturing attempt from 1953; refrac resulted in sustained production increase and jump in estimated ultimate recovery (Sallee and Rugg, 1953)

Vincent (2010a) pointed out that about 35% of the 500,000 frac jobs up to 1970 had been restimulation treatments, whereas in 1996 the Gas Research Institute estimated

that only 2-3% of frac jobs were restimulations. An important question in need of attention is whether the potential success involved with refracturing warrants an increase in usage to past levels.

METHODS AND MECHANISMS

A variety of mechanisms have been offered as motivation for conducting refracturing treatments. These mechanisms can be divided into two areas: ones that extend the fracture into new parts of the reservoir containing virgin pressure, and ones that enhance fracture conductivity.

Contacting New Parts of the Reservoir

The extension of a fracture network into new parts of a reservoir, which clearly offers higher production rates and better drainage of the reservoir, can be accomplished in a variety of ways. The simplest one is to increase the half-length of the transverse or longitudinal fractures. Increasing the fracture half-length in a refracturing treatment can most easily be achieved when the initial treatment was not optimized and the half-length fell short of its potential. Problems with the initial treatment can be caused by a variety of factors, such as compatibility issues between the fluid and the formation, inadequate width created in the near wellbore region, use of a fluid with poor proppant transport characteristics, and early screenout.

Refrac field studies typically alter several factors, and so it is difficult to attribute the success or failure of a treatment to any one change. For instance, Shaefer (2006) detailed a refracturing program of four vertical wells in a low-permeability gas sand of the Greater Green River Basin in Wyoming. A production analysis technique indicated that the observed low production rates were caused by low fracture half-lengths. Refracturing treatments were conducted using stronger man-made proppants than those

used in the original treatment and a crosslinked gel fluid instead of an energized one. The problem with the energized fluid is that it is not able to deliver the proppant as far into the fracture as the cross-linked gel, resulting in smaller fracture half lengths. All of the refracturing treatments were successful, resulting in sustained increases in production and longer fracture half-lengths as determined by the analysis technique (see Figure 2-2). While the increase in production likely resulted from longer fracture-half lengths, the use of higher quality proppant certainly contributed to the production gains as well. As a result, the cause of refracturing success could not be specifically determined.

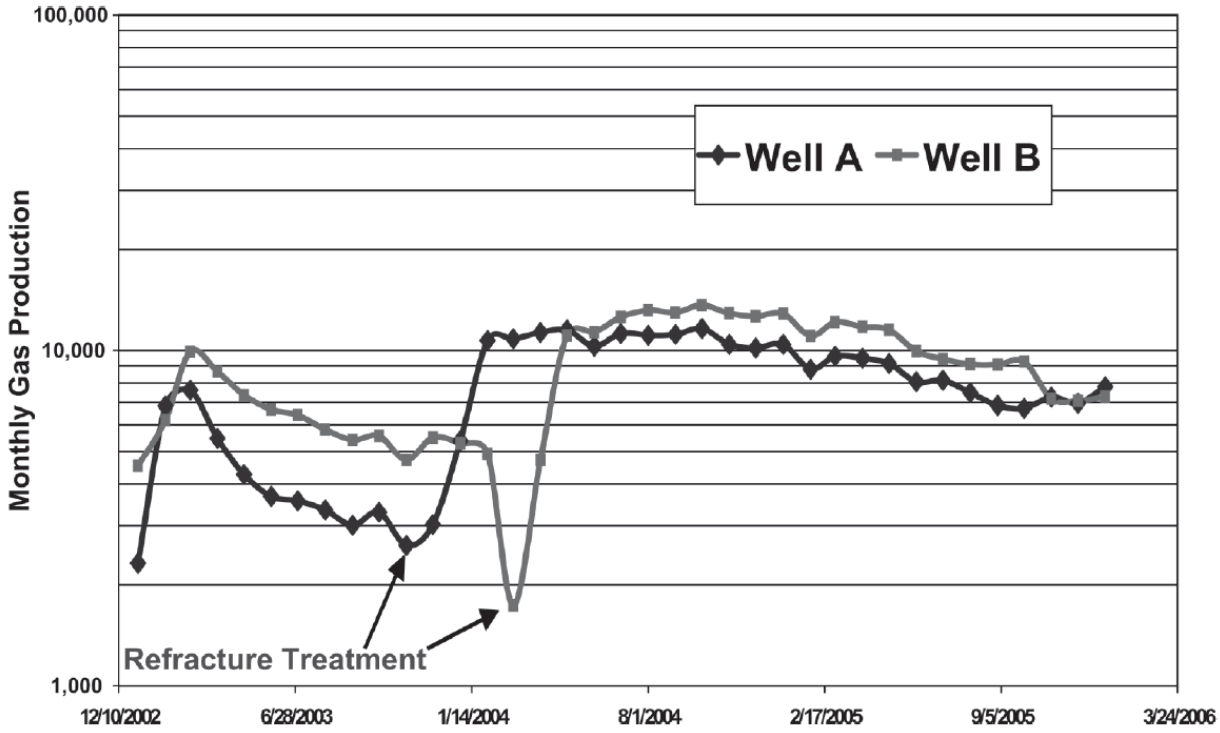

Figure 2-2 – Sustained production gains from refracturing treatments attributed to an increase in fracture half length due to better proppant transport capabilities in the fracturing fluid (Shaefer, 2006).

Two other common ways to access new parts of the reservoir in a refracturing stimulation are extending the fracture height to cover previously untouched payzones and reperforating the wellbore to create new fractures. The former method is applicable in vertical wells that have a multitude of interspersed pay zones. The operators may have missed some of these pay zones in the original treatment for a variety of reasons, including a lack of knowledge of the pay zone or a limited fracture height. In some cases, the number of pay zones is so high that it would be unreasonable for a single fracturing treatment to contact all of them, leading to an obvious motivation for an additional treatment. For instance, Craig and Brown (1999) report that in massively stacked lenticular tight-gas sands, the number of individual pay sands can range from 4 to 40 within a 1,000 to 2,000 ft thick gas-saturated interval.

Fisher et al. (1995) sought to determine the extent and frequency that pay zones were understimulated in fracturing treatments. They studied over 100 fracture treatments using radioactive tracers, which can identify propped fracture height along the wellbore. The analysis showed that "in nearly 40% of the completions, one or more zones did not receive any or all of the designed treatment". Furthermore, the authors presented tracer logs before and after a refracturing treatment. The tracer identifies proppant along the vertical wellbore. As can be seen in Figure 2-3, the refracturing treatment resulted in better coverage along the length of the perforated section, especially in the upper most portion. The perforations are identified on the left side of the log, and all of the perforations were open during the initial treatment (i.e no reperforating was conducted for the restimulation). Stabilized production thereafter doubled from 200 Mcfd to 400 Mcfd at roughly the same flowing tubing pressure (Figure 2-4).

Analogous results may be expected when simply increasing the height of a single fracture. Doing so will make an impact in both horizontal and vertical wells. Height

growth can be limited by proppant settling for many reasons, including poor fluid selection. Conway et al. (1985) detailed a successful refracturing program that used higher proppant concentrations to alleviate proppant settling thought to be caused by long closure times.

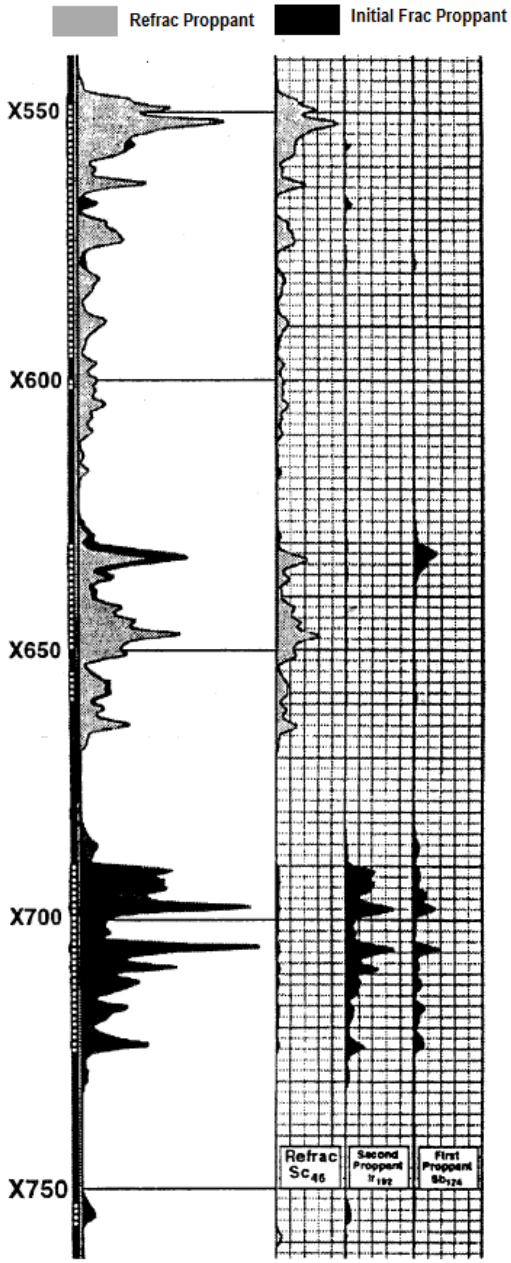

Figure 2-3 – Log of radioactive tracer along wellbore. The tracer indicates that the refracture delivered proppant to previously bypassed zones in the top portion of the wellbore (Fisher 1995).

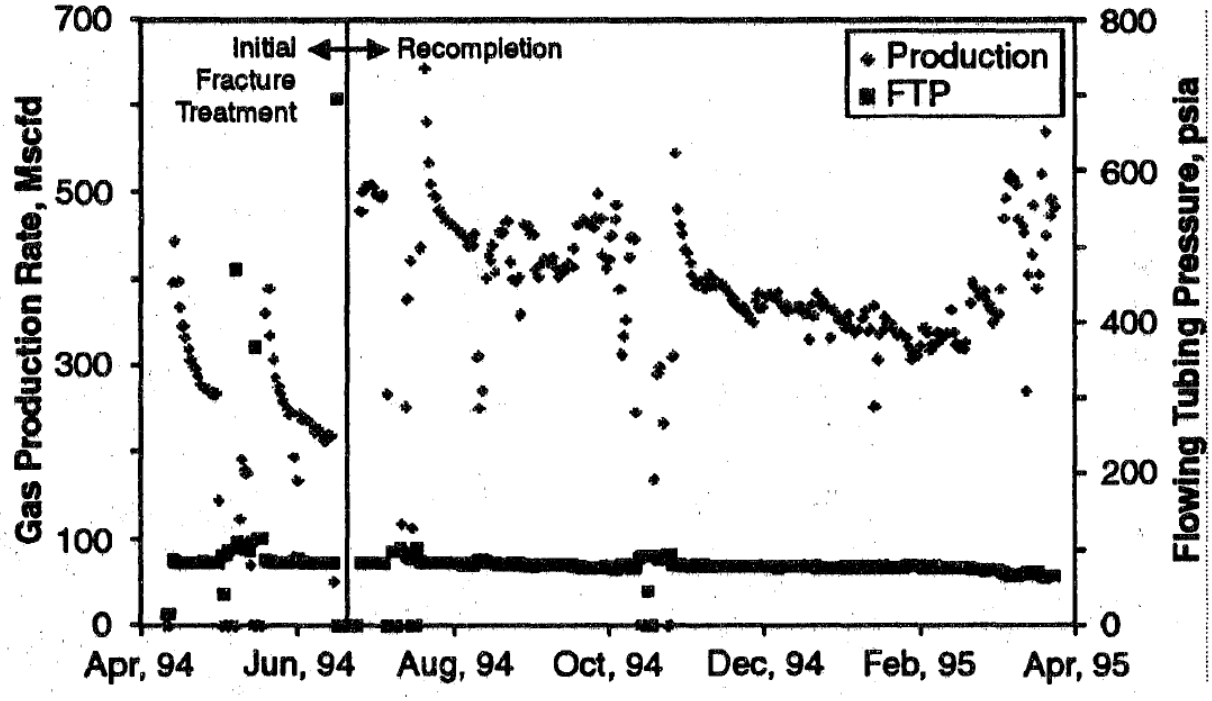

Figure 2-4 – Production in the well from figure 3, before and after the recompletion. The refrac doubled the stabilized gas rate (Fisher 1995).

In a similar fashion, new parts of the reservoir can be accessed by reperforating new sections along a horizontal well, thereby creating new fractures in the subsequent treatment. Unlike a vertical well, an ideal horizontal well remains in the pay zone throughout the length of the lateral. As a result, an optimized completion will maximize contact between the fractures and the lateral. For a longitudinal fracture, the length of the fracture should be maximized. For transverse fractures, the number of fractures along the wellbore should be maximized (this will maximize recovery; maximizing economic return must balance the benefit of extra fractures against the cost of additional stages and larger treatments). The effect of increasing the number of fractures per unit length of the lateral can be seen in Figure 2-5 below, taken from a paper by Waters et al. (2009). The images show the results from a reservoir simulator of a 400 nd shale gas reservoir with an initial reservoir pressure of 3,000 psi. In the image on the left, the fractures are spaced at

1,000 ft intervals and in the image on the right, the fractures are spaced at 250 ft intervals. The tighter spacing greatly increases the recovery factor: the 250 ft fracture spacing case produces as much from the reservoir in 10 years as the 1,000 ft fracture spacing case does in 60 years.

In an older well, tighter spacing can be achieved by reperforating and subsequently creating new fractures in between existing fractures. A diversion stage is often added to the fracturing treatment in order to ensure all perforations receive the treatment. This technique is discussed in further detail later in this chapter. An example of a successful refrac in a reperforated well is shown in Figure 2-6. Vincent (2010a) compiled the work of Lantz and Greene (2007) to show an increase in coverage along the lateral after the refrac. The refrac consisted of reperforating sections along the lateral (Figure 2-7) and then using ball sealers as diverters during the treatment. The log identifies proppant with the use of a radioactive tracer, and areas that were missed by the original frac were clearly stimulated during the subsequent treatment. After the refrac, the average GOR declined by almost half to near original rates, and the pressure generated in the refrac was about 50% greater than in the original treatment. Both measurements indicate that the refrac contacted previously undrained portions of the reservoir. Figure 2-8 displays the well's production and shows a sustained increase in oil production following the refrac. Both this and Fisher's examples demonstrate the intuitive concept that by contacting undrained portions of the reservoir in a refracturing treatment, sustained production increases can be achieved.

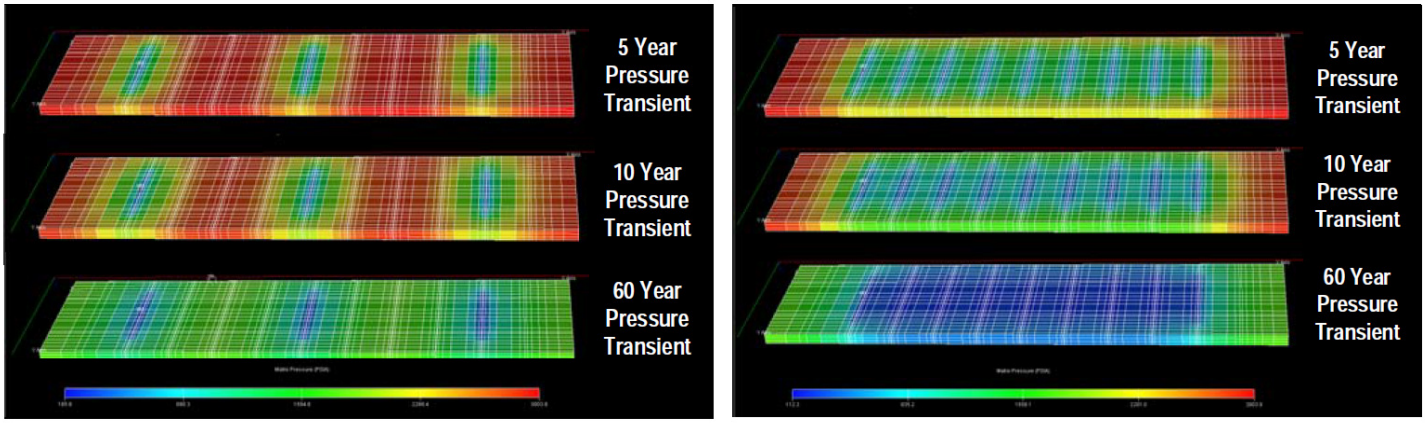

Figure 2-5 – fracture comparison spacing using a reservoir simulator. The formation is a 400 nd shale gas reservoir with an initial pressure of 3,000 psi. In the left image, fractures are spaced at 1,000 ft intervals and in the right image, fractures are spaced at 250 ft intervals (Waters et al., 2009).

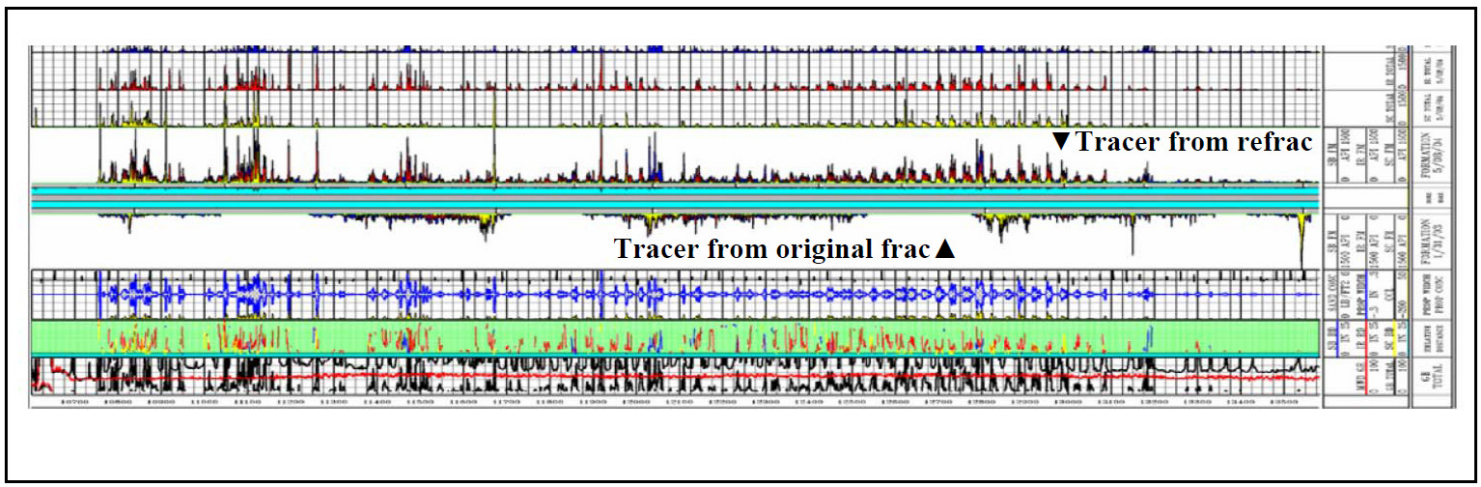

Figure 2-6 – radioactive tracer log that shows the presence of proppant from both the original fracturing treatment and the subsequent refracturing treatment. Prior to the refracturing treatment, new perforations were shot; during the refracturing treatment, ball sealers were used to divert flow to other perforations. The log clearly shows that the refracture resulted in greater coverage along the length of the lateral (Vincent, 2010a; adapted from Lantz and Greene, 2007)

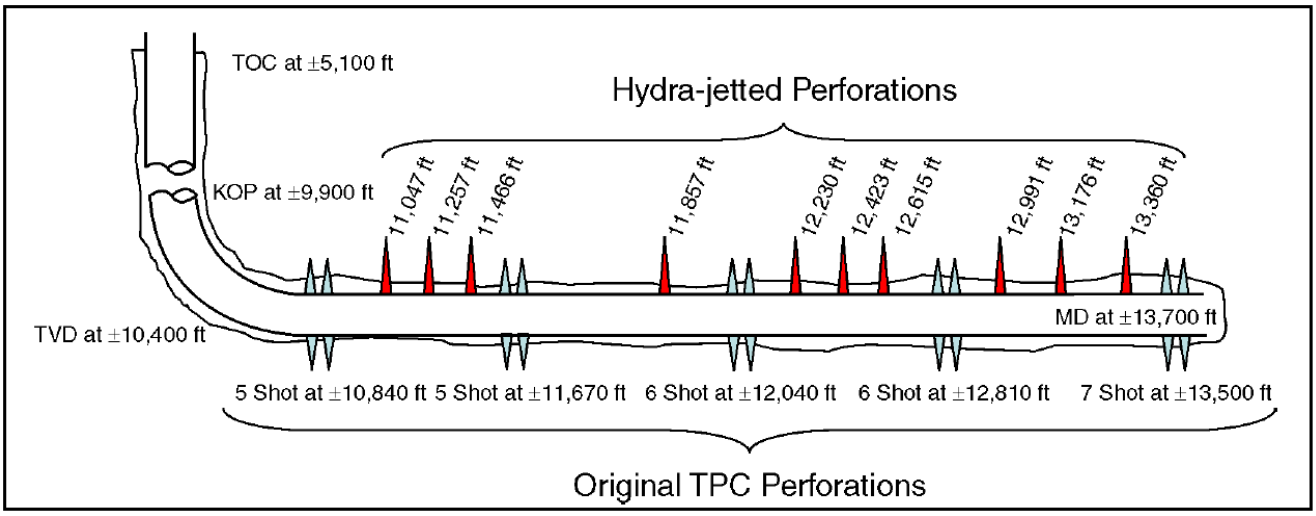

Figure 2-7 – Wellbore schematic of a typical well from the refracturing program described by Lantz and Greene. The hydra-jetted perforations are the new perforations added for the refracturing treatment (Lantz and Greene, 2007).

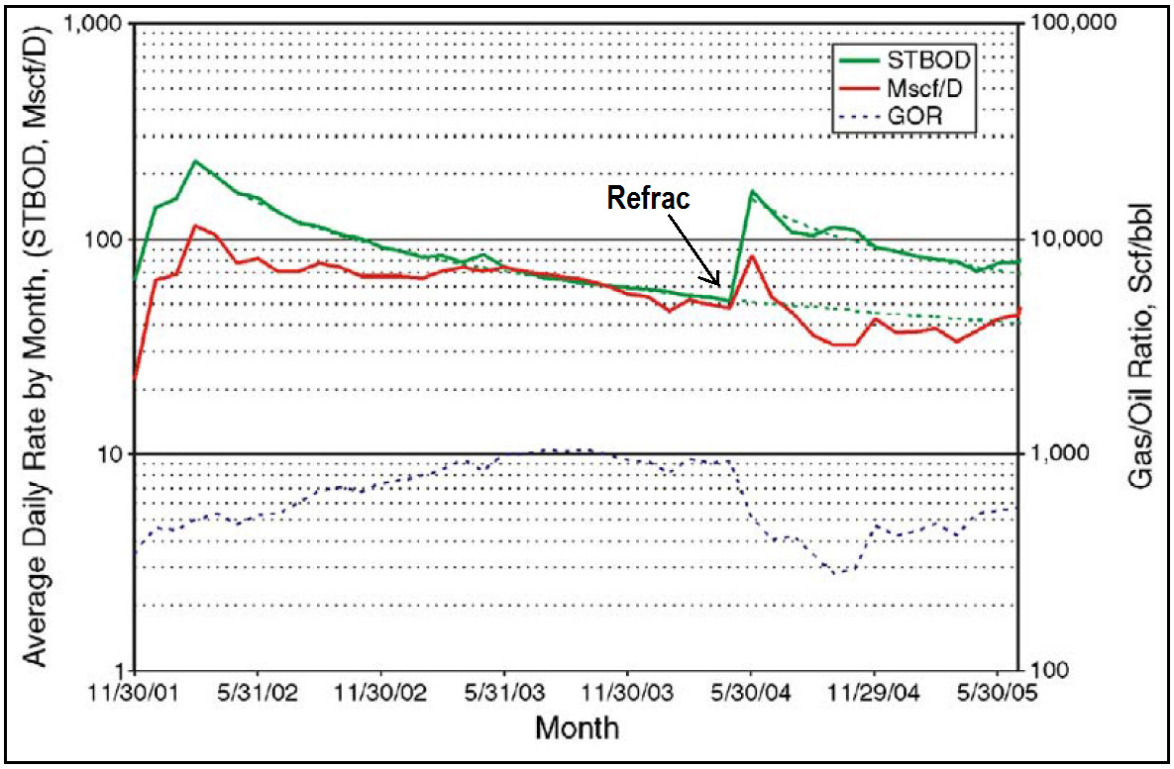

Figure 2-8 – Production rates of the well from Figure 2-6. Oil production saw a sustained increase after the refrac (adapted from Lantz and Greene, 2007).

Fracture reorientation is another mechanism that may allow engineers to contact new portions of the reservoir. Fractures propagate in the direction of maximum horizontal stress (Gidley et al., 1989), and after a period of time the direction of maximum horizontal stress may change (Wright and Conant, 1995). As detailed by Roussel and Sharma (2010), the in-situ stress profile of a fractured formation changes over time due to poroelastic and mechanical effects caused by the fracture. The poroelastic effects are caused by reservoir drainage and pressure depletion of the reservoir, and the mechanical effects are caused by the physical opening of the fracture. Since the pressure drops more rapidly in the direction of fracture propagation than away from it, the maximum horizontal stress decreases faster than the minimum horizontal stress during production (Roussel and Sharma, 2010). If the initial difference between the minimum and maximum horizontal stress is small, then it is possible that the maximum horizontal stress and minimum horizontal stress will switch directions. A subsequent fracture will continue to propagate in the direction of the maximum horizontal stress, so it will also switch directions from the original fracture and reorient. The mechanical and poroelastic effects decline rapidly with distance away from the fracture such that the stress profile will return to its initial state and any reoriented fracture will again reorient into the direction of the initial fracture (Figure 2-9). The reorientation allows contact with undrained portions of the reservoir, thereby supporting production increases if it occurs during a refracturing stimulation. Figure 2-10 shows a field example that demonstrates fracture reorientation with the use of microseismic monitoring.

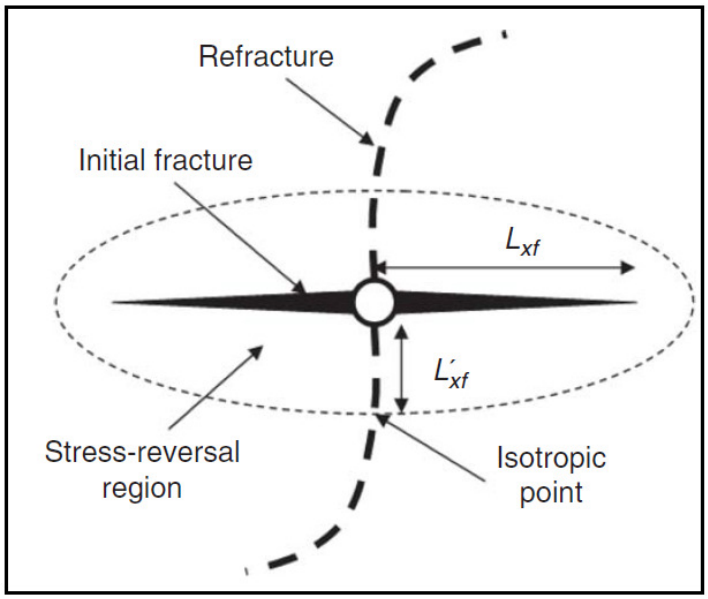

Figure 2-9 – The refracture reorients in a new direction inside the stress-reversal region, before returning to the orientation of the initial fracture (Roussel and Sharma, 2010).

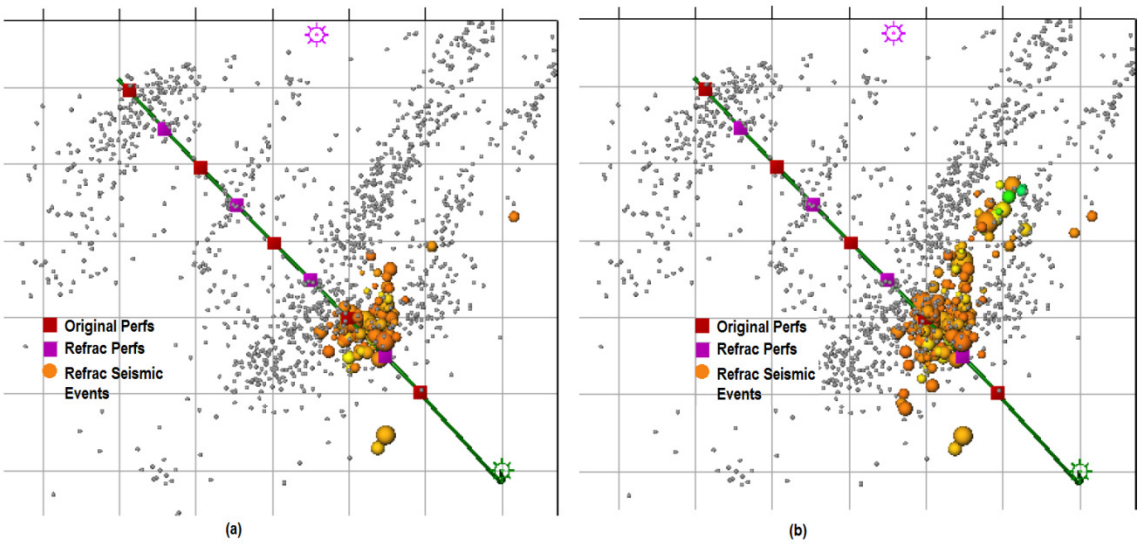

Figure 2-10 – Evidence of fracture reorientation. (a) is a mapview of microseismic events during a refracture; reorientation of the refrac to a North-South orientation is seen. (b) displays the same event, but at a later time; the fracture reorients back to the initial direction, orthogonal to the wellbore.

Enhancing Fracture Conductivity

Refracs can also improve recovery by increasing fracture conductivity, and two mechanisms that are responsible for this behavior are described below.

Proppant Degradation

Proppant degradation is a reduction in the permeability of the proppant pack over time and can be caused by several factors. While it is commonly understood that weaker proppants, such as sand, result in fractures with less conductivity, it is also possible that such proppants lose conductivity over time at a faster rate than the stronger ceramic proppants. Vincent (2010a) provides a robust summary of the various laboratory tests that illustrate proppant degradation. McDaniel (1986) tested the change in fracture conductivity over an extended time using five different proppants. The tests differed from conventional tests by employing higher temperatures, longer test times, and different test fluids. Most conductivity measurements up to the time were conducted at ambient temperatures and for short periods of time, and McDaniel's work showed these conditions led to overly optimistic results (see Figure 2-11). The drop in conductivity ranged from about 25% to 80%, with the ceramic proppants performing the best. As expected, conductivity reductions were highly correlated with confining stress.

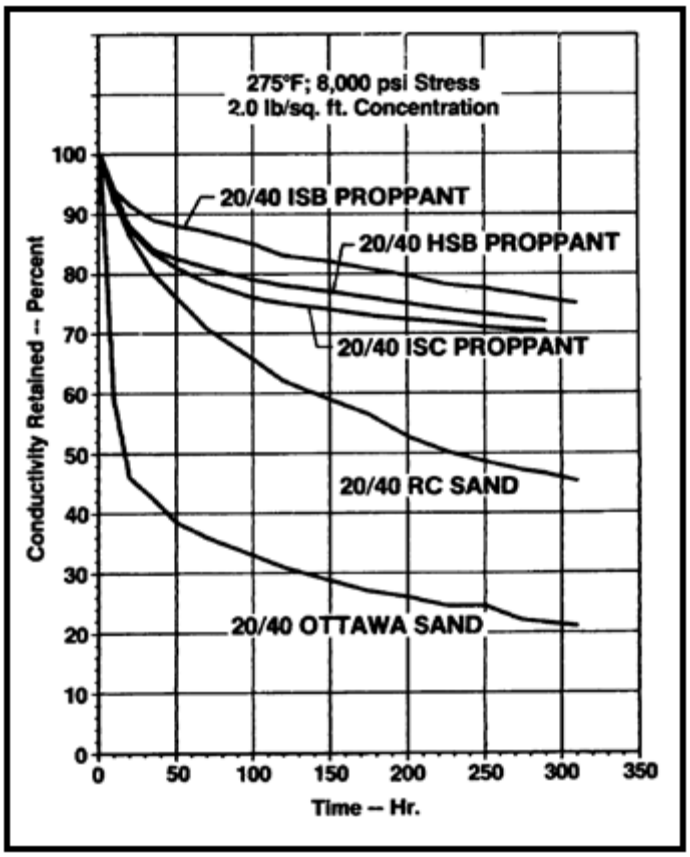

Figure 2-11 – Reduction in fracture conductivity over time for five different properties (McDaniel, 1986)**. ISB, HSB, and ISC are different types of ceramic proppant.**

Montgomery and Steanson (1985) showed similar results. The conductivity through proppant was tested with a cell composed of metal plates as fracture faces. At a closure stress of 5,000 psi, conductivity was reduced after 10 months by 50% and 60% for 20/40 sand and 10/20 sand, respectively.

Several mechanisms for proppant degradation have been identified, including mechanical failure of the proppant grains, plugging by formation fines, and proppant dissolution (Duenckel et al., 2011). Plugging by formation fines or by asphaltene production would clearly lead to reductions in fracture conductivity. Another possible mechanism is proppant diagenesis. According to this theory, geochemical reactions occur

between the formation and the proppant that alter the structure of the proppant bed, thereby reducing fracture conductivity. While diagenesis in rocks occurs over vast time scales, the process in fractures is greatly accelerated because the rock is already at reservoir stress and temperature. Rayson and Weaver (2012) physically observed this diagenesis in the form of crystal growth on the surface of proppant (see Figure 2-12). Duenckel et al. (2011) agreed that diagenesis does occur and can occur on all types of proppants, but they did not believe that it would be common at reservoir conditions or that it would result in significant conductivity degradation. Instead, the authors thought that the observed degradation was due to stress corrosion and static fatigue caused by exposure to water.

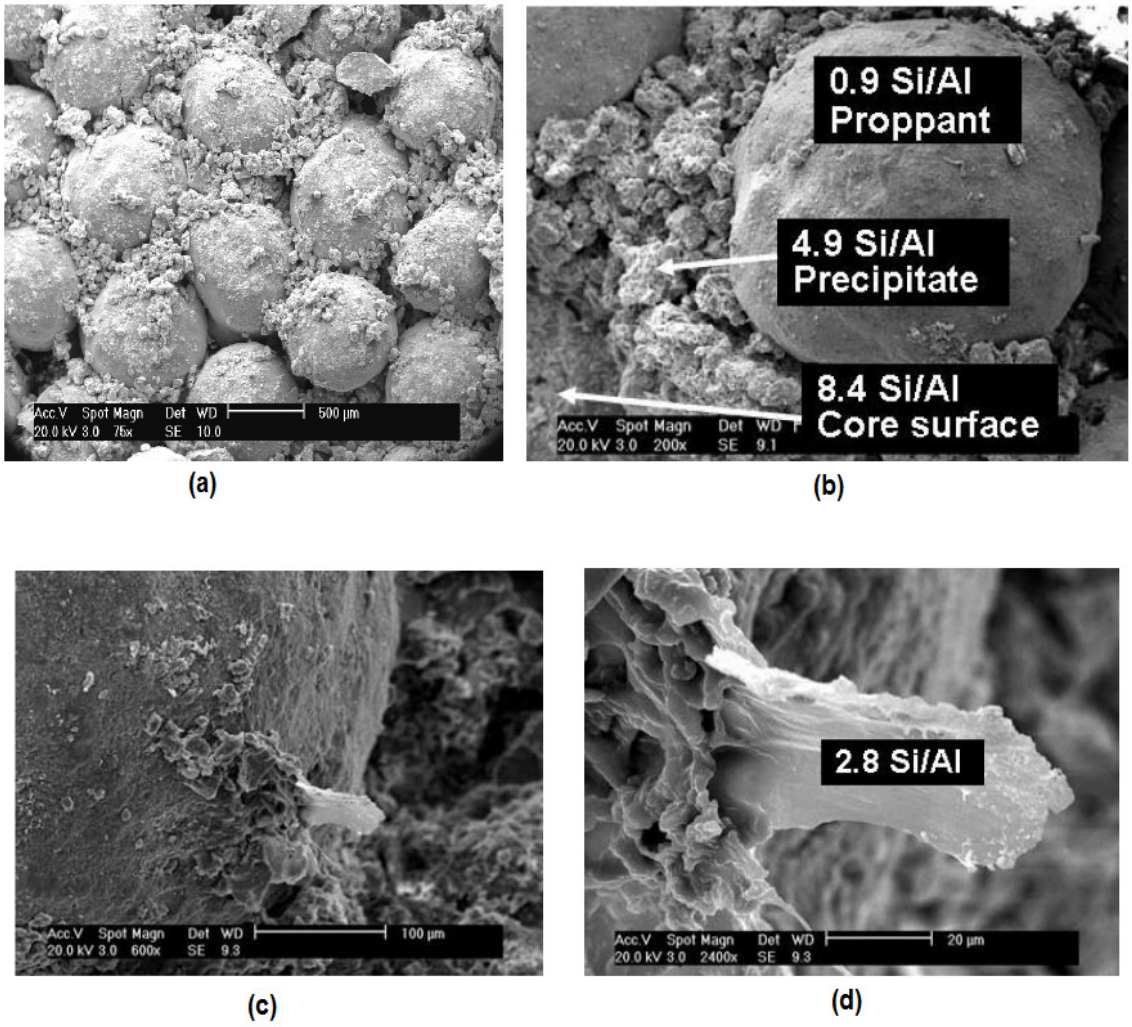

Figure 2-12 – Images of proppant diagensis captured using electron microscopy and energy dispersive X-ray (Rayson and Weaver, 2012)**. (a) ceramic proppant after exposure to 10,000-psi closure stress and 275 F for 140 hr in 2% KCl water. The debris is not thought to be crushed proppant; (b) a ceramic proppant grain embedded in Ohio sandstone after exposure to 10,000-psi closure stress at 250 F for 140 hr in 2% KCl solution under static flow condition; chemical makeup differs between proppant, precipitate, and core surface (c) and (d) closeup view of proppant from (b) showing an aluminosilicate crystal growing on the surface of the ceramic proppant**

Whatever the cause of the degradation in proppant quality, the lab results strongly suggest that the degradation is partly responsible for the large decline rates seen in shale wells. Vincent (2010a) provides strong evidence for the potential of refracing to "replace degraded proppant." He points out that, while it is not possible to isolate single variables

in a refracturing treatment, one field trial in horizontal wells in the Bakken resulted in successful refracs in 100% of the wells that were initially propped with sand (Lantz and Greene, 2007). On the other hand, only half of the refractured wells that were initially propped with ceramic were successful in another study in the Bakken (Besler et al., 2007; Besler, 2008).

Preventing Proppant Embedment

The embedment of proppant into the reservoir damages fracture conductivity by reducing fracture width (see Figure 2-13). Embedment occurs in formations that are sufficiently ductile. Alramahi and Sundberg (2012) conducted experiments measuring proppant embedment and fracture conductivity over a range of closure pressures with different shale samples. They found that embedment was highly correlated with the clay content of the sample (higher clay content resulted in more ductile samples and more embedment), but that other factors such as organic content and porosity were also important. The effect of closure pressure on fracture conductivity varied widely between samples, but in even the best case, fracture conductivity declined by an order of magnitude at a closure stress of 10,000 psi.

Terracina et al. (2010) showed that embedment could be mitigated by proper proppant selection. They employed new methods to test three varieties of proppant: curable resin coated sand (CRCS), uncoated frac sand, and lightweight ceramic. They showed that, in addition to other benefits, CRCS underwent less embedment in Bakken and Haynesville cores than the other samples did. In addition, wells that were treated with CRCS recorded superior production rates in the areas studied. The authors postulated that the superior embedment quality of CRCS is caused by grain-to-grain bonding, which allows the high closure stress to be more evenly distributed along the fracture. Kurz et al.

(2013) showed that fracturing fluid selection was also important for reducing embedment. In a standard fracture test conducted in an API conductivity cell for over fifty hours, slickwater consistently reduced the hardness of the rock by a larger margin than the other fluids tested, thereby increasing the potential for embedment. By designing treatments that reduce proppant embedment in a formation known to suffer from this problem, fracture conductivity and production rates can be increased.

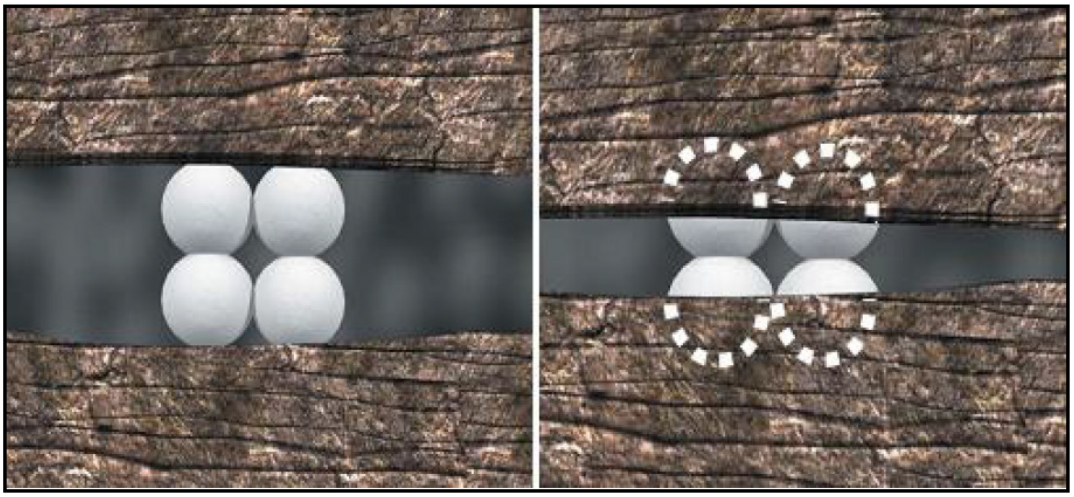

Figure 2-13 – Proppant embedment reduces fracture width (Terracina et al., 2010)

DIVERSION METHODS

During a refrac, a diversion method is commonly employed to ensure that the treatment is distributed evenly along the targeted section of the wellbore. Without the use of diversion techniques or isolation, it is possible that some portions of the lateral will remain untreated, resulting in a smaller production gain from the refrac. The original treatment typically does not need a diversion method, since the stages are often already isolated. For example, in plug and perf operations, a bridge plug is set between the current stage and the last set of treated perforations. Since stages of fracturing and perforating occur in an alternating manner, open perforations exist in only one direction

away from the targeted set of perforations. As a result, only one bridge plug is needed to isolate the targeted section and the treatment fluid will only be able to access these newly created perforations. In a refracturing treatment, all of the perforations have already been opened, so isolation would be more difficult. Furthermore, reducing the use of downhole equipment is an effective way to limit the cost of the treatment. A variety of diversion techniques have been employed in an effort to treat all of the targeted areas equally. All of these techniques rely on the ability to limit flow through perforations and fractures that would otherwise take proportionally larger amounts of the injected fluid.

One of the oldest techniques used to accomplish flow diversion is the limited entry technique (Lagrone and Rasmussen, 1963). The process essentially uses the friction force caused by the fluid moving through perforations as the diverting mechanism. In order to increase the friction force to sufficient levels, each zone limits the number of perforations through which the fluid may flow. As the pressure and flow rate of the injected fluid increases, the friction force and pressure drop through the perforations rises. Eventually, the pressure resistance may be high enough that the fluid will be diverted to other perforations and fractures. A step by step illustration of the process is given in Figure 2-14. The authors discuss successful field trials that employed the limited entry technique. Full coverage of the targeted zones was confirmed with the use of a radioactive tracer in the proppant.

Ball sealers provide a more direct form of diversion. In this method, balls of varying sizes are pumped downhole with the fracturing fluid. They are designed to restrict flow by seating in the perforations (a picture of ball sealers is given in Figure 2-15). The technique begins with a standard fracturing stage. After sufficient treatment fluid has been pumped, ball sealers are added to the injected fluid, and they seal the perforations that are taking the most flow. Fracturing continues without any ball sealers,

and since the fracture that would normally take the most fluid is now plugged, the fracture that normally takes the second most fluid now grows preferentially. This process is continued as long as desired. Wang et al. (2011) discussed the use of ball sealers in three horizontal wells in an Inner Mongolia field. The technique described above was used, except these wells had not been hydraulically fractured previously. To cover the entire perimeter of the horizontal well, ball sealers with densities lower than water, equal to water, and higher than water were used. As a result, some balls float to the top of the wellbore, some sink, and some float in between. Direct confirmation of diversion was not possible in this example, but the wells showed significant production gains after the treatment. Confirmation of diversion using ball sealers is seen in Figure 2-6 from Lantz and Greene (2007). Radioactive proppant confirmed better distribution of treating fluid in a refracturing treatment when ball sealers were used.

There are two notable disadvantages of using ball sealers. First, as with any diversion technique, the operator does not have the precise control over the location of created fractures offered by conventional isolation schemes such as plug-and-perf. Second, the seating of the ball sealers on the perforations relies on precise, regular perforation geometry. Irregular geometry will prevent complete plugging of the perforation, or, worse, will prevent the balls from even engaging the perforation. Adulteration of the perforation geometry can occur due to erosion caused by the pumping of the proppant. Figure 2-16 shows the degree to which proppant can erode perforations.

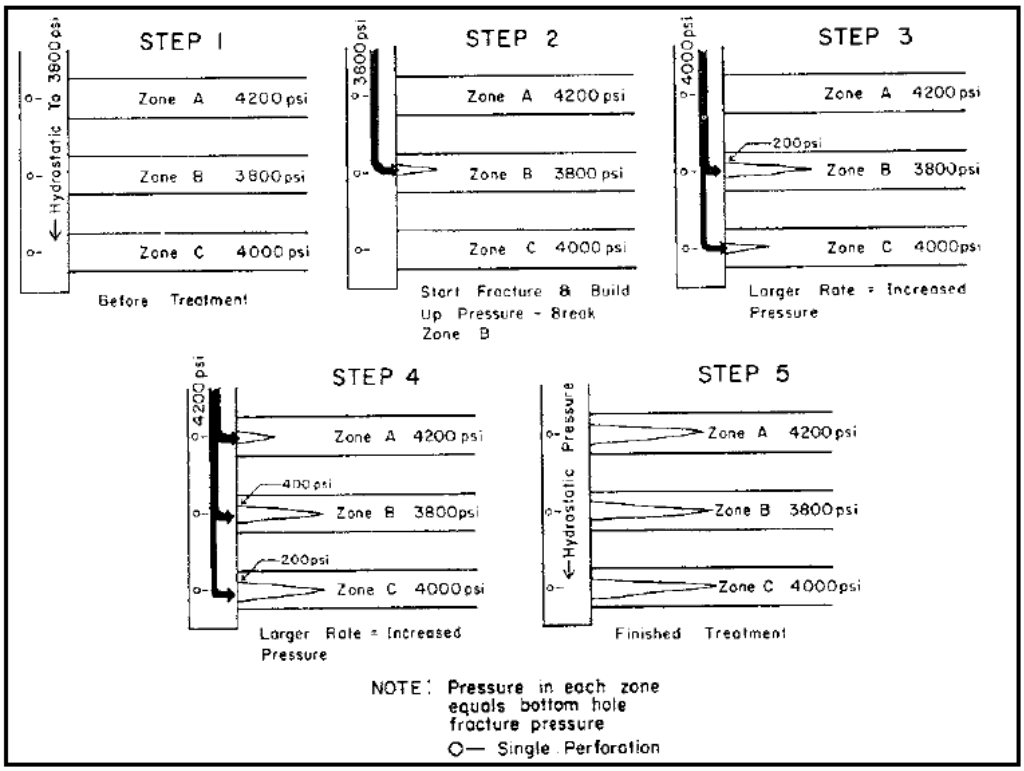

Figure 2-14 – An illustration of the limited entry technique for diverting treatment fluids. The method limits the number of perforations in a zone in order to use the increased friction forces in the perforations as a means to govern flow through a zone and accomplish diversion (Lagrone and Rasmussen, 1963).

Figure 2-15 – Ball sealers are designed to seat on perforations (Wang et al., 2011)

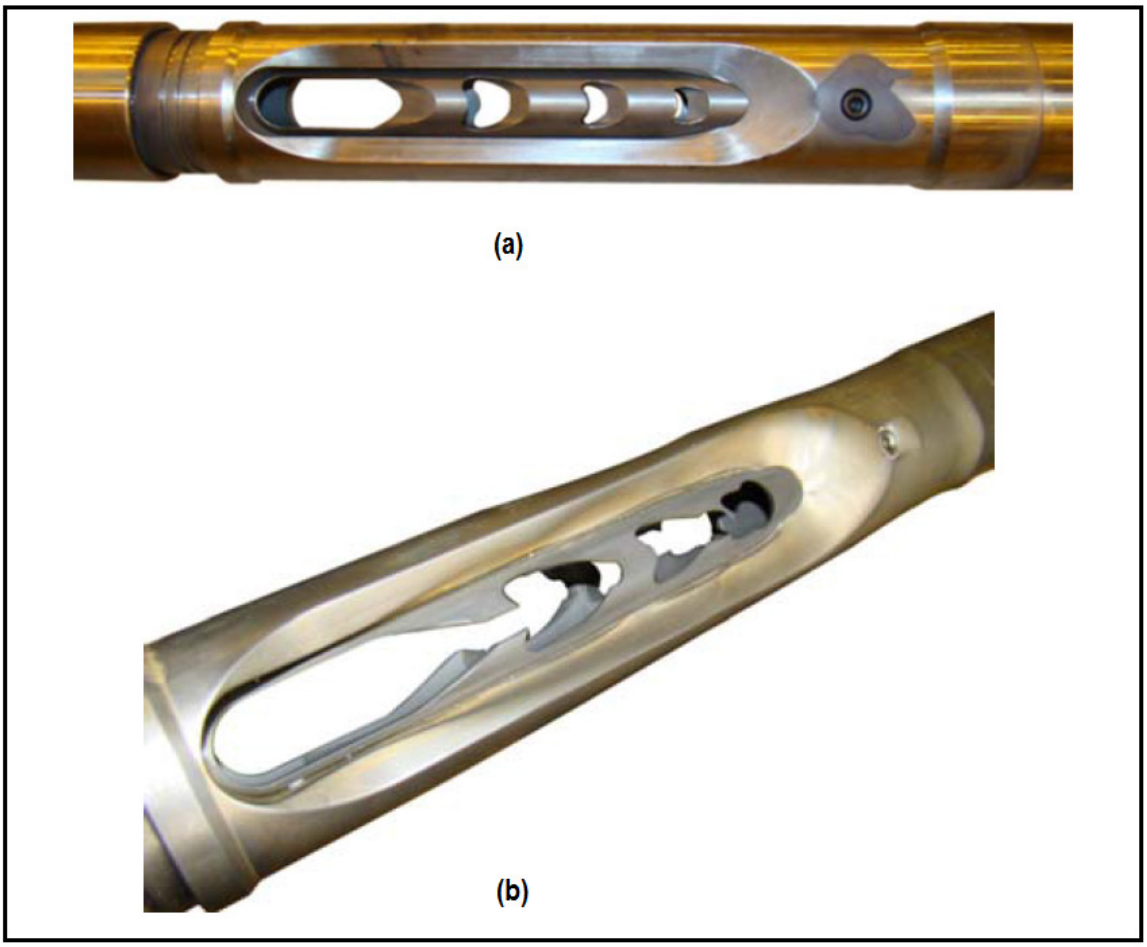

Figure 2-16 – (a) Initial configuration of perforation holes before an erosion test; (b) eroded perforations caused by pumping 250,000 lbm of sand

Diverting agents are likely a more robust tool for creating diversion. These are small particles that are pumped with the treatment fluid to bridge and form a filter cake plug in either the perforation tunnel or the fracture. To create a strong plug, different sized particles are mixed together (see Figure 2-17 for a picture of one diverting agent product). The diverting agents are designed to bridge on a variety of perforation and fracture geometries. The procedure for using diverting agents in a refrac is very similar to the one for using ball sealers. After a fracturing stage is pumped, diverting agent is added

to the fluid. The diverting agents are assumed to bridge on the fracture that is growing preferentially, so that in the subsequent fracturing stage, a new fracture will begin to grow. The diverting agents break down with time at reservoir temperature so production will not be disrupted.

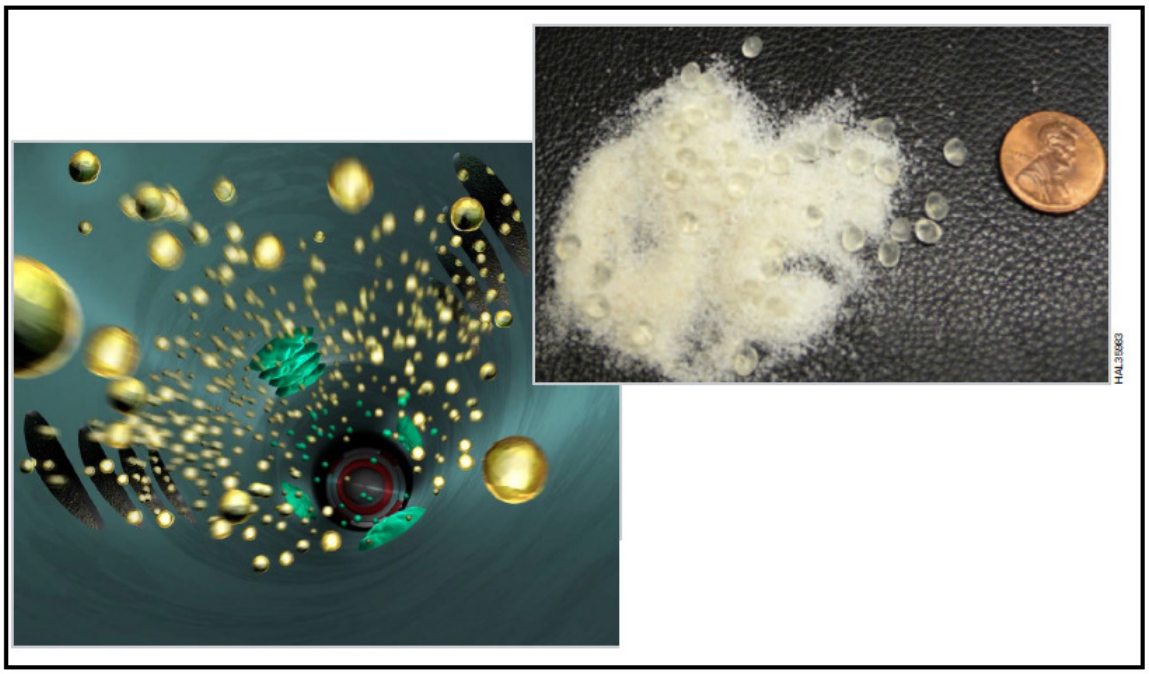

Figure 2-17 – A depiction of Biovert, Halliburton's diverting agent product. Different sized particles are injected simultaneously to enhance the plug. (Halliburton)

Several successful field trials with diverting agents have been documented and will be discussed in more detail later on in this chapter (Potapenko et al., 2009; Allison et al., 2011; Craig et al., 2012). Potapenko et al. (2009) observed diverting agent plugging in the lab and also detailed the results of a field trial in which diverting agents were used in horizontal wells in the Barnett. The authors observed a variety of factors that controlled the bridging of a slot by diverting agents, but noted that it was primarily controlled by the diverting agent material and the base fluid viscosity. They also collected the filter cake formed by the diverting agent and found the permeability to range from 1.7

to 15 Darcies. Successful diversion was confirmed in the field trial. Microseismic, which was used before and after the application of the agent, displayed a clear shift in seismic events to a different portion of the lateral (Figure 2-18).

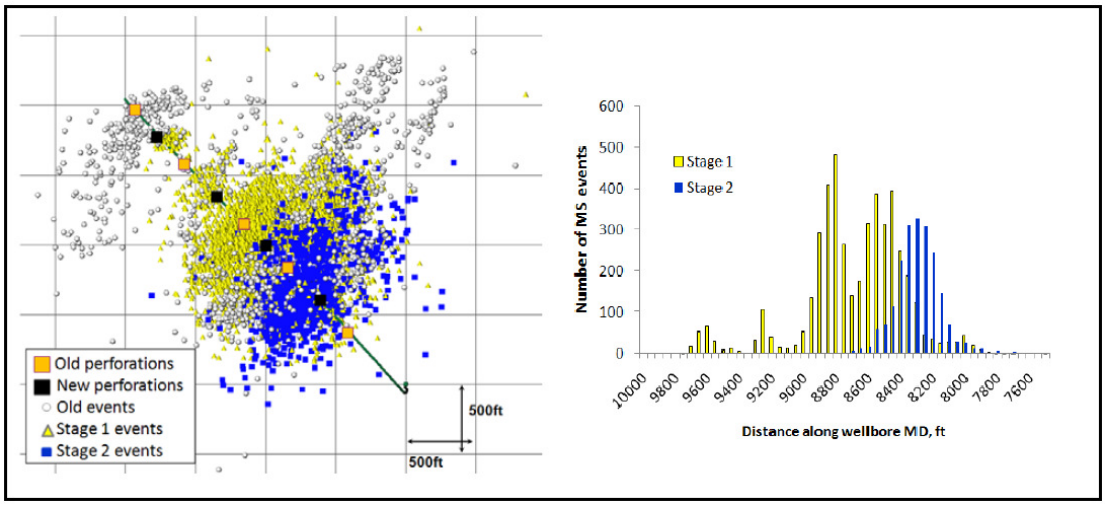

Figure 2-18 – Microseismic events during a refrac treatment before application of diverting agent (Stage 1) and afterwards (Stage 2). Diversion is clearly seen (Potapenko et al., 2009).

CANDIDATE SELECTION

To a large degree, the success of a refracturing program depends on which of the candidate wells are selected to be restimulated. While many successful refracs have been recorded, many wells have seen no production increases or, in some cases, drops in production. Vincent (2010a) discusses the result of a survey regarding restimulation treatments conducted on operators in the Rocky Mountain region. One third of the respondents stated that production increases exceeding 100% were observed, and another third of the respondents reported that wells failed to respond to restimulation. In regards to candidate selection criteria, "intuition" was the second most frequent technique employed, following well production trends. Standardized candidate selection criteria

would make the selection process more efficient and remove some of the uncertainty in refrac performance.

Interestingly, many authors have observed that the best wells actually make the best candidates for refracturing treatments (Reeves et al., 2000). As Vincent (2010a) notes, this observation suggests that initial fractures are often not sufficient nor optimized. However, operators are sometimes reluctant to treat high performing wells out of fear that the high performance will be damaged. As a result, wells with poor production are sometimes picked as refrac candidates instead. If poor production is a result of poor reservoir quality, then refracturing will likely not yield large production improvements and a negative bias toward refracturing in general may form. The development and use of an effective candidate selection methodology would reduce the risk of a failed refracturing treatment as well as the guesswork involved in the selection process. Reeves et al. (2000) remark that the need to develop better candidate selection methods is underscored by an observation from the Gas Research Institute that 85% of the restimulation potential for a given field appears to exist in only 15% of the wells.

Candidate Selection Study by the Gas Research Institute

Early studies by the Gas Research Institute suggested that the restimulation of tight gas sand wells could yield a large supply of low-cost reserves, and the organization launched a study to identify the best methods for candidate well selection (Reeves et al., 1999). Three different selection methods were employed on wells from the Piceance basin, the Green River basin, and the East Texas basin. The three different methods used were based on virtual intelligence, production statistics, and type curves. All three methods were applied at each site to pick wells from more than two hundred candidates.

Before discussing the results from this study, a brief background on each of the selection methodologies will be given. Methods based on production statistics compare a wells production to its offsets or to other similar wells. Engineers then select wells for refracturing based on the gap between expected production and actual production. This is perhaps the simplest method for selecting wells, and while it may be effective in identifying some wells that do not live up to their potential, the method suffers from two primary drawbacks. First, production data alone does not allow one to determine reservoir quality. As discussed earlier, a well with low production may be caused by poor reservoir quality and as a result would not be a good well for a restimulation treatment. The second drawback is that this method will not select high productivity wells that still hold potential for reserve growth. However, in reservoirs that show little variability in quality, selection methods based on production statistics may be effective.

Mohaghegh et al. (2000) provides background on three different virtual intelligence techniques and the application of virtual intelligence to the selection method used in the GRI study. The method begins by employing a tool called artificial neural networks. These networks attempt to solve problems in a similar fashion as biological neural networks. The connections between the neurons relate input parameters to a specified output parameter. The network is then "trained" by feeding it multiple examples. In response to each example, the connections of the network adjust in order to better describe the example. After many examples, the network reaches a steady state, and can then be used to map a set of different input parameters to the output parameter. This technique has been applied in multiple industries and is best suited for complex problems.

After the use of neural networks, genetic algorithms are employed. These algorithms are used to optimize a set of parameters. The algorithm operates by first

creating a set of different inputs, termed a population. Each input has multiple parameters. In the case of candidate selection, each input is an individual well, and the parameters are the proppant type, volume of fluid injected, date of initial treatment, etc. When creating the inputs, each parameter is randomly selected. The population is then evaluated using the artificial neural network to find the output for a given set of parameters. The worst inputs (i.e members of the population) are disregarded, and new inputs are created by mixing the parameters of the most successful inputs. Several random inputs are created as well. This process is continued multiple times (termed "generations") and ideally, the inputs that remain are the ones that contain the optimum parameters. For the candidate selection case, the optimized production for a well is the result of the neural network using the optimum parameters identified by the genetic algorithm. The difference between actual production and optimized production is the potential gain that can result from a refrac.

The last technique used in the virtual intelligence method is fuzzy logic. In the case of candidate well selection, fuzzy logic applies a rule about good candidates and places a well into one of several categories based on how well it meets the rule. The results of the genetic algorithms are used as an input to the fuzzy logic, in addition to other parameters identified by the rules. After applying each virtual intelligence technique, the candidate wells can then be ranked based on the suitability for a refrac. The primary drawbacks of this method relate to the examples used to train the neural network. The sample size of the examples must be large enough so that parameters are neither overvalued nor undervalued. One anomalous example in a small sample size would result in a poorly tuned neural network. Furthermore, all of the relevant parameters affecting a fracture treatment must be identified and accurately measured.

Type curves are the last of the candidate selection methodologies tested and employed in the GRI study. These curves have been formulated for hydraulically fractured wells and can allow one to estimate the well's permeability and skin. Wells with high permeability and skin are then selected as good candidates for refracturing. This technique involves a few drawbacks (Reeves et al., 1999). Most type curves have only been made for single layered reservoirs, making it difficult to apply them to wells with multiple fractures. Also, type curves often do not result in unique solutions for the various output parameters.

The GRI study ultimately selected nine wells from the three different basins. The wells were selected by shortlisting the top wells identified by each selection methodology and the wells that made the top fifty list for more than one methodology. The wells were further evaluated on a variety of factors such as the mechanical integrity of the wellbore. Casting doubt on the effectiveness of the selection methods used, only six of the more than two hundred wells considered were identified in the top fifty list for all three selection methods; twenty-nine wells were identified in more than one list, and eighty-six wells were identified in only one list (Reeves et al., 1999). The authors explained that each methodology selects different wells because each one uses different parameters to assess refracturing potential.

While the wells selected by each methodology were not consistent, the production results after the refrac were very positive overall. Six of the nine treatments were economically successful. Considering all nine wells, the program as a whole was economically successful as well, increasing incremental reserves by 2.9 bcf at an average $0.26/Mcf cost. Furthermore, each selection methodology performed almost equally. The methodologies were compared by their number of successful picks. A pick was determined to be successful if the methodology either ranked it near the top of its list and

the refrac was successful, or if the methodology ranked it as a poor candidate and the refrac then turned out to be unsuccessful. Both the production statistics method and the type curve method had successful picks in four out of nine wells. The virtual intelligence method made accurate picks in five out of nine wells. While the percentage of successful picks leaves much to be desired, the results of the program indicate that economic success is still possible despite the performance of the selection methodologies.

Other Candidate Selection Methods

A variety of other candidate selection methods have been proposed and tested. Shelley (1999) applied an artificial neural network to select wells for restimulation in the Red Oak field of southeast Oklahoma. This neural network differed from the one described by Mohaghegh et al. (2000) in that it incorporated refracture treatment properties as inputs to the network. As a result, Shelley's network directly attempts to estimate refracture production, whereas Mohaghegh only attempts to estimate the production after an ideal initial treatment in order to determine the gap in production from actual levels to the ideal levels. The refracture production rates predicted by the neural network matched actual production rates with an R squared value of 0.99. The predictions were based on twenty-five wells – seventeen were used to train the neural network and eight were used only for testing the neural network. The network was then used to evaluate the remaining wells for refracture potential; 30% were projected to be good economic candidates, 50% were projected to offer minimal potential for production improvement, and 20% were projected to see a production decrease from a refracture attempt.

Conway et al. (1985) described a simple, but likely effective method for selecting candidate wells. Essentially, the authors looked at wells that were underperforming.

Wells in areas that showed signs of depletion or insufficient reserves were not considered. Next, the initial fracturing treatment was analyzed for problems that may have caused poor production, and a refracturing treatment that would correct these problems was designed. The authors also discussed results from a refracturing field trial. In the A.W.P. Olmos field, they determined that higher than expected closure times resulted in proppant settling and poor production performance. They designed refracturing treatments that had higher sand concentrations to counteract this problem, resulting in successful refracs.

Sinha and Ramakrishnan (2011) describe a method designed to rapidly eliminate wells from consideration and to select wells for further analysis. The method relies on a completion index that identifies understimulated wells and a production index that indicates wells that have strong reservoir qualities. The wells to be selected for further analysis have a high production to completion index. The authors present example formulas for the completion and production indexes, but these formulas can be tailored based on operator experience. Roussel and Sharma (2011) described a new candidate selection method based on dimensionless criteria. One of the main advantages of this method is that only production data of the wells under consideration is needed, as extensive examples are not needed for the tuning required by artificial neural networks. The dimensionless criteria are as follows: stress reorientation number, which quantifies the potential for stress reorientation in a refracture; well completion number, which estimates the effectiveness of the initial completion based on initial production figures; reservoir depletion number, which uses production data from neighboring wells to determine the extent of remaining reservoir pressure and reserves; and the production decline number, which estimates reservoir quality by the magnitude of production

decline. The method was tested on a set of refractured wells in the Wattenberg field, and the wells selected by the method outperformed a random selection by 35%.

FIELD STUDIES OF REFRACTURING TREATMENTS ON HORIZONTAL WELLS WITH THE USE OF DIVERSION

The original research described in later sections of this thesis concerns the modeling of refrac treatments with the use of diverting agents. The results from several published field studies have been promising, and the works are summarized below.

Restimulation of Wells using Biodegradable Particulates as Temporary Diverting Agents

In their recent paper, Allison et al. (2011) first describe the design process that resulted in a diverting agent product, and then discuss the results of the application of this diverting agent to a refracturing treatment on two wells in the Barnett shale. The design process began with the identification of several criteria needed in a diversion mechanism, including the capability to self-degrade (i.e., cease plugging of the fracture and allow for uninhibited production); to assemble and form plugs in a variety of unknown downhole geometries; and to integrate seamlessly into the pumping process. The authors rated common diversion mechanisms, such as rock salt and ball sealers, on these criteria and ultimately settled upon biodegradable particulates (i.e., diverting agents) as the best solution. These diverting agents utilize small particles that will bridge on an opening and form a plug. The product described in this paper is designed to plug in the perforation tunnel or early part of the fracture.

The paper also presented the results from the refracturing of two wells in the Barnett. One well (Well A) was a horizontal well that pumped four treatment stages and three diverting agent stages. New perforations were added before the fracturing treatment to improve coverage along the lateral, and acid treatments were also pumped to reduce

perforation friction. The other well (Well B) was vertical and pumped three treatment stages with two diverting agent stages. Perforations were also added in this well. In both wells, large pressure increases were seen during the pumping of the diverting agent (from 500 psi to 1250 psi) and between the end of one stage and the start of another (from 306 psi to 828 psi). These pressure differences due to pumping of the diverting agent are taken as evidence of successful diversion into flow paths of higher resistance. The refracturing treatments were very successful, resulting in sustained production increases that resulted in peak rates that were 55% and 70% of the original production rates (see Figure 2-19). Figure 2-20 shows the refrac pumping schedule for the horizontal well.

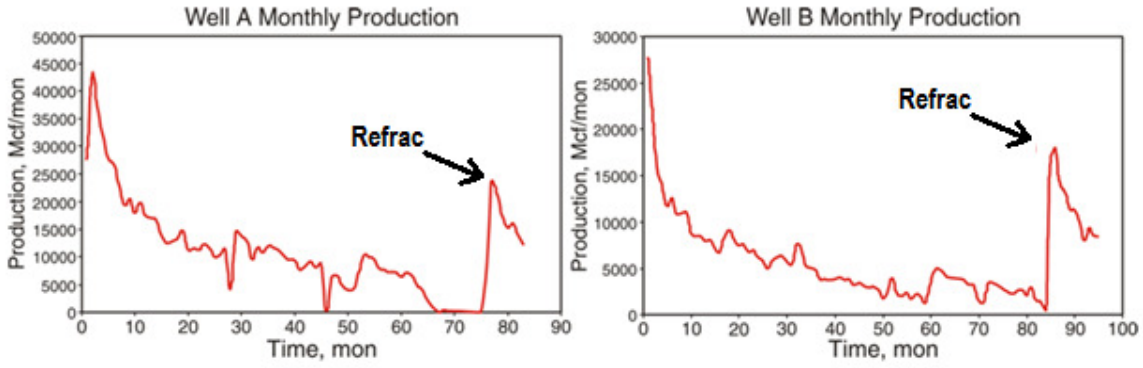

Figure 2-19 – Monthly production for wells refractured with diverting agent. Production rates after the refracture reached 55% and 70% of the initial rates (Allison et al., 2011).

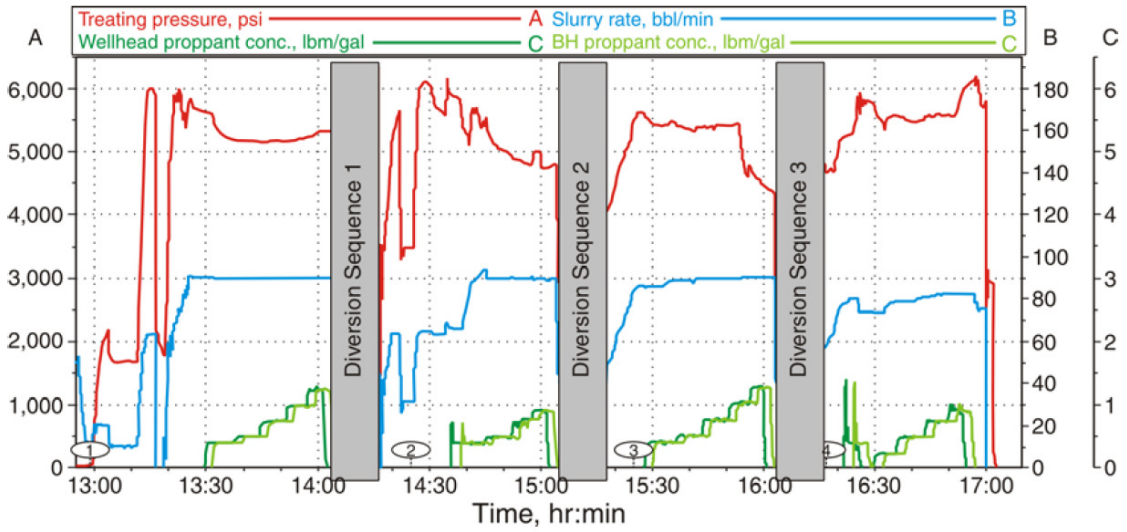

Figure 2-20 – Treatment schedule for the refracturing of Well A with the use of a diverting agent (Allison et al., 2011).

Barnett Shale Refracture Stimulations Using a Novel Diversion Technique

Potapenko et al. (2009) discusses the results of lab testing on a fiber based diverting agent before detailing the results of refracturing treatments on two horizontal wells in the Barnett shale. The lab experiments consisted of pumping a slurry containing diverting agent into a restricted slot. The goal was to understand the physics of bridging, identify the parameters that control the bridging event, and determine the pressure increase resulting from the bridged material in the flow path. The results illustrated the pressure increase following a bridging event and the amount of diverting agent volume fraction needed to form a bridge in the slot based on the fluid velocity and proppant volume.

A unique aspect of the diversion method outlined by the authors is that it attempts to customize the treatment in real time based on data provided by microseismic measurements. Results from the lab experiments allow the treatment to be optimized based on fracture and formation parameter estimates. These properties are evaluated by

microseismic data and are then used to tailor the treatment to the well in real time. The microseismic data also provides confirmation of diversion. Figure 2-18, which presents a map view of microseismic events measured during the refracturing of one (Well A) of the two wells discussed in the paper, is reprinted below. The events clearly shift along the lateral after multiple applications of the diverting agent. In turn, production increased significantly after the restimulation, and the production histories of both wells is given in Figure 2-21. The authors estimated that the EUR for well A increased by 20%.

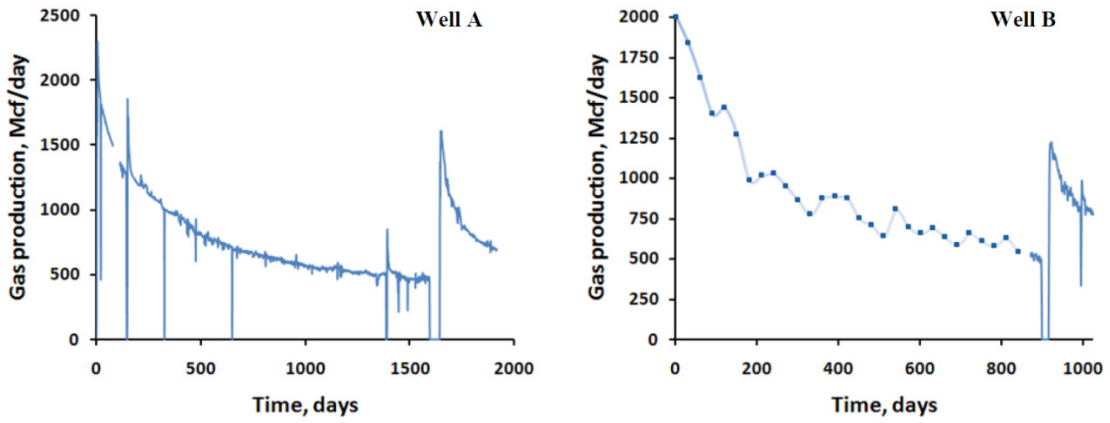

Figure 2-21 – Monthly production figures of two horizontal wells restimulated with the use of a diverting agent (Potapenko et al., 2009).

Restimulation of Unconventional Reservoirs: When Are Refracs Beneficial?

Vincent (2010b) compiled results from refracturing stimulations in the Bakken and in Canada. Much of the data presented in this work is only from publically available data, and detailed information about the refracturing treatment is not listed. The results are mixed, with some wells showing apparent damage from the treatment, some showing mild improvement, and some proving to be economic successes. The results from two

different areas in the Bakken are presented below. Both wells were successful in Figure 2-22 (a), and only some showed improvement due to the refracture in Figure 2-22 (b).

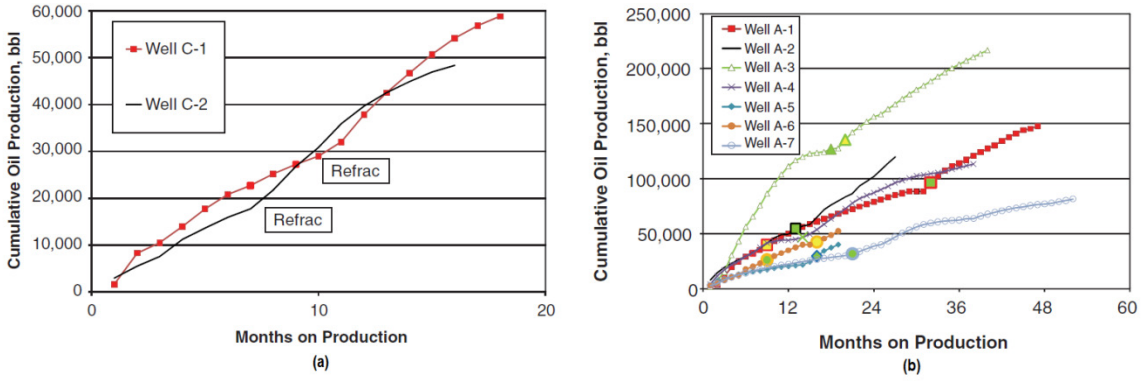

Figure 2-22 – (a) shows cumulative oil production of a well that was initially fractured using sand and subsequently refractured using ceramic proppant. Results from (b) were mixed, with some refracs a success and some had little effect. Green symbols represent refracs, and yellow symbols denote dates when pumping equipment was run/rerun (Vincent, 2010b).

Barnett Shale Horizontal Restimulations - A Case Study of 13 Wells

The horizontal well refracturing program reported by Craig et al. (2012) occurred in one of the most productive areas in the Barnett Shale. The wells were primarily screened by reservoir depletion. This value was calculated by combining the cumulative production of a particular well with a fraction of the cumulative production of offset wells that are close enough to the original well that the stimulated reservoir volumes overlap. Subtracting this number from the original gas and oil in place gives the remaining reserves.

Of the thirteen wells refractured, twelve showed increases in reserves and one actually showed a loss. In the well that experienced a loss, the fracture job went according to plan and the authors are not sure how to explain the failure. Cost figures are

included and the authors used a minimum ratio of 1 incremental Bcf gas to $1 MM cost to justify a refrac. With this stipulation, six of the thirteen wells were justified. Most refractures were conducted with the use of a diverting agent. As diverting agent costs proved to be high, the operators moved away from diverting agents and instead accomplished refrac control through cement squeezing and reperforating (an operation that uses cement that plugs leak paths and then reperforates in desired areas). The new method resulted in better economics. A normalized production plot for the thirteen wells is shown in Figure 2-23. The increase in EUR achieved by all but one of the wells can be seen in the graph as a sustained increase in production after the refrac.

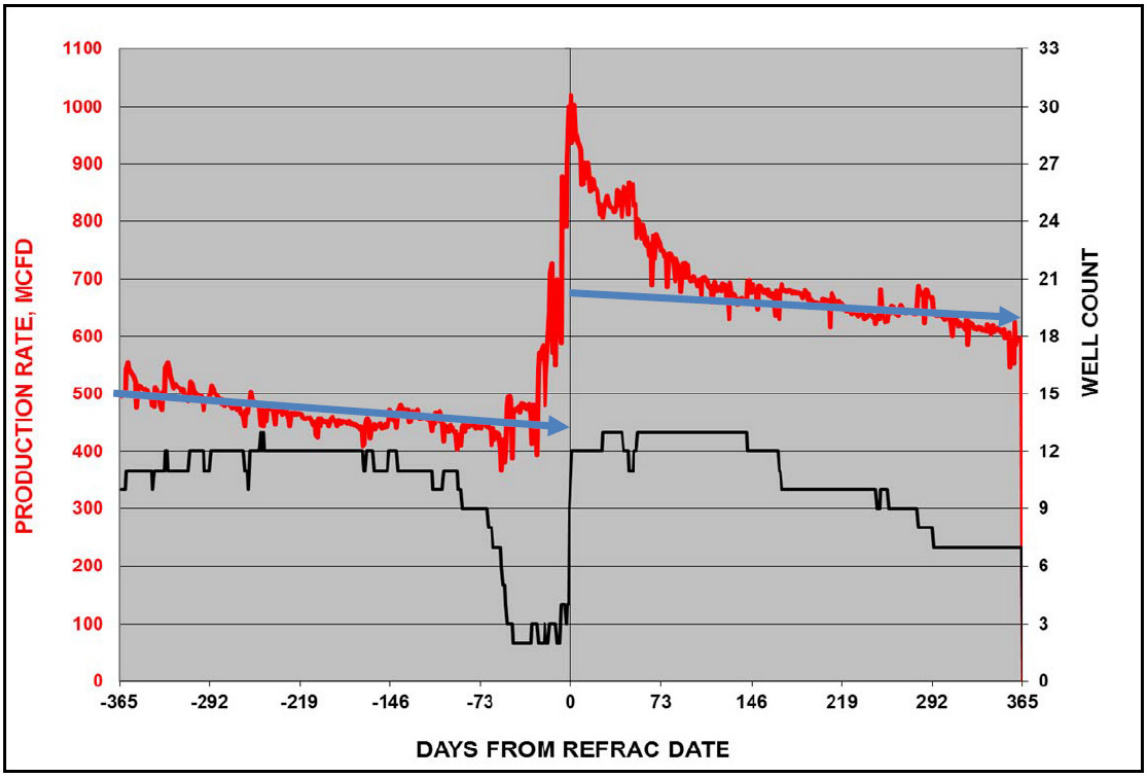

Figure 2-23 – Normalized graph of production rate for 13 wells from date of refracturing treatment. The refrac resulted in sustained increases in production and EUR gains (Craig et al. 2012).

The case studies described here demonstrate the potential success associated with refracs. However, the failures that have occurred underscore the importance of selecting the most suitable wells and understanding the mechanisms that will improve production performance.

Chapter 3: Model Formulation

This thesis describes the results of simulations of refracture treatments with the use of a diverting agent. The simulations were conducted by combining a fracture propagation model with a model that calculates the pressure drop caused by an injected diverting agent. The principles and equations that underlie these models are described in this chapter.

SUMMARY OF UTWID

The fracture modeling feature of UTWID was used as the standard fracture propagation model. UTWID is an injection well modeling simulator developed at the University of Texas at Austin. UTWID can create initial fractures intersecting the wellbore and calculate the propagation of competing multiple fractures caused by an injected fluid.

ASSUMPTIONS

UTWID incorporates a variety of assumptions, listed below.

1. The reservoir is homogeneous and isotropic.

2. The vertical stress exceeds the horizontal stresses; therefore, the fractures created are vertical.

3. There is a large difference between the minimum and maximum horizontal stresses which lead to fracture propagation as a single two-winged fracture (Figure 3.6).

4. The fracture is contained and extends vertically through the entire thickness of the reservoir.

5. Formation damage due to particle plugging is uniform over the entire fracture face.

6. The leak-off is uniform over the entire fracture face.

7. The leak-off is one dimensional and perpendicular to the fracture face.

8. The temperature front is approximated as a step profile and heat conduction to overlying and underlying formations is neglected.

9. The injection rate is constant.

10. The reservoir fluid displacement is piston like, with step profiles having residual reservoir fluid (usually oil) saturation behind the water flood front and initial water saturation ahead of the water flood front.

UTWID FEATURES

UTWID includes a variety of features to describe injection behavior. The User Guide for UTWID (The University of Texas, 2009; also see Suri et al., 2010) provides a detailed description of this model, but an overview of the different features described in the User Guide is given below. Subsequent sections describe how the code was modified to accommodate the use of diverting agents.

Fracture Propagation

The model assumes that the minimum horizontal stress is less than the overburden stress. As a result, the created fracture is vertical and the fracture propagates in the direction of the maximum horizontal stress. Since the strains created by hydraulic fractures are relatively small, the formation can be assumed to deform in an elastic manner. However, the linear theory predicts an infinite stress singularity at the fracture

tip, a condition not sustainable in real materials. As a result, inelastic behavior has been proposed for the area around the fracture tip. Under this theory, the fracture propagation pressure is the pressure that will equate the work done during fracture propagation to the total energy in the fracture system. An equation utilizing this theory proposed by Perkins and Krech is used in this model (3.1).

$$p = s + \sqrt{\frac{\pi UE}{2(1-\nu^2)r_f}} \tag{3.1}$$

where p is the average pressure in the circular area near the extending ends of the fracture, s is the earth stress perpendicular to the fracture plane, U is the specific surface energy, E is Young's Modulus, ν is Poisson's ratio and r_f is the radius of the extending end of the fracture. Since the direction of fracture propagation is normal to the direction of the minimum stress, the fracture propagation pressure is given by

$$p_{frac} = \sigma_{H,\min} + \sqrt{\frac{\pi UE}{2(1-\nu^2)r_f}} \tag{3.2}$$

For each timestep, the program calculates the tip pressure for a given fracture length and injection rate. If the tip pressure (p_{tip}) exceeds the fracture extension pressure of the rock (p_{frac}), then the fracture grows. The fracture length will be increased, and, consequently, the pressure drop will change from the wellbore to the tip. The fracture length is iterated until the correct one is found such that p_{tip} equals p_{frac}. The injected fluid is distributed in each fracture in accordance with the flow resistance offered by each set of open perforations and fractures.

Thermoelastic Stresses

Thermoelastic stresses are created when the injected fluid is at a lower temperature than the formation. In this case, a thermal front propagates from the well. Assuming a two-winged vertical fracture and a fluid of constant viscosity, the flow geometry is elliptical with the outer boundary of the thermal front at any time being approximately an ellipse that is confocal with the fracture (Figure 3-1). The change in temperature results in a reduction of the fracture propagation pressure. For a formation with height h, the thermoelastic stresses $\Delta\sigma_{1T}$ perpendicular to the major axis of the ellipse are expressed as

$$\frac{(1-\nu)}{E\alpha\Delta T}\Delta\sigma_{1T}=\frac{(b_0/a_0)}{1+b_0/a_0}+\left(\frac{1}{1+b_0/a_0}\right)\left[1+0.5\left\{1.45\left(\frac{h_{for}}{2b_0}\right)^{0.9}+0.35\left(\frac{h_{for}}{2b_0}\right)^{2}\right\}\left\{1+\left(\frac{b_0}{a_0}\right)^{0.774}\right\}\right]^{-1} \quad \textbf{(3.3)}$$

The thermoelastic stresses $\Delta\sigma_{2T}$ parallel to the major axis of the ellipse are expressed as

$$\frac{(1-\nu)}{E\alpha\Delta T}\Delta\sigma_{2T}=\frac{(b_0/a_0)}{1+b_0/a_0}+\left(\frac{b_0/a_0}{1+b_0/a_0}\right)\left[1+0.5\left\{1.45\left(\frac{h_{for}}{2b_0}\right)^{0.9}+0.35\left(\frac{h_{for}}{2b_0}\right)^{2}\right\}\left\{1+\left(\frac{b_0}{a_0}\right)^{0.774}\right\}\right]^{-1} \quad \textbf{(3.4)}$$

The major and minor axes are

$$a_0=\frac{L_f}{2}\left(\sqrt{X_0}+\frac{1}{\sqrt{X_0}}\right) \quad \textbf{(3.5)}$$

$$b_0=\frac{L_f}{2}\left(\sqrt{X_0}-\frac{1}{\sqrt{X_0}}\right) \quad \textbf{(3.6)}$$

where

$$X_0 = \frac{2V_c}{\pi L_f{}^2 h_{for}} + \frac{1}{2}\sqrt{\left(\frac{4V_c}{\pi L_f{}^2 h}\right)^2 + 4} \tag{3.7}$$

$$V_c = \frac{\rho_w C_w W_i}{\rho_{gr} C_{gr}(1-\phi) + \rho_w C_w \phi(1-S_{or}) + \rho_o C_o \phi S_{or}} \tag{3.8}$$

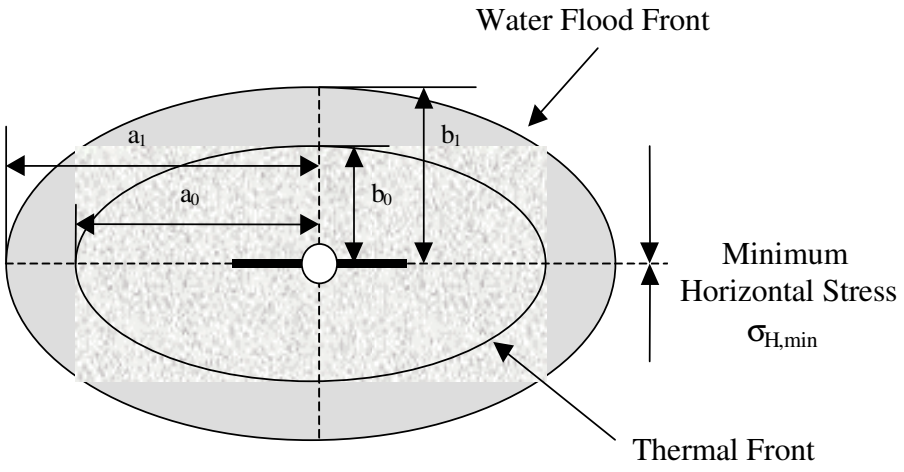

Figure 3-1 – Thermal front with elliptical geometry in the presence of a two-wing fracture (The University of Texas, 2009)

Particle Plugging

The ability to model plugging due to suspended particles in the injected water is included in UTWID. This process can have a large impact on the economic feasibility of a waterflooding operation; however, for the hydraulic fracturing case considered here, particle plugging is less significant. The particles are distributed to two areas: an internal filter cake and an external filter cake. Initially, the particles invade the formation from the fracture, reducing the porosity and permeability of the formation in the vicinity of the

fracture. The invaded area is known as the internal filter cake. After a period of time known as the transition time, particles are no longer able to invade the formation and begin to form an external filter cake at the fracture face.

The equations for the internal filter cake are derived below. The general mass conservation for the particles is given in (3.9).

$$\nabla.(uc - D\nabla c) + \frac{\partial}{\partial t}(\varphi c + \sigma_{sd}) = 0 \qquad \textbf{(3.9)}$$

where u is the Darcy velocity, c is the concentration of the suspended particles, D is the dispersion coefficient, φ is the porosity and σ_{sd} is the specific deposit (volume of deposited particles per unit bulk volume). The equation can be simplified by assuming incompressible flow and negligible dispersion to arrive at (3.10).

$$u.\nabla c + \frac{\partial}{\partial t}(\varphi c + \sigma_{sd}) = 0 \qquad \textbf{(3.10)}$$

Assuming that particle plugging is the only mechanism changing the porosity,

$$\frac{\partial}{\partial t}\varphi = -\frac{\partial \sigma_{sd}}{\partial t} \qquad \textbf{(3.11)}$$

The rate of deposition is assumed to be proportional to the particle concentration and the Darcy velocity, so that

$$\frac{\partial \sigma_{sd}}{\partial t} = \lambda uc \qquad \textbf{(3.12)}$$

where λ is the filtration coefficient. With these assumptions, Equation (**3.10**) simplifies to

$$u.\frac{\partial c}{\partial x_f} + \varphi \frac{\partial}{\partial t} c + \lambda u c = 0 \qquad \textbf{(3.13)}$$

The above equation can be solved by assuming that λ is constant and equal to λ_0, that the injection velocity and porosity are independent of time, and that the initial and boundary conditions are

$$c(x_f, 0) = 0 \qquad \textbf{(3.14)}$$

$$c(0, t) = c_{in} \qquad \textbf{(3.15)}$$

The solution for (3.13) is then

$$c(x_f, t) = 0 \qquad \text{for } t < \frac{\varphi x_f}{u} \qquad \textbf{(3.16)}$$

$$c(x_f, t) = c_{in} \exp(-\lambda_o x_f) \qquad \text{for } t > \frac{\varphi x_f}{u} \qquad \textbf{(3.17)}$$

Using these results, the solution for Equation (**3.12**) is

$$\sigma_{sd}(x_f, \theta) = \lambda_0 u \theta c_{in} \exp(-\lambda_o x_f) \qquad \text{for } \theta > 0 \qquad \textbf{(3.18)}$$

$$\sigma_{sd}(x_f, \theta) = 0 \qquad \text{for } \theta \le 0 \qquad \textbf{(3.19)}$$

where θ is the corrected time and defined as

$$\theta(x_f) = t - \int_0^x \frac{dx_f'}{u(x_f')/\varphi(x_f')} \tag{3.20}$$

For large values of *t,* the decrease in porosity due to the internal filter cake can be expressed as

$$\varphi(x_f, t) = \varphi_0 - \sigma_{sd}(x_f, t) \tag{3.21}$$

The degradation of permeability due to the internal filter cake is related to the decrease in porosity. (3.22) calculates the drop in permeability due to three factors: reduced porosity (k_{dp}), increased surface area (k_{ds}), and increased tortuosity (k_{dt}).

$$k/k_o = k_{dp}k_{ds}k_{dt} \tag{3.22}$$

$$k_{dp} = \frac{\phi^3(1-\phi_0)^2}{\phi_0^3(1-\phi)^2} \tag{3.23}$$

$$k_{ds} = \left(\frac{1+\sigma_{sd}/(1-\phi_0)}{1+(d_g/d_p)\sigma_{sd}/(1-\phi_0)}\right)^2 \tag{3.24}$$

$$k_{dt} = \frac{1}{1+\beta\sigma_{sd}} \tag{3.25}$$

d_g and d_p are the grain and particle size, respectively. The default value for the damage factor, β, is 0. Darcy's law is then used to calculate the pressure drop due to the internal filter cake using the calculated permeability for the internal filter cake. After a period of time, no more particles are able to invade the formation and buildup of the internal filter cake ends. At this point, the particles begin to form an external filter cake on the wall of

the fracture face. The time at which this occurs is known as the transition time (t^*), which occurs when the formation face reaches a critical porosity (φ^*). Experimental data on the transition time is not available, so an estimate of the critical porosity (3.26) is used to calculate the transition time.

$$\phi^* = \phi_{formation} \times \phi_{cake} \tag{3.26}$$

$$t^* = \frac{1}{buc\lambda_0} \ln[b(\phi_0 - \phi^*)] \qquad \text{for } b \neq 0 \tag{3.27}$$

$$t^* = \frac{\phi_0 - \phi^*}{uc\lambda_0} \qquad \text{for } b = 0 \tag{3.28}$$

The pressure drop due to this external filter cake is then calculated using Darcy's Law and a filter cake permeability given by the user.

Flow Resistance / Pressure Drop Calculations

To calculate both the volume of fluid going into each pre-existing fracture and the propagation of the fracture, it is necessary to compute the flow resistance from the wellbore to the reservoir boundary for each fracture that is exposed to the injected refracturing fluids. The injected fluid can then be allocated to the fractures in accordance with the resistances by relating the system to a parallel circuit.

In the unmodified version of UTWID, the pressure drops are related by the following equation:

$$P_{wf} = P_r + \Delta P_1 + \Delta P_2 + \Delta P_3 + \Delta P_4 + \Delta P_s + \Delta P_f + \Delta P_p \quad \textbf{(3.29)}$$

where P_{wf} is the bottom hole pressure at the fracture; P_r is the pressure at the reservoir boundary; ΔP1, ΔP2, ΔP3, and ΔP4 are the pressure drops across different regions of the reservoir, ΔP_s is the additional pressure drop due to particle plugging as well as any initial damage, ΔP_f is the pressure drop along the fracture from the wellbore to the tip of the fracture, and ΔP_p is the pressure drop across the perforations. The pressure at the fracture tip is then calculated as

$$P_{tip} = P_i - \Delta P_f - \Delta P_p = P_r + \Delta P_1 + \Delta P_2 + \Delta P_3 + \Delta P_4 + \Delta P_s \quad \textbf{(3.30)}$$

As discussed in the thermoelastic stresses section, the flow geometry around a two-winged vertical fracture is elliptical. For typical waterflood applications, flow is steady state and four regions develop (Figure 3-2): the region ahead of the flood front where oil is the mobile phase, the region behind the flood front where the formation may have displaced connate water at original temperature, the region behind the connate water front with injected fluid at reservoir temperature and the region with the injected fluid at injected fluid temperature. These regions are elliptical and confocal with the fracture. The pressure drops are calculated as follows:

For the region between the drainage boundary and the waterflood front:

$$\Delta P_1 = \frac{q\mu_o}{2\pi k k_{ro} h_{for}} \ln\left(\frac{2r_e}{a_2 + b_2}\right) \quad \textbf{(3.31)}$$

For the region between the connate water front and the injected fluid front:

$$\Delta P_2 = \frac{q\mu_{wr}}{2\pi k k_{rw} h_{for}} \ln\left(\frac{a_2 + b_2}{a_1 + b_1}\right) \tag{3.32}$$

For the region between the injected fluid front and the thermal front:

$$\Delta P_3 = \frac{q\mu_{wi}}{2\pi k k_{rw} h_{for}} \ln\left(\frac{a_1 + b_1}{a_0 + b_0}\right) \tag{3.33}$$

For the region between the thermal front and the fracture, assuming water is the injected fluid:

$$\Delta P_4 = \frac{q\mu_{wi}}{2\pi k k_{rw} h_{for}} \ln\left(\frac{a_o + b_o}{L_f}\right) \tag{3.34}$$

where a and b are the lengths of the major and minor axes, respectively.

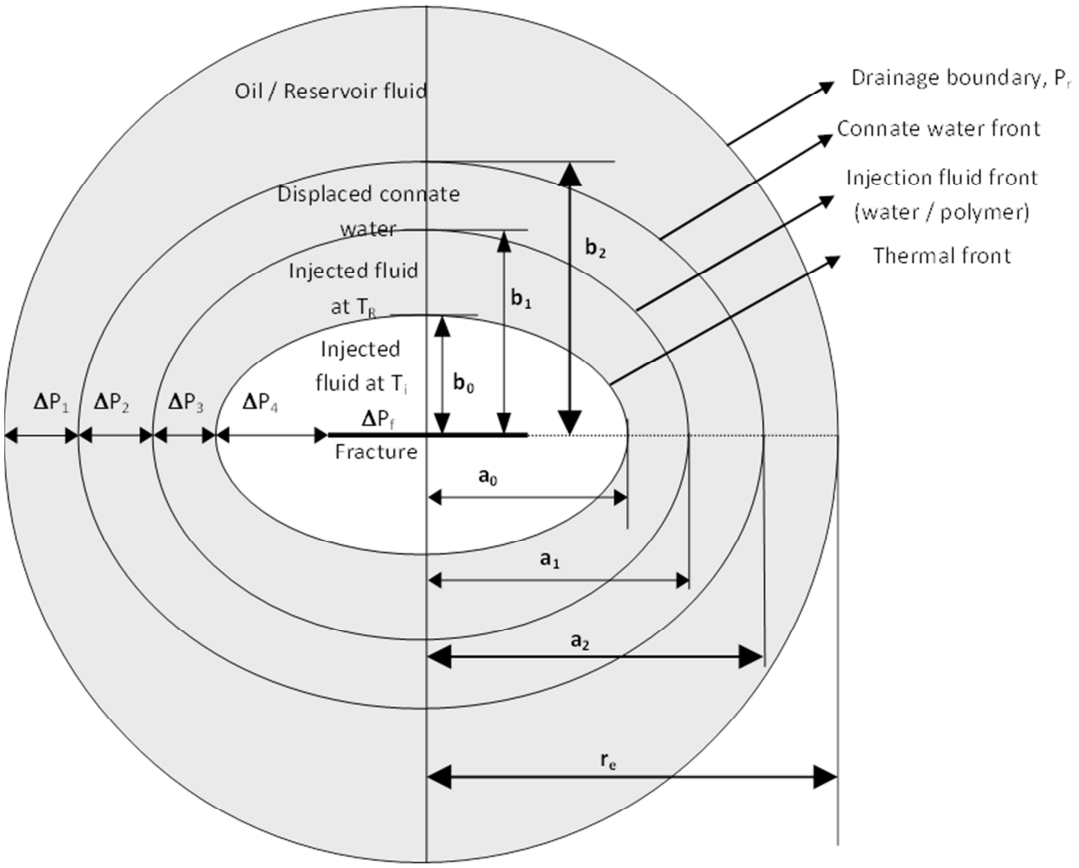

Figure 3-2 – Map view of the fluid fronts due to elliptical flow geometry (The University of Texas, 2009)

In the refracturing operations described in this work, fluid flow occurs primarily under transient flow conditions, so instead of calculating the pressure drops across the four different regions, early time pressures are estimated using a transient model described by Gringarten (1972). The implementation of this model into UTWID is detailed by Suri and Sharma (2010), and a summary is provided here. Equations (**3.35)** through (**3.39)** describe the behavior of the transient flow condition and allow for the calculation of P_{tip} (note that these equations are derived for oil field units).

$$P_{wf}(t_{Dxf}) = P_R + \left(\frac{141.2q(\mu/k)_{eff}}{h} \right) P_D(t_{Dxf}) \tag{3.35}$$

where

$$P_D(t_{Dxf}) = \frac{1}{2}\sqrt{\pi t_{Dxf}} \left[erf\left(\frac{0.134}{\sqrt{t_{Dxf}}} \right) + erf\left(\frac{0.866}{\sqrt{t_{Dxf}}} \right) \right] + 0.067E_1\left(\frac{0.018}{t_{Dxf}} \right) + 0.433E_1\left(\frac{0.750}{t_{Dxf}} \right) \tag{3.36}$$

and

$$t_{Dxf} = \frac{0.0002637t}{\phi(\mu/k)_{eff}(c_t)_{eff}\, {x_f}^2} \tag{3.37}$$

The effective mobility and compressibility is approximated as follows:

$$\left[\frac{\mu}{k} \right]_{eff} = \frac{\frac{(\mu_w)_{T_w}}{kk_{rw}} \ln\left[\frac{(a_c + b_c)}{x_f} \right] + \frac{(\mu_w)_{T_R}}{kk_{rw}} \ln\left[\frac{(a_w + b_w)}{(a_c + b_c)} \right] + \frac{(\mu_o)_{T_R}}{kk_{ro}} \ln\left[\frac{2r_e}{(a_w + b_w)} \right]}{\ln(2r_e / x_f)} \tag{3.38}$$

The mobilities of the different zones are captured in the numerator of the above equation

$$(c_t)_{eff} = \frac{c_{tcool}(a_c b_c) + c_{tcw}(a_w b_w - a_c b_c) + c_{ti}({r_e}^2 - a_w b_w)}{{r_e}^2} \tag{3.39}$$

The effective c_t for the reservoir is calculated using the volume of the different regions where S_w and S_o are a function of time,

$$c_{tcool} = c_f(T_{wi}) + (1 - S_{or})c_w(T_{wi}) + S_{or}c_o(T_{wi}) \tag{3.40}$$

$$c_{tcw} = c_f(T_R) + (1 - S_{or})c_w(T_R) + S_{or}c_o(T_R) \quad \textbf{(3.41)}$$

$$c_{ti} = c_f(T_R) + S_{wi}c_w(T_R) + (1 - S_{wi})c_o(T_R) \quad \textbf{(3.42)}$$

The above equations rely on the definition of total compressibility for a single phase flow in a two phase system:

$$c_t = c_f + S_w c_w + S_o c_o \quad \textbf{(3.43)}$$

The P_D solutions defined above are for an infinite acting reservoir. However, the constant pressure drainage boundary will be somewhere between the injector and the end of the reservoir and is assumed to be the midpoint distance. The infinite acting solution for P_D is used until it becomes equal to the steady state P_{DSS}. After this time, the steady state solution is used. The exact solution for a finite reservoir will be slightly different when approaching P_{DSS}, and the approximate solution to the pressure transients is given below:

$$P_{DB} = \min[P_D, P_{DSS}] \quad \textbf{(3.44)}$$

$$P_{DSS} = \frac{2\pi h}{q(\frac{\mu}{k})_{eff}}\Delta P_{SS} \quad \textbf{(3.45)}$$

where ΔP_{SS} is the sum of the four pressure drops described above (i.e., ΔP1, ΔP2, ΔP3 and ΔP4). Then, the transient pressure drop can be calculated using

$$\Delta P_{trans} = \frac{\left(\frac{\mu}{k}\right)_{eff}}{2\pi h}[q_1 P_{DB}(t_D) + (q_2 - q_1)P_{DB}([t - t_1]_D) + \cdots \\ \ldots + (q_N - q_{N-1})P_{DB}([t - t_{N-1}]_D)] \quad \textbf{(3.46)}$$

where q_N and t_N are the injection rate and time for the N^{th} stage. P_{tip} can be calculated using

$$P_{tip} = P_r + \Delta P_{trans} + \Delta P_s \quad \textbf{(3.47)}$$

The two remaining pressure drops to be calculated are caused by flow through the fracture and through the perforations. The reduced flow area through the perforations restricts flow, and the pressure drop is calculated as follows (Perkins and Gonzales, 1985):

$$\Delta P_p = 0.8338 \rho v_p^{\ 2} \quad \textbf{(3.48)}$$

where ρ is the injected fluid density and v_p is the velocity of the injected fluid through the perforations. Realistically, an additional pressure drop is experienced as the fracturing fluid extends from the diameter of the wellbore to the full height of the fracture. However, explicit expressions are not available to predict this pressure drop, and the pressure drop is taken to be negligible by assuming that the height of the fracture is constant and equal to the net pay, even in the near wellbore region.

The pressure drop along the fracture is calculated by modeling the fracture with the PKN model (Nordgren, 1972). Under this model, the height of the fracture is held constant as the length and width changes with time. As derived in Chapter 4 of the

UTWID manual, the flow resistance, fracture width, and pressure drop along the fracture is calculated as follows:

$$R_{fi} = \left[\frac{16}{3\pi} \frac{(2n_p+1)^{n_p} k_p L_f E^{2n_p+1}}{n_p{}^{n_p} 2^{2n_p-1} (1-\nu^2)^{2n_p+1} h_f{}^{3n_p+1}} \right]^{\frac{1}{2n_p+2}} q_f{}^{-\left[\frac{n_p+2}{2n_p+2}\right]} \quad \textbf{(3.49)}$$

$$w_{fi} = \frac{2(1-\upsilon^2)h_f}{E} q_f * R_{fi} \quad \textbf{(3.50)}$$

$$\Delta P_f = \frac{w_{fi} E}{2(1-\upsilon^2)h_f} \quad \textbf{(3.51)}$$

where resistance is defined as

$$R = \frac{\Delta P}{q} \quad \textbf{(3.52)}$$

Under transient conditions, these pressure drops are all related by the equation

$$P_{wf} = P_r + \Delta P_{trans} + \Delta P_s + \Delta P_f + \Delta P_p \quad \textbf{(3.53)}$$

For each time step, the program calculates a new fracture length for each fracture. This is done by guessing a fracture length and then comparing the fracture tip pressure for the guessed length and the fracture propagation pressure. The fracture length is then iterated until the tip pressure equals the fracture propagation pressure. Using the new fracture length, the program then calculates the flow resistance from the bottom of the well to the tip of the fracture. Using the resistance from each fracture (R_i), the fracture flow rates (q_i) for the next time step are then calculated using Equation (**3.54**).

$$q_i = \frac{R_{total}}{R_i} q \tag{3.54}$$

The procedures describe above are used in the currently released version of UTWID. The next section describes the modifications made to implement the use of diverting agents during a refracturing treatment.

MODIFICATIONS TO UTWID TO ACCOMMODATE APPLICATION OF DIVERTING AGENT

Several modifications were made to UTWID to accommodate the modeling of diverting agent plugging. Frictional forces were added to the model, as the asymmetry of friction along the wellbore has an important impact on the distribution of diverting agent. In the model, each fracture is positioned along a horizontal lateral (see Figure 3-3), and as the fluid travels along the lateral to the fractures, there is a frictional pressure drop in the wellbore. Fracturing fluids often incorporate drag reducers, a high molecular weight polymer that significantly reduces friction. As a result, common correlations tend to overestimate this frictional pressure drop in hydraulic fracture operations. A correlation designed to account for the lower friction factor observed under fracturing conditions is described by Valko and Economides (1995) and used in this work. The correlation is defined as follows:

$$\ln(f) = 28.135 + (-29.379 + (8.2405 - 0.86227a)a)a \tag{3.55}$$

where

$$a = \ln(\ln(N_{Re,w})) \tag{3.56}$$

And $N_{Re,w}$, the wall Reynolds number, is defined as

$$N_{Re,w} = \left(\frac{1+3n_p}{4n_p}\right) N_{Re} \tag{3.57}$$

The generalized Reynolds number, N_{Re}, is

$$N_{Re} = \frac{8^{1-n_p} v^{2-n_p} \rho {D_w}^{n_p}}{k_p} \tag{3.58}$$

The pressure drop due to friction is then calculated using the equation

$$\Delta P = \frac{2x_w f \rho v^2}{D_w} \tag{3.59}$$

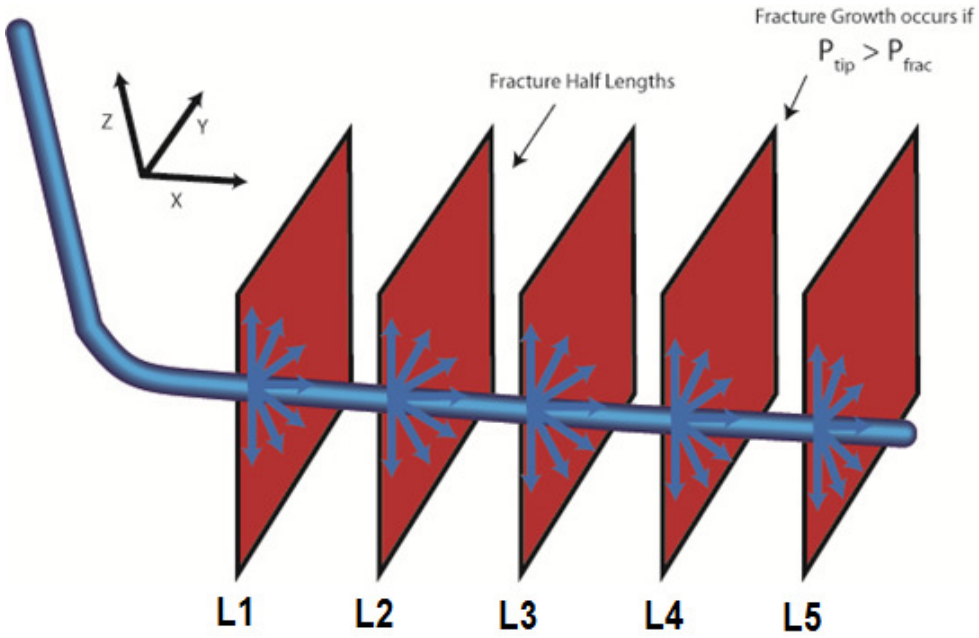

Figure 3-3 – Diagram of five fractures along a wellbore. The cumulative amount of friction exerted on a fluid particle increases as it moves away from the heel.

The deposition of diverting agent to the fractures is calculated from fracture flow rates. The volume of the diverting agent injected into the wellbore is user defined as a volume fraction or concentration in the fracturing fluid. Consequently, the distribution of diverting agent between the many open fractures is the same as the ratio of flow rates between the fractures. That is, if one fracture is receiving twice as much injected fluid as another, it will also receive twice as much diverting agent.

UTWID includes the ability to pump in multiple stages, and an added identifier marks stages in which diverting agent is pumped. The user can vary the number of diverting agent stages as well as the length of each stage. A typical pumping schedule used in the field and in the simulations is presented in Table 3-1.

Table 3-1 – A typical pumping schedule used in simulations

0 to 30 minutes	Stage 1: Pad Stage begins refrac treatment
30 minutes to 144 minutes	Stage 2: Proppant is pumped
144 minutes to 158 minutes	Stage 3: Diverting agent is pumped
158 minutes to 165 minutes	Stage 4: Pad stage is pumped
165 minutes to 360 minutes	Stage 5: Proppant is pumped

Two separate models for diverting agent plugging are included. The first models the diverting agent plug to form in the perforation tunnel, and the second models the agent to plug inside the fracture itself. Once the volume of diverting agent pumped into a

given fracture is known, the pressure drop is calculated based on the geometry of the plug (determined by the model selected) and Darcy's law (Equation (**3.60**)).

$$\Delta P = \frac{q\mu}{k_{DA}} \frac{h_c}{A} \tag{3.60}$$

where h_c is the thickness of the diverting agent cake.

Diverting Agent Plugging in the Perforation Tunnel

In this model, the diverting agent is assumed to plug in the perforation tunnel, beginning at the face of the fracture (see Figure 3-4). In so doing, all of the fluid that flows into a fracture must flow through the diverting agent once the plug is set. In the model, the pumped diverting agent is distributed equally between all of the perforations that feed into a particular fracture. This is assumed to be the total perforated interval (the perforation density and interval is defined by the user). The thickness of the diverting agent cake is then calculated from the geometry of the perforations inputted by the user. Darcy's law is used to find the pressure drop due to the plug in a particular perforation. The total pressure drop through the diverting agent in all of the perforations that feed a particular fracture is calculated by modeling the perforations as resistors in a parallel configuration. From the definition of resistance given in Equation (**3.52**), the diverting agent filter cake resistance is:

$$\mathrm{R} = \frac{\Delta P}{q} = \frac{\mu}{k_{DA}} \frac{h_c}{A} \tag{3.61}$$

Then the total resistance of the system is calculated from the equation of resistors in parallel:

$$R_{total} = \frac{R}{N} \tag{3.62}$$

Once the total resistance is found, the pressure drop is calculated as the product of the flow resistance and the flow rate in the fracture. This pressure drop is then added to the other pressure drops in order to calculate the overall resistance from the bottom of the wellbore to the tip of the fracture. This resistance in turn controls the flow rate into the fracture during the next time step, which will then affect further fracture propagation.

Since preferentially growing fractures will have a higher flow rate, they will also take a larger share of the pumped diverting agent. The faster growing fractures will then have a higher pressure drop due to the diverting agent, so flow will be redirected toward the slower growing fractures. Since the plug is assumed to form in the perforation tunnel, it remains in place as the fracture propagates (the plug remains only for the duration of the treatment; this form of diverting agent is still designed to break down with time and heat to allow for unhindered production). A problem with this assumption is that it does not allow for flow of proppant past the diverting agent. Future work may address this problem by modeling a mechanism that allows for only a fraction of the perforations to be plugged, or by modeling new channels in which the proppant can flow to the fracture. One important characteristic response caused by leaving the plug in the perforation is the equalization of flow and, as a result in most cases, the equalization of fracture lengths. The timing of diverting agent application, permeability of the agent cake, and amount of agent pumped all determine this response. Chapter 6 offers more detail about this behavior.

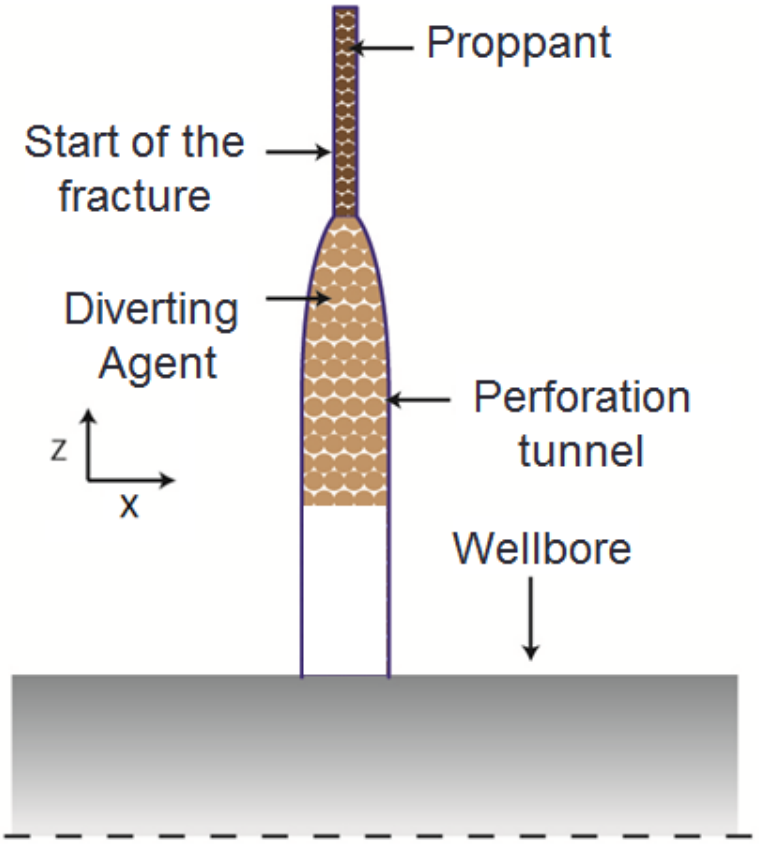

Figure 3-4 – Diagram of diverting agent plugging for one of the two models used. In this model, the agent is assumed to plug in the perforation tunnel, beginning at the face of the fracture and proppant.

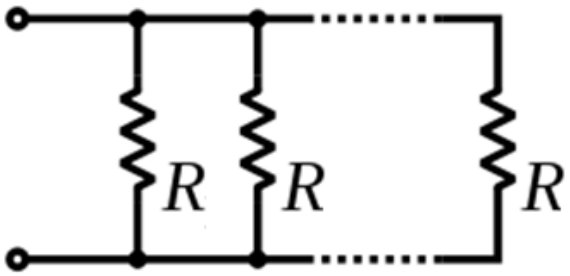

Figure 3-5 – Resistors configured in a parallel configuration. The total resistance due to diverting agent is calculated by combining the resistance from each perforation into a system of parallel resistors.

Diverting Agent Plugging in the Fracture

In this model the diverting agent is assumed to form a plug in the fracture. As discussed earlier, the fracture height is assumed to be the full height of the pay zone, even at the wellbore. In addition, the PKN model is used to determine fracture geometry and propagation. Once the volume of diverting agent pumped to a given fracture is known, the thickness of the diverting agent cake is calculated. This calculation is more involved than the one conducted in the first model because the geometry of the fracture is more complex than that of the perforation tunnel. Figure 3-6 and Figure 3-7 illustrate the diverting agent and proppant in the fracture. The process of plug formation (known as bridging) is not modeled in this work. Instead it is assumed that sufficient diverting agent is pumped for a given flow rate and fracture width to bridge over the fracture. Bridging is defined as the process of a material to collect in a specific location and restrict flow in a slot that is larger than the particle size of the material. Bridge formation conditions are highly dependent on the specific product of diverting agent used, as well as the flow rate of the injected fluid and the width of the fracture.

The thickness of the diverting agent cake can be calculated using the condition that the volume it takes up in the fracture is equal to the volume pumped in the fracture (the volume of diverting agent pumped in the fracture is known). This condition is shown in the below equation:

$$V_{DA} = 2\int_0^{h_c} A(x_f)dx_f \tag{3.63}$$

where h_c is the thickness of the diverting agent cake, and the multiple of two is used to account for both wings of the fracture. A(x) is the cross-sectional area of the fracture at a particular time and is defined by Nordgren (1972) as

$$A(x_f) = \int_{-\frac{h_f}{2}}^{\frac{h_f}{2}} w_{fi}(x_f, z)dz = \frac{\pi}{4} W_{fi}(x_f)h_f \tag{3.64}$$

where h_f is the height of the fracture, z is the vertical axis of the fracture, and z = 0 represents the middle of the fracture. Lowercase w_{fi} is the width of the fracture and varies along both the horizontal and vertical axes. Uppercase W_{fi} is the maximum width of the fracture at a given cross section and is defined as w(x,z=0). An approximate solution for $W_{fi}(x)$ is taken from Nordgren (1972) and is derived from Perkins and Kern (1961) assuming a Newtonian fluid. It neglects fluid-loss and rate of fracture volume change in the continuity equation:

$$W_{fi}(x) = 4\left[\frac{(1-\nu)\mu q_f L_f}{\pi G}\left(1 - \frac{x_f}{L_f}\right)\right]^{1/4} \tag{3.65}$$

Using

$$G = \frac{E}{2(1+\nu)} \tag{3.66}$$

Equation (**3.65**) becomes

$$W_{fi}(x) = 8\left[\frac{(1-\nu^2)\mu q_f L_f}{\pi E}\left(1 - \frac{x_f}{L_f}\right)\right]^{1/4} \tag{3.67}$$

The solution for Equation (**3.63**) using Equation (**3.64**) and Equation **(3.67)** is

$$V_{DA} = 4.48993 h_f \left((h_c - L) \left(\frac{\mu(\nu^2 - 1) q_f (h_c - L)}{E} \right)^{1/4} + \left(\frac{-L\mu(\nu^2 - 1) q_f}{E} \right)^{1/4} L \right) \quad \textbf{(3.68)}$$

For a given time step, Equation (**3.68**) can be solved for h_c – the thickness of the diverting agent filter cake. Next, the pressure drop caused by the diverting agent cake is calculated by adding an expression for a changing cross sectional area to the equation for the pressure drop of a filter cake (The University of Texas, 2009).

$$\Delta P = \frac{q\mu}{k_{DA}} \int_0^{h_c} \frac{dx_f}{A(x_f)} \quad \textbf{(3.69)}$$

Using Equation (**3.64**), the solution for Equation (**3.69**) is

$$\Delta P_{DA} = \frac{.475137 q_f \mu}{h_f k_{DA} \left(\frac{q_f \mu (1 - \nu^2)}{E} \right)^{1/4}} \left(L^{3/4} - (L - h_c)^{3/4} \right) \quad \textbf{(3.70)}$$

The calculated pressure drop due to the diverting agent is then added to the other pressure drops in order to calculate the total resistance from the bottom of the wellbore to the fracture tip. This resistance is then used to calculate the flow rate to the fracture for the next time step.

This model includes a mechanism for plug disassociation in order to allow for the subsequent pumping of proppant, which is unable to flow past the diverting agent. Disassociation of the bridge is assumed to occur if, after the bridge is set and during

pumping of a pad stage, the width of the fracture at the bridge increases. Since the pad stage contains no proppant, it is able to flow past the diverting agent and propagate the fracture, subject to the pressure drop created by the diverting agent. If a bridge dissociates, no pressure drop is attributed to diverting agent in that fracture. If a proppant stage begins and a plug still exists in a fracture, then the program does not allow flow in that fracture, because the proppant in the slurry prevents it from flowing past the diverting agent. The half-length and width is held fixed at the values from before the pumping of the proppant.

As a result of these conditions, the timing of the diverting agent stage and subsequent pad stage is important to the resulting behavior. In general, the expected behavior is that the fastest growing fractures, which receive more diverting agent, will maintain diverting agent plugs after the pad stage. Their growth will then be cutoff, and the remaining fractures will grow much faster because the entire injected flow rate will be split among fewer fractures. The result is that this model allows for a specific set of fractures to receive all of the subsequent treatment after fluid diversion. The ideal situation for this occurrence is when there is a large disparity between fracture growth rates. In such a case, the operator may prefer the vast majority of a refrac treatment to target a selection of underperforming fractures. Results from simulations using this model are presented in Chapter 4.

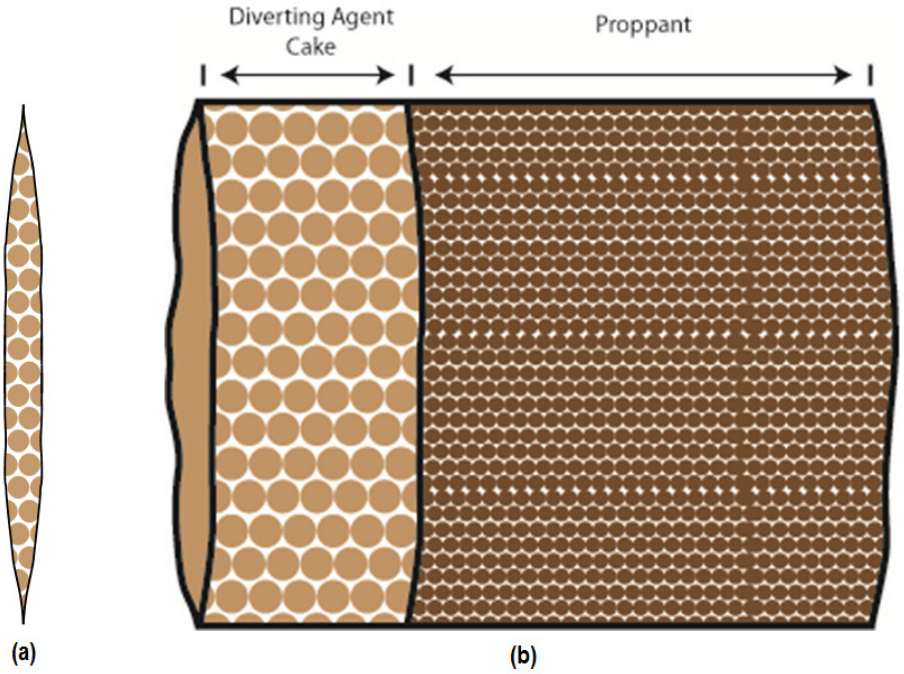

Figure 3-6 – (a) cross sectional view of the fracture with diverting agent inside. (b) Side view of diverting agent cake deposited adjacent to proppant. Note that the diverting agent particles are larger than the proppant

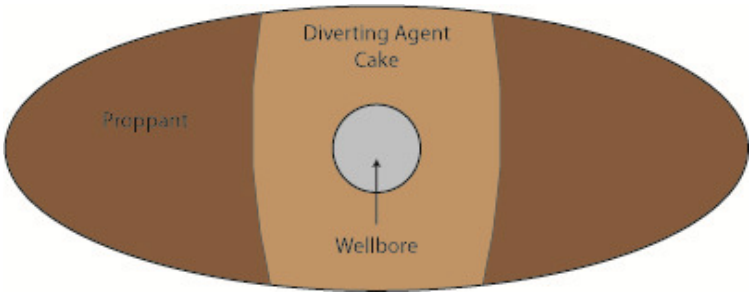

Figure 3-7 – Side view of the fracture including the wellbore. The diverting agent cake surrounds the well.

NOMENCLATURE

A	Area
a_0	Major axis of the thermal front ellipse
a_1	Major axis of the injected fluid ellipse
a_2	Major axis of the connate water ellipse
b_0	Minor axis of the thermal front ellipse
b_1	Minor axis of the injected fluid ellipse
b_2	Minor axis of the connate water ellipse
c	concentration of suspended particles (volume of particles per unit fluid volume)
c_f	Compressibility of the reservoir fluid
C_{gr}	Specific heat of the mineral grains
C_o	Specific heat of oil
c_o	Compressibility of oil
c_t	Total compressibility
c_{tcool}	Compressibility of the region at injected water temperature
c_{tcw}	Compressibility of the connate water front region at reservoir temperature
c_{ti}	Compressibility of the constant pressure boundary region at reservoir temperature
C_w	Specific heat of water
c_w	Compressibility of water
D	Dispersion coefficient
D_w	Diameter of the wellbore
E	Young's modulus
f	Friction factor
G	Shear modulus
h_c	Filter cake width
h_f	Height of the fracture
h_{for}	Formation height
k	Permeability
k_{DA}	Permeability of the diverting agent cake
k_{dp}	Drop in permeability due to reduced porosity
k_{ds}	Drop in permeability due to increased surface area

k_{dt}	Drop in permeability due to increased tortuosity
k_o	Original permeability
k_p	Power law coefficient for the injected fluid at injection temperature
k_{ro}	End point permeability to oil
L_f	Fracture half length
n_p	Power law exponent for the injected fluid at injection temperature
N_{Re}	Reynolds number
$N_{re,w}$	Wall Reynolds number
p	Average pressure in the circular area near the extending ends of the fracture
P_D	Dimensionless pressure
P_{DSS}	Dimensionless pressure, assuming steady state conditions
p_{frac}	Fracture propagation pressure
P_r	Reservoir pressure
P_{tip}	Pressure at the fracture tip
P_{wf}	Bottomhole pressure
ΔP	Pressure drop over a given length
ΔP_1	Pressure drop along the first region from the drainage boundary to the connate water front
ΔP_2	Pressure drop along the second region from the connate water front to the injection fluid front
ΔP_3	Pressure drop along the third region from the injection fluid front to the thermal front
ΔP_4	Pressure drop along the fourth region from the thermal front to the tip of the fracture
ΔP_{DA}	Pressure drop along the diverting agent cake
ΔP_f	Pressure drop along the fracture from the wellbore to the tip of the fracture
ΔP_p	Pressure drop across the perforations
ΔP_s	Pressure drop due to particle plugging as well as any initial damage
ΔP_{SS}	Sum of the four pressure drops assuming steady state conditions
ΔP_{trans}	Pressure drop from the fracture tip to the reservoir during the transient period
q	Flow rate

q_f	Flow rate through the fracture
R	Resistance
r_e	Length from the wellbore to the reservoir boundary
r_f	Radius of the extending end of the fracture
R_{fi}	Resistance of the fracture
s	Earth stress perpendicular to the fracture plane
S_{or}	Residual saturation of oil
S_{wi}	Initial water saturation
T	Temperature
t	Time
t^*	Transition time
t_{Dxf}	Dimensionless time
U	Specific surface energy
u	Darcy velocity
v	Velocity of the injected fluid through the well
V_c	Volume of the cooled zone
V_{DA}	Volume of the diverting agent cake
v_p	Velocity of the injected fluid through the perforations
w_{fi}	Width of the fracture
W_{fi}	Maximum width of the fracture for a given cross section along the length of the fracture
Wi	Total volume of water injected up to time t
x_f	Horizontal distance along the fracture
x_w	Horizontal distance along the wellbore

α	Coefficient of thermal expansion
β	Damage factor
λ	Filtration Coefficient
ν	Poisson's ratio
ϕ	Porosity
ϕ_o	Original porosity
ϕ^*	Critical porosity
ρ	Density of the injected fluid

ρ_{gr}	Density of the mineral grains
ρ_o	Density of oil
ρ_w	Density of water
$\sigma_{H,\ min}$	Minimum horizontal stress
σ_{sd}	Specific Deposity
σ_{1T}	Thermoelastic stresses perpendicular to the major axis of the thermal front ellipse
σ_{2T}	Thermoelastic stresses parallel to the major axis of the thermal front ellipse
θ	Corrected time
μ	Viscosity
μ_0	Viscosity of the oil
μ_{wr}	Viscosity of the water at reservoir temperature
μ_{wi}	Viscosity of the water at the injected water temperature

Chapter 4: Refracture Simulation Results and Discussion for Diverting Agent that Plugs in the Fracture

This chapter discusses the results from simulations of a refracturing treatment with diverting agent that is modeled to plug in the fracture. The simulations are divided into scenarios, which represent fracture systems with particular conditions. Some scenarios contain multiple cases, each of which is a unique system that still adheres to the conditions of the relevant scenario. For instance, each case in Scenario IV begins with the same fracture lengths, but the permeability is varied in each case. The parameters for the baseline case are presented in Table 4-1. Unless otherwise specified, these parameters are used in all of the simulations.

SCENARIO I – BASELINE CASE

Since the other scenarios generally utilize the parameter values used in the baseline case, this scenario serves as a foundation for the subsequent simulations. The most relevant parameters are summarized in Table 4-1.

Table 4-1 – Selection of Input Parameters

Permeability (μD)	100
Porosity	.15
Pore Pressure (psi)	10,000
Fluid Type	oil
Net Pay (ft)	250
Minimum Horizontal Stress (psi)	12,500
Injected Fluid Type	slickwater
Injected Fluid Rate (bpm)	42
Diverting Agent Cake Permeability (D)	1
Volume Fraction of Diverting Agent Stage	.001

In the baseline case, five fractures are modeled along a horizontal wellbore. All the fractures begin with a half-length of 150 ft. This represents the length of the fracture that resulted from the previous treatment. The names L1 through L5 are assigned to each fracture, with L1 being the fracture closest to the heel of the well. The pumping schedule begins in the same manner as does a traditional treatment - a pad stage is followed by a proppant stage. After the proppant stage, the diverting agent is pumped, in this case for about 15 minutes. Next, a pad stage is pumped so that the fluid can break through some of the diverting agent bridges, forcing them to disassociate. The pad stage is able to flow

through the diverting agent bridge, subject to the associated pressure drop. Disassociation of the bridge is assumed to occur if the fracture widens during this stage and will only occur in the fractures containing the smallest amount of diverting agent (only a pad stage can break through the diverting agent; proppant cannot flow through the plugs). The final proppant stage is then pumped and the slurry will only be able to travel in the fractures that no longer contain a diverting agent bridge. Only one diverting stage is pumped in the baseline case, but more stages could be added. Table 4-2 details the pumping schedule.

Table 4-2 – Refrac Pumping Schedule

0 to 30 minutes	Stage 1: Pad Stage begins refrac treatment
30 minutes to 144 minutes	Stage 2: Proppant is pumped
144 minutes to 158 minutes	Stage 3: Diverting agent is pumped
158 minutes to 165 minutes	Stage 4: Pad stage is pumped to open fractures
165 minutes to 360 minutes	Stage 5: Proppant is pumped and only flows to fractures without diverting agent bridges

For comparison purposes, the simulation results of the baseline case without the use of diverting agents are presented first (see Figure 4-1). Since the properties of each fracture are identical, the only difference between them is the position along the wellbore. L1 is closest to the heel and therefore experiences a smaller pressure drop due to friction than the other layers. The discrepancy seen in growth and flow rates is caused only by

friction. As a result of this difference, the L1 and L2 fractures grow preferentially and take a larger share of the fracturing fluid.

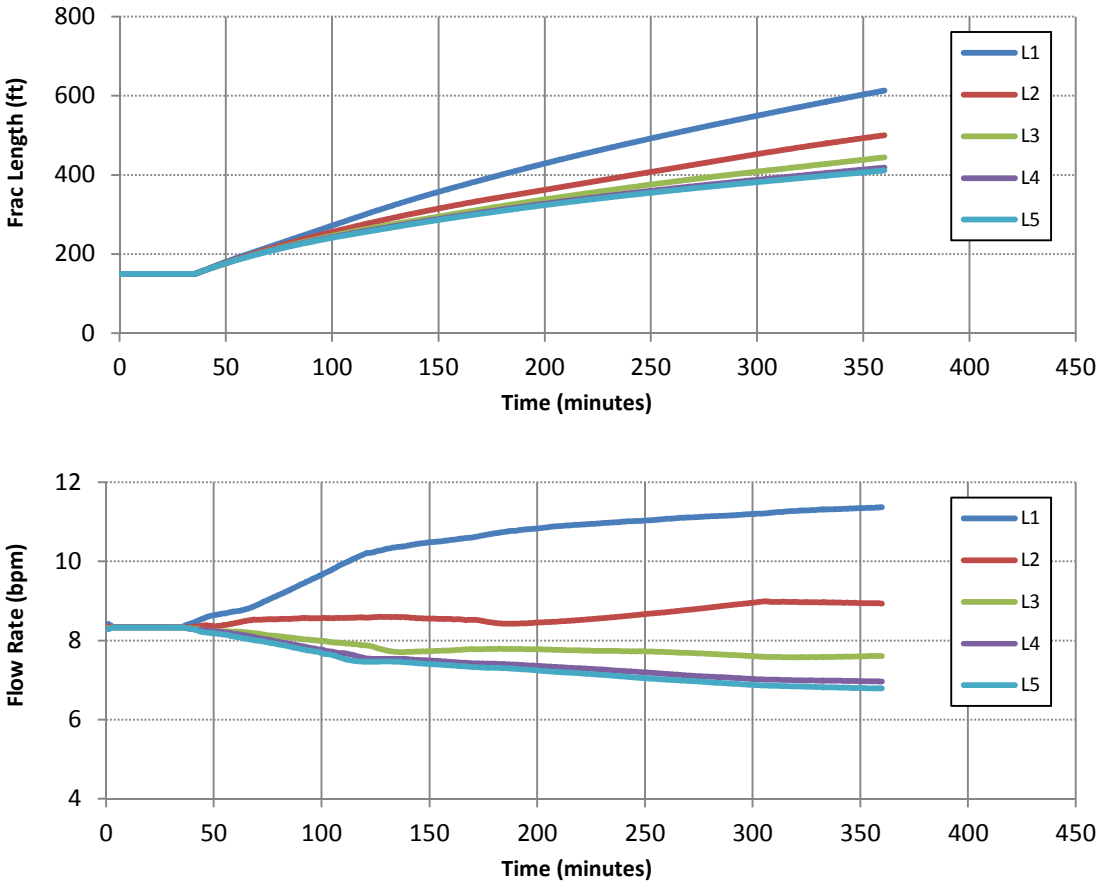

Figure 4-1 – Scenario I: Baseline case without the use of diverting agent. All fractures are identical, except for their positions along the wellbore and consequently their frictional pressure drop. Select properties are given in Table 4-1

Figure 4-2 shows the large effect a diverting stage has on the system. At the beginning of the diverting agent stage (i.e 144 minutes), L1 and L2 fractures have higher flow rates. Since the diverting agent is deposited to each fracture in proportion to the fracture's flow rate, L1 and L2 will therefore take higher amounts of diverting agent and

see higher pressure drops due to the diverting agent. The pressure drop in this case is sufficiently high for the diverting agent bridge to remain in L1 and L2 during pumping of the pad in stage 4. As a result, when proppant is pumped in stage 5, it is unable to pass through the bridge in these fractures. The flow rate drops to zero and the fracture length remains static. As before, the fractures that experience less friction have faster growth rates, so L3 is the fastest growing of the trio of three unplugged fractures and L5 is the slowest growing. The simulation shows that the diverting agent was successfully able to isolate and divert treatment to the fractures that were previously growing less preferentially.

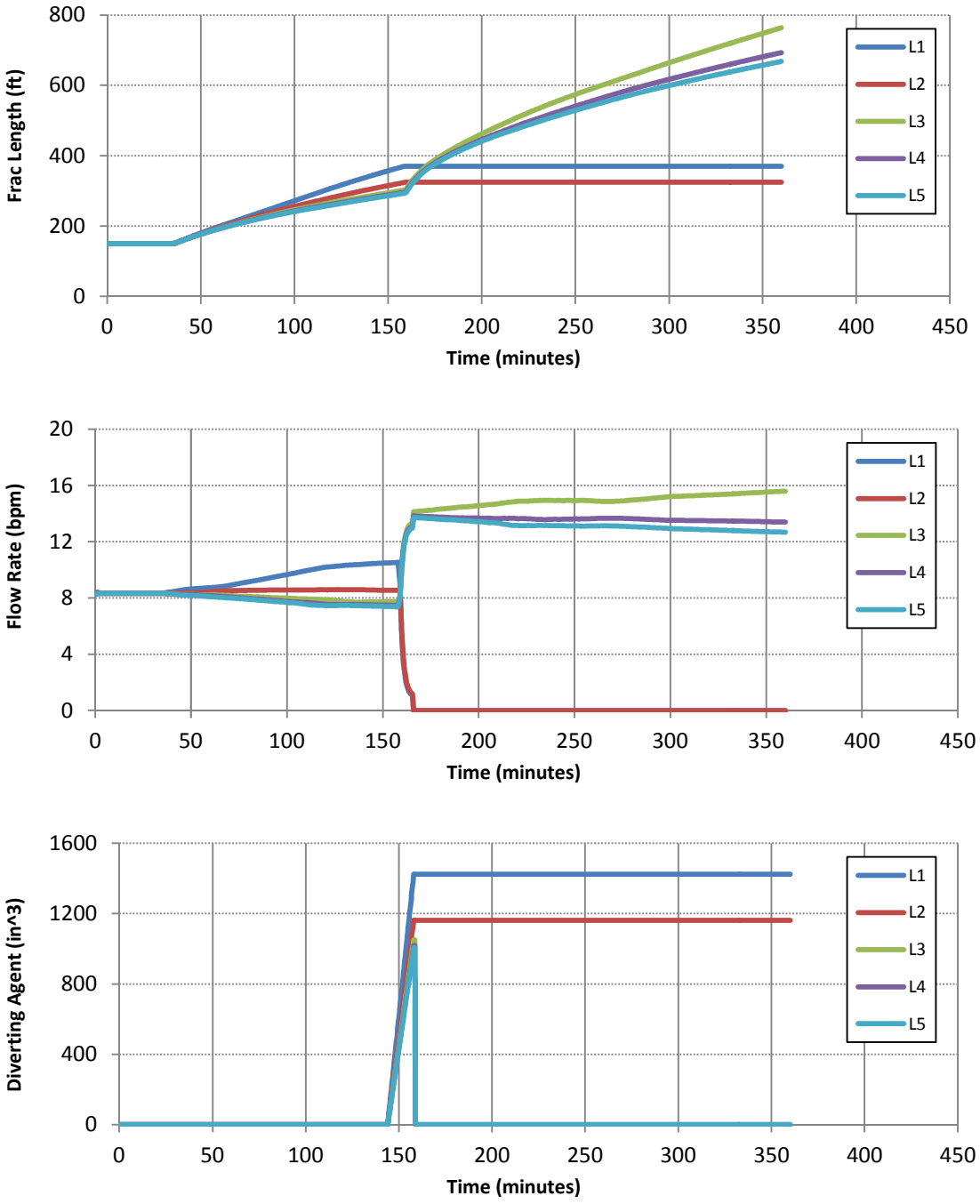

Figure 4-2 – Scenario I: The baseline case with the standard diverting agent stage included. All fractures are identical, except for their positions along the wellbore. The fractures closest to the heel initially grow the fastest due to less friction, but also take more diverting agent and as a result become plugged. Successful diversion is seen.

SCENARIO II – ONE FRACTURE WITH REDUCED LENGTH

Scenario II shows the effect of reducing the half-length of one of the fractures. In scenario II, case A, L1 is reduced from 150 ft. to 50 ft. In scenario II, case B, L4 is reduced from 150 ft. to 50 ft. All other properties are identical to Scenario I. As before, the simulation with no diverting agent (Figure 4-3) is presented first, followed by the one with diverting agent (Figure 4-4) for both Case A and Case B. It is interesting to contrast the two cases when there is no diverting agent present. For Case A, the initially short fracture L1 grows more quickly than the rest due to its reduced level of friction. However, it is important to note that in the flow rate graph, it still shows a lower flow rate for the first half of the treatment. It is able to maintain faster growth rates despite lower flow rates because the shorter fracture length requires less flow for the same amount of fracture growth. Alternatively, in Case B the fracture with reduced length is not able to catch up to the other fractures because it experiences a higher friction force due to its position near the toe.

The fact that L1 in Case A has the lowest flow rate despite having the fastest growth rate becomes very important once the diverting stage is added. Since the diverting agents are deposited to the fractures based on fracture flow rates, fracture L1 will receive the lowest amount of diverting agent. As a result, the pad stage is able to remove the plugging bridge in fracture L1, along with the ones in fractures L4 and L5. The bridges in fractures L2 and L3 hold, and they will not grow once the proppant stage is pumped. The refracturing treatment then successfully targets the fracture with reduced length from the previous treatment along with the other fractures that grow less preferentially (i.e., fractures L4 and L5).

In Case B, the flow rate for the fracture with reduced length is even lower than in Case A, so it too will have treatment fluid diverted to it. The result of this simulation is

very similar to the one for the baseline case – fractures L1 and L2 are plugged, and growth occurs in L3, L4, and L5. The primary difference is that fracture L4 is recovering from a shorter fracture length. While the shorter fracture is never able to catch up to the position it held in the baseline case, its growth rate and flow rate is faster than that of L5. As a result, given more time, it would recover to its position between fracture L3 and L5.

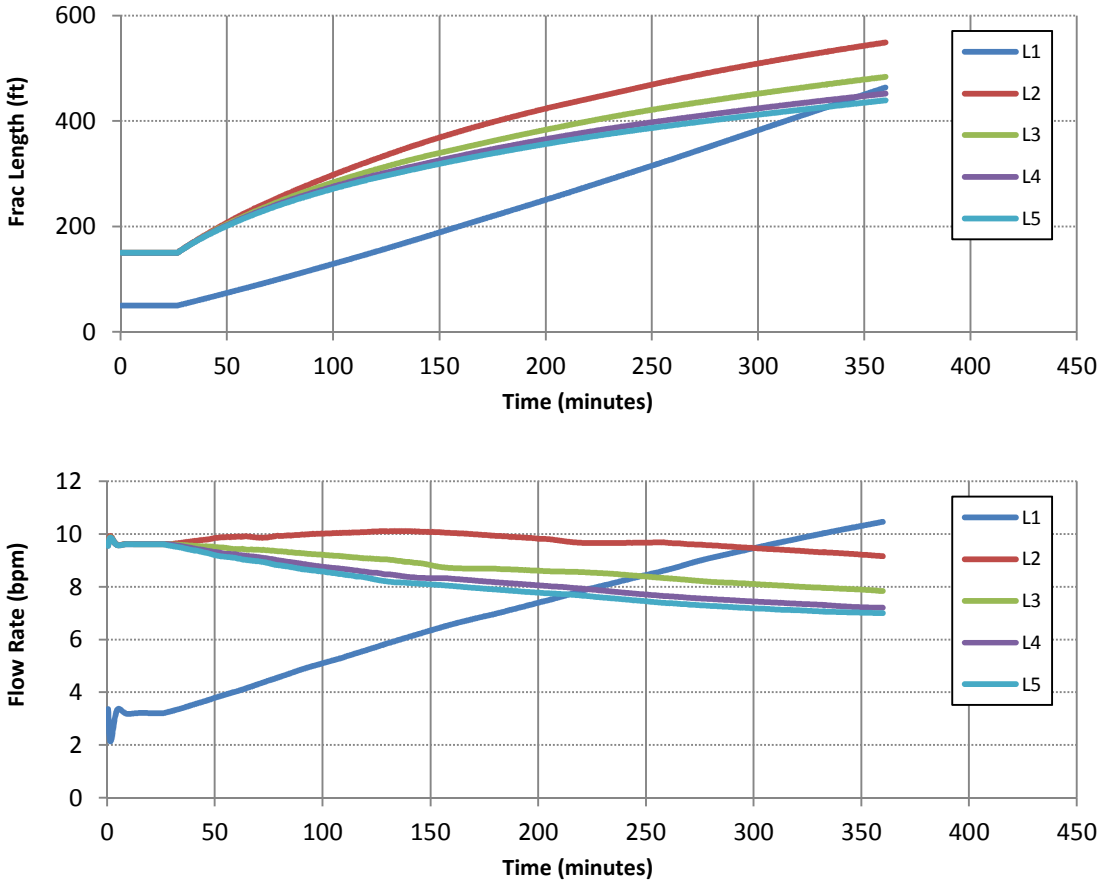

Figure 4-3 – Scenario II, Case A without diverting agent. All fractures are identical except fracture L1 begins the treatment with a shorter fracture length

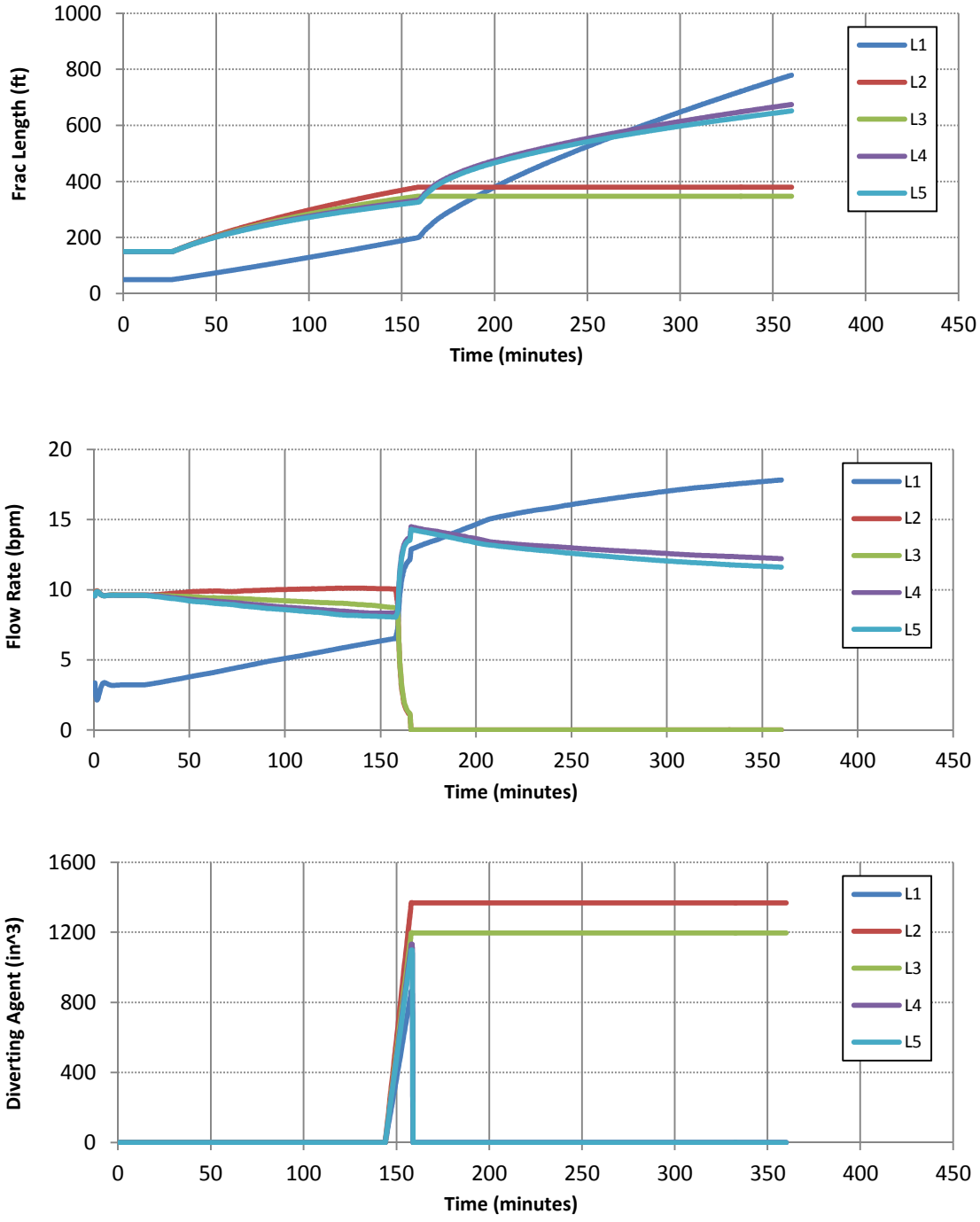

Figure 4-4 – Scenario II, Case A with diverting agent. All fractures are identical except fracture L1 begins the treatment with a shorter fracture length

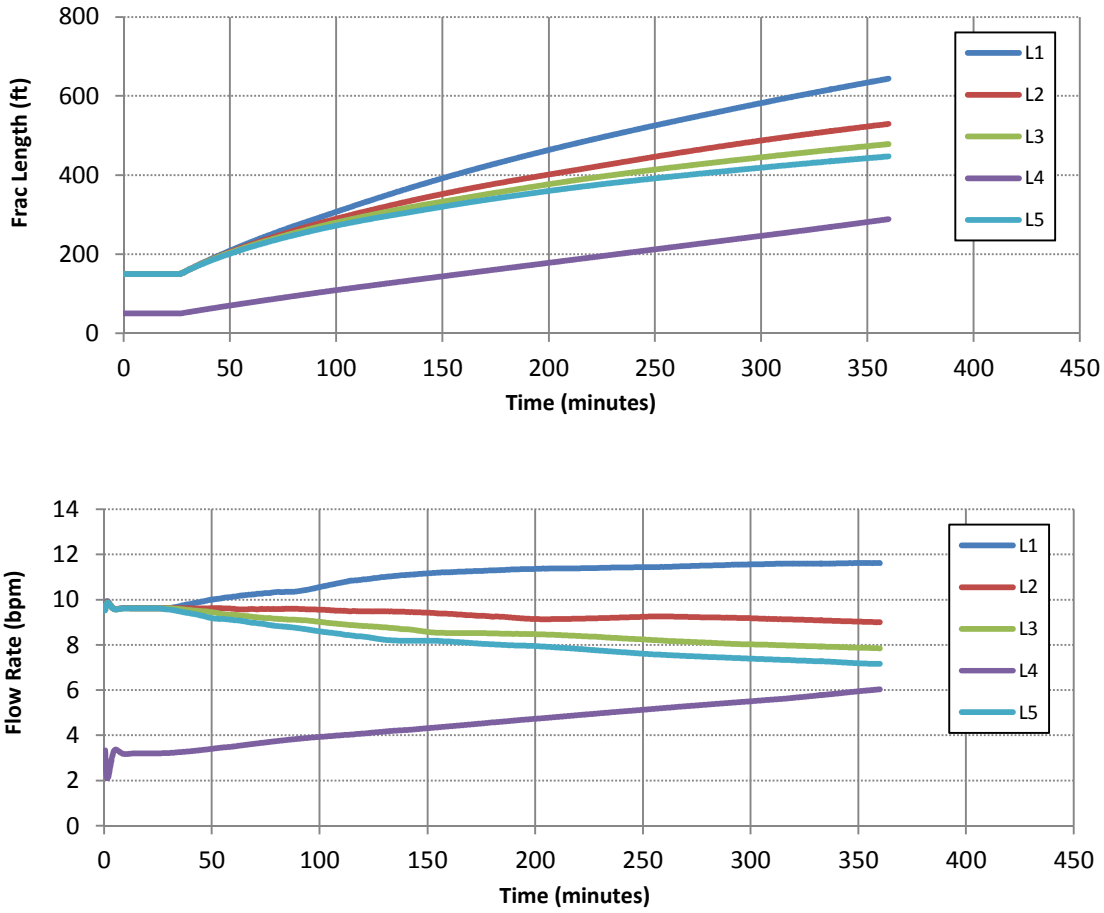

Figure 4-5 – Scenario II, Case B without diverting agent. All of the fractures are identical, except fracture L4 begins the treatment with a shorter fracture length

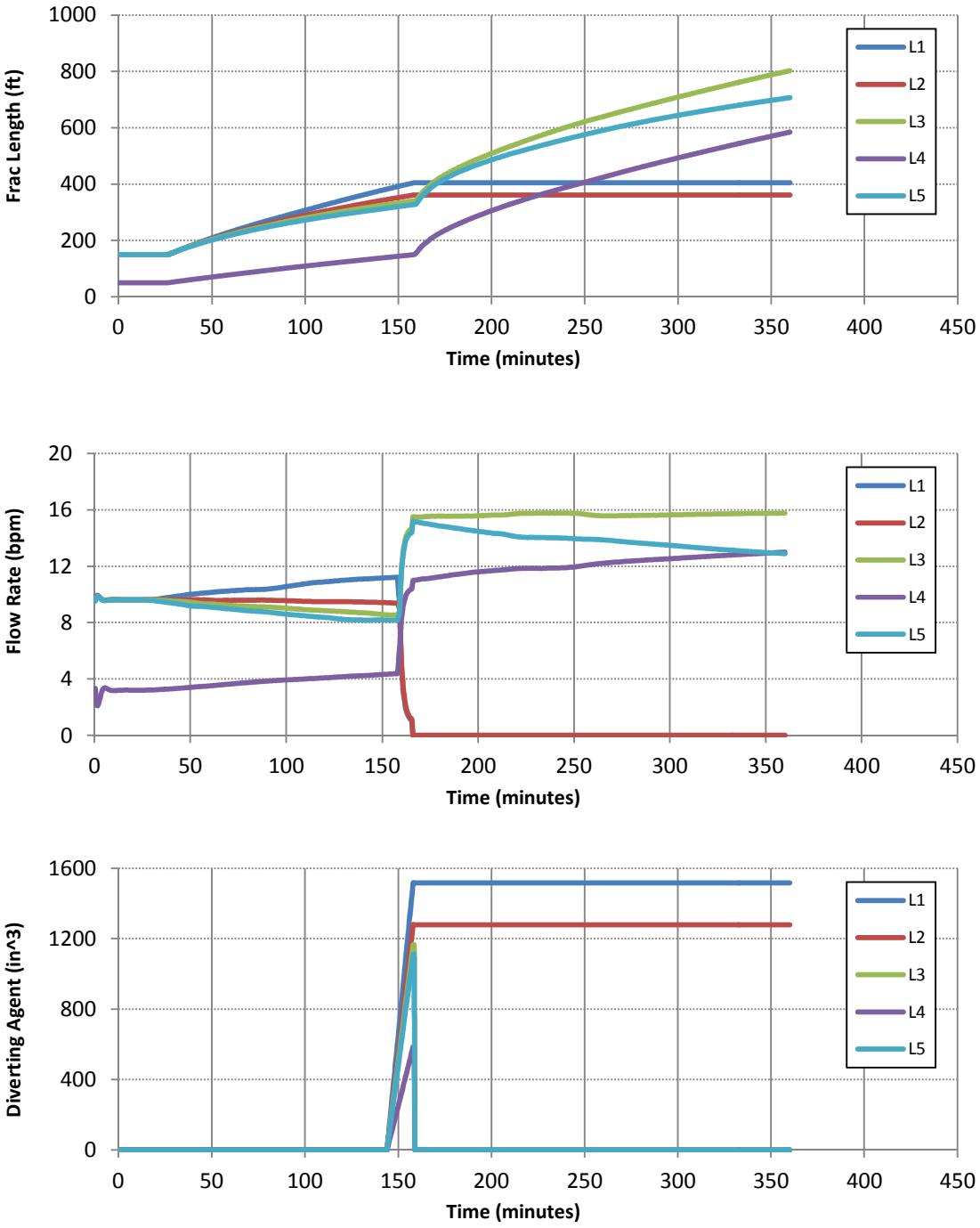

Figure 4-6 – Scenario II, Case B with diverting agent. All fractures are identical, except fracture L4 begins the treatment with a shorter fracture length

SCENARIO III – MIX OF FRAC LENGTHS

Scenario III adds to scenario II by adjusting the half lengths of multiple fractures. Similar principles that were observed in the past scenario underlie the behavior seen here. In cases without diverting agent, the fractures with reduced half lengths are unable to reach the positions they would have attained if they had started at equal lengths. On the other hand, friction forces are still important, and the fractures closer to the heel are growing faster than the remaining fractures at the end of the treatment.

When diverting agent is added, the fractures with the highest flow rates will form a permanent plug. Since the fractures with reduced half lengths have not increased flow rates beyond those of the other fractures, the treatment will be diverted to these smaller fractures, which will then grow preferentially. As in the simple case of Scenario II where only one fracture length was reduced, this simulation shows successful isolation of the smaller fractures. It should be noted that these results indicate that the timing of the diverting stage is important to the subsequent behavior of the system. For instance, if the diverting agent stage in Case B had been applied around the 250 minute mark, then fracture L1 would have been plugged even though its half-length had not yet exceeded that of fracture L2 and L4. This result occurs because the flow rate of fracture L1 exceeds that of L4 after the 250 minute mark (see the flow rate graph of Figure 4-9), meaning L1 will consequently receive a larger amount of diverting agent. As a result, a fracture with a shorter length would be plugged, likely a situation that operators would wish to avoid.

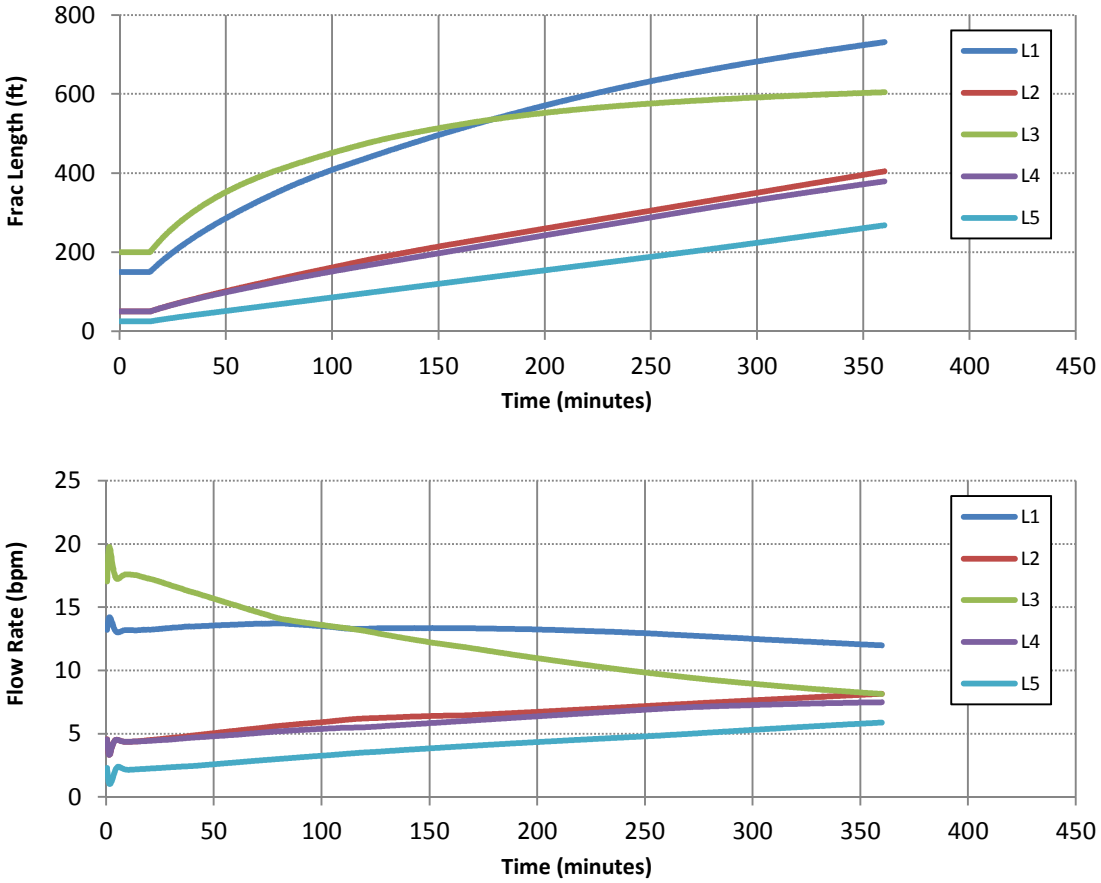

Figure 4-7 – Scenario III, Case A without diverting agent. The fractures begin the treatment with a mix of fracture lengths

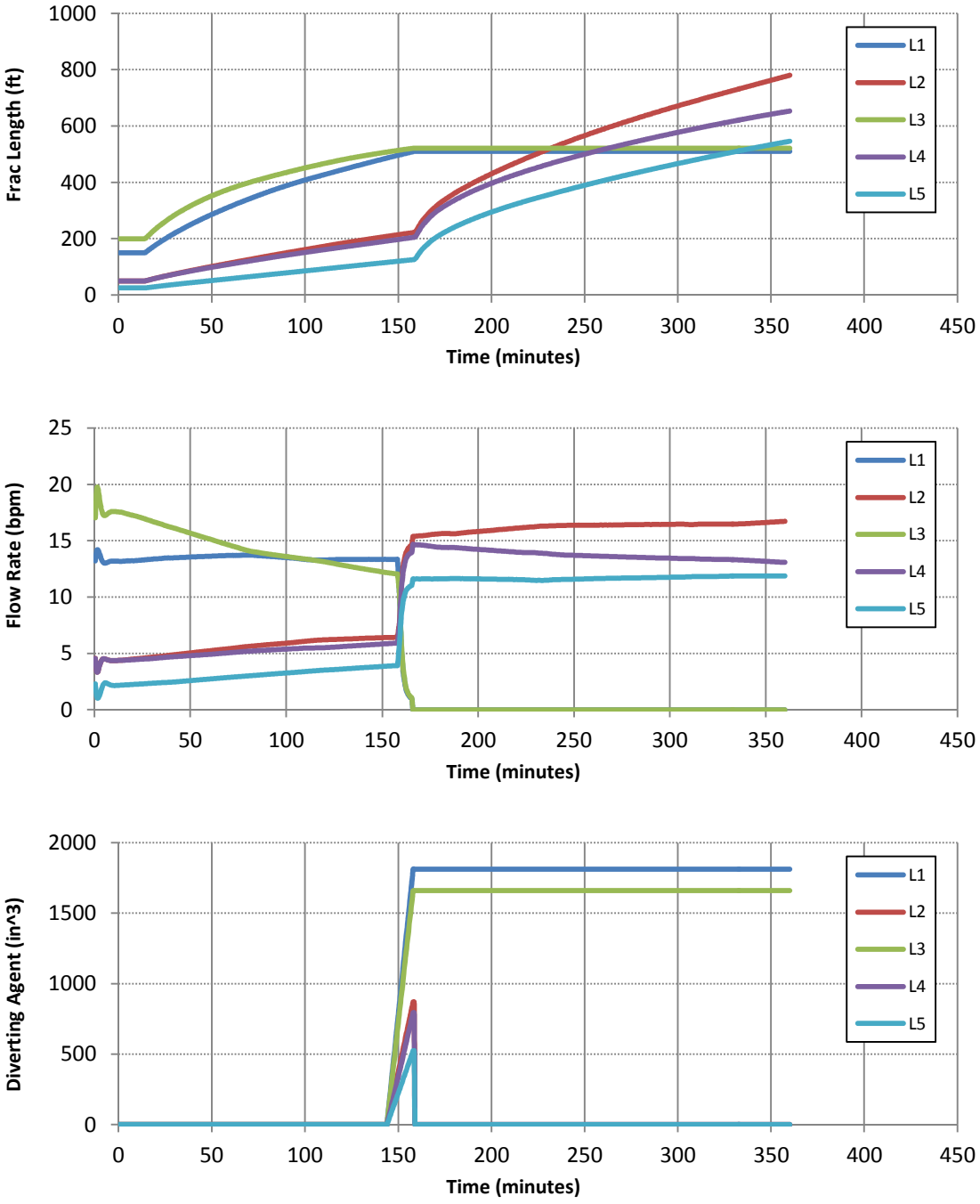

Figure 4-8 - Scenario III, Case A with diverting agent. The fractures begin the treatment with a mix of fracture lengths

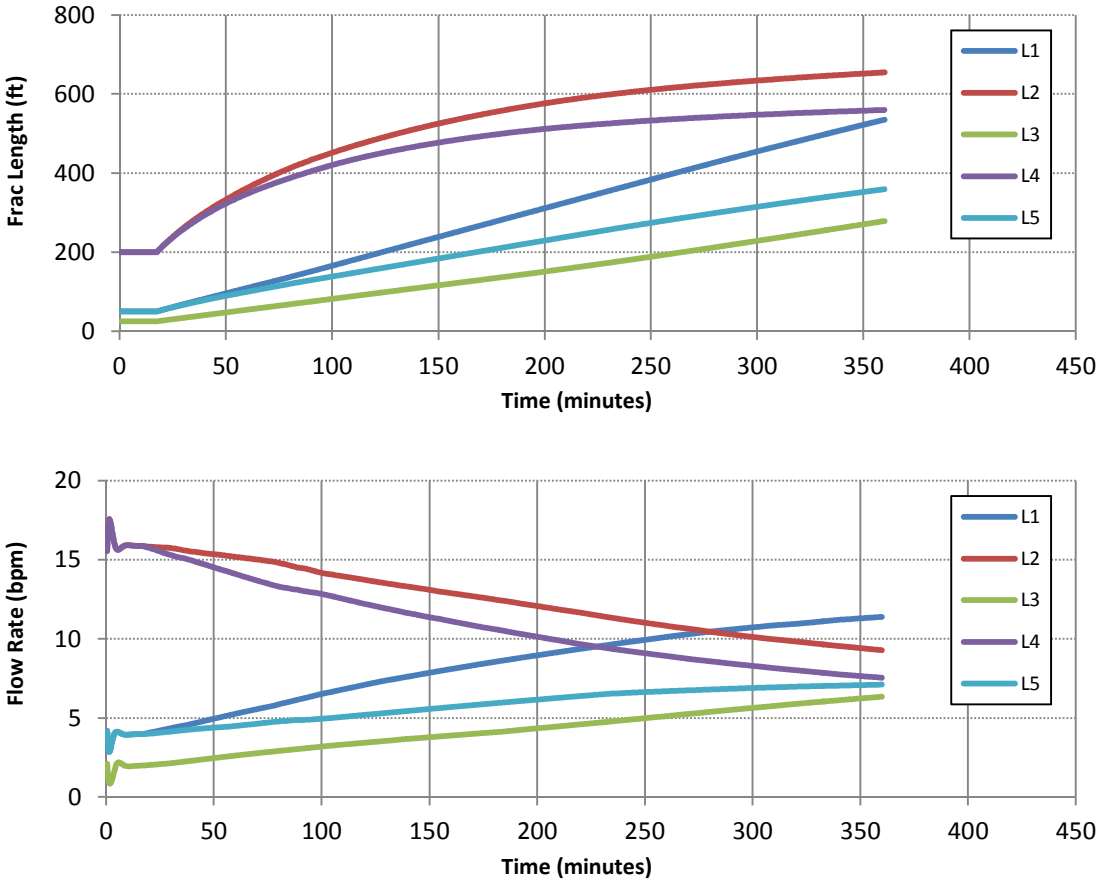

Figure 4-9 - Scenario III, Case B without diverting agent. The fractures begin the treatment with a different mix of fracture lengths than those in Case A

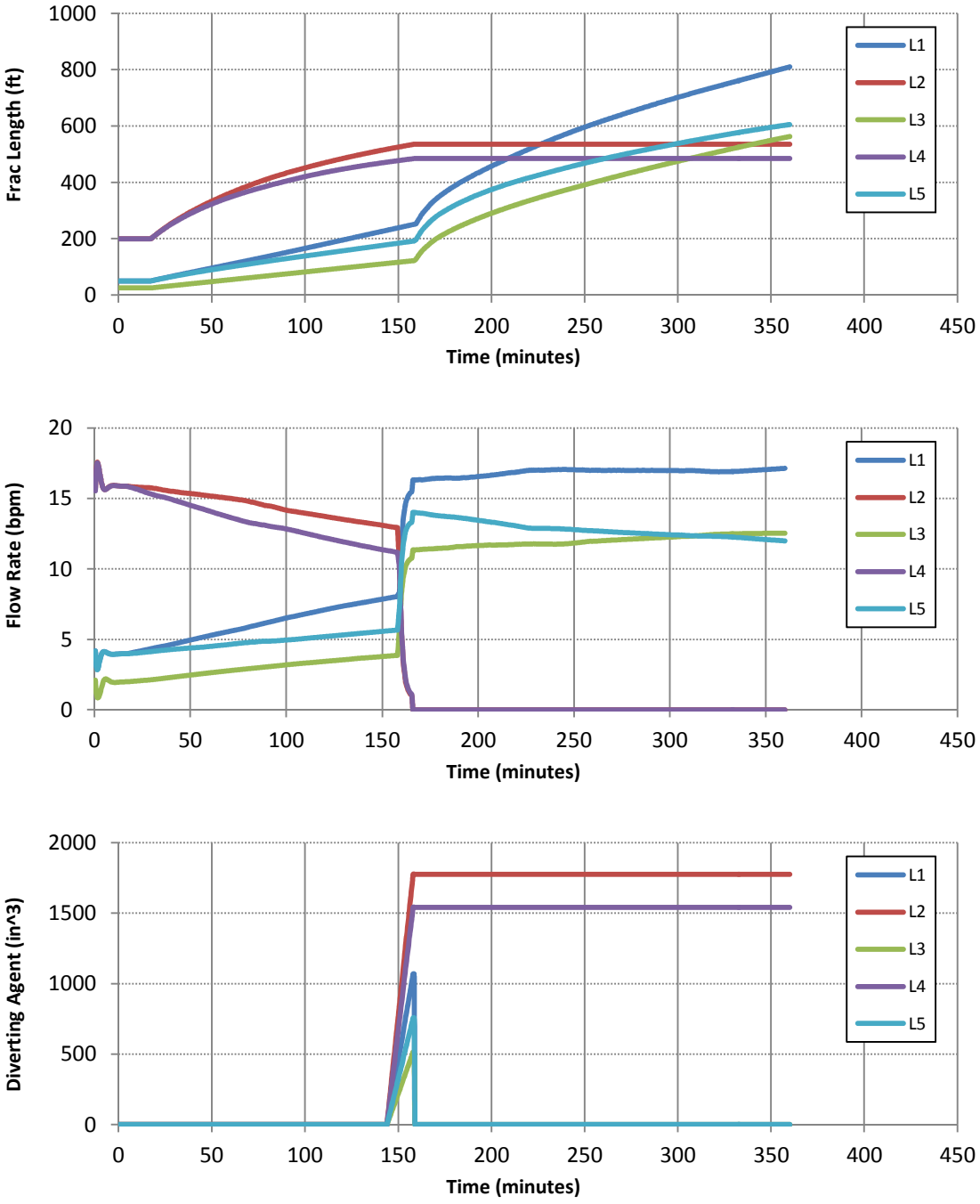

Figure 4-10 - Scenario III, Case B with diverting agent. The fractures begin the treatment with a different mix of fracture lengths than those in Case A

SCENARIO IV – SENSITIVITY TO THE DIVERTING AGENT CAKE PERMEABILITY

In Scenario IV the permeability of the diverting agent cake is adjusted from the standard 1 Darcy value. From Case A to Case D, the permeability ranges from 50 mD to 5000 D. Case D uses the extremely large permeability value to show the insensitivity to high values of permeability. The simulations are all based off of the fracture system from Scenario III, Case B. All properties are identical to this case except for the diverting agent permeability. As a result, Figure 4-10 should be used for comparison.

In Case A, the diverting agent cake permeability is lowered to 100 mD. The lowered value does not affect which fractures grow and which are plugged, but it does change the growth rates of the three growing fractures. A larger degree of diversion results from the lowered permeability, and so the fractures with initially lower flow rates will see a higher spike in flow rates after the diverting agent stage. This is easily seen when comparing the flow rate graph of Figure 4-11 to that of Figure 4-10. In the latter figure, the fracture with the lowest flow rate (L3) before the diverting agent stage continues to have the lowest flow rate of the three growing fractures after diversion. When the permeability is reduced, the situation reverses. The fracture with the lowest flow rate also has the lowest amount of diverting agent (see the diverting agent graph of Figure 4-11). The effect of the lowered permeability on the diverting agent is strong enough to offset the lower flow rate a shorter fracture normally receives. As a result the fracture now has the highest flow rate and its length exceeds that of the next fracture (L5). Also, the fastest growing fracture now has less flow, and its growth rate diminishes. Essentially, the lowered permeability accomplishes more diversion, which in turn changes the relative growth rates and flow rates of the fractures.

A much larger effect is seen in Case B when the permeability is reduced further to 50 mD. Fractures L2 and L4 remain plugged, but an additional plug forms in fracture L1.

The formation of the plug is somewhat surprising because the amount of diverting agent in fracture L1 is much closer to the amount in the unplugged fractures than in the plugged fractures (see the diverting agent graph of Figure 4-12 - the difference in diverting agent between fractures L4 and L1 is about 50% greater than the difference between L1 and L5). The reduced permeability increases the pressure drop due to the diverting agent in fracture L1 to a level that prevents the pad from opening the plug. In effect, the increase in pressure drop from the diverting agent caused by the reduced permeability narrowly plugs L1, but is also small enough to keep L5 unplugged. Since only two fractures are growing instead of three, the flow rates and resulting fracture lengths are higher than in the previous scenario.

In Case C, the diverting agent permeability is increased to 100 Darcies. Little difference is seen when comparing this case to the benchmark case of 1 Darcy permeability from Scenario III, Case B. Some growth and flow is shifted from fracture L5 and L3 to fracture L1 due to the increase in permeability and lower resulting diversion, but the effect is minimal. Further demonstrating the insensitivity of the system to increases in diverting agent permeability, the value had to be increased to 5000 Darcies in Case D before a change in the overall pattern of the system could be observed. At this high value, the plugs do not hold in any of the fractures, so the result is very similar to the benchmark case with no diverting agent (see Figure 4-9). While this permeability value is larger than any that would practically be expected, it shows that successful diversion can be accomplished even when the diverting cake is very permeable.

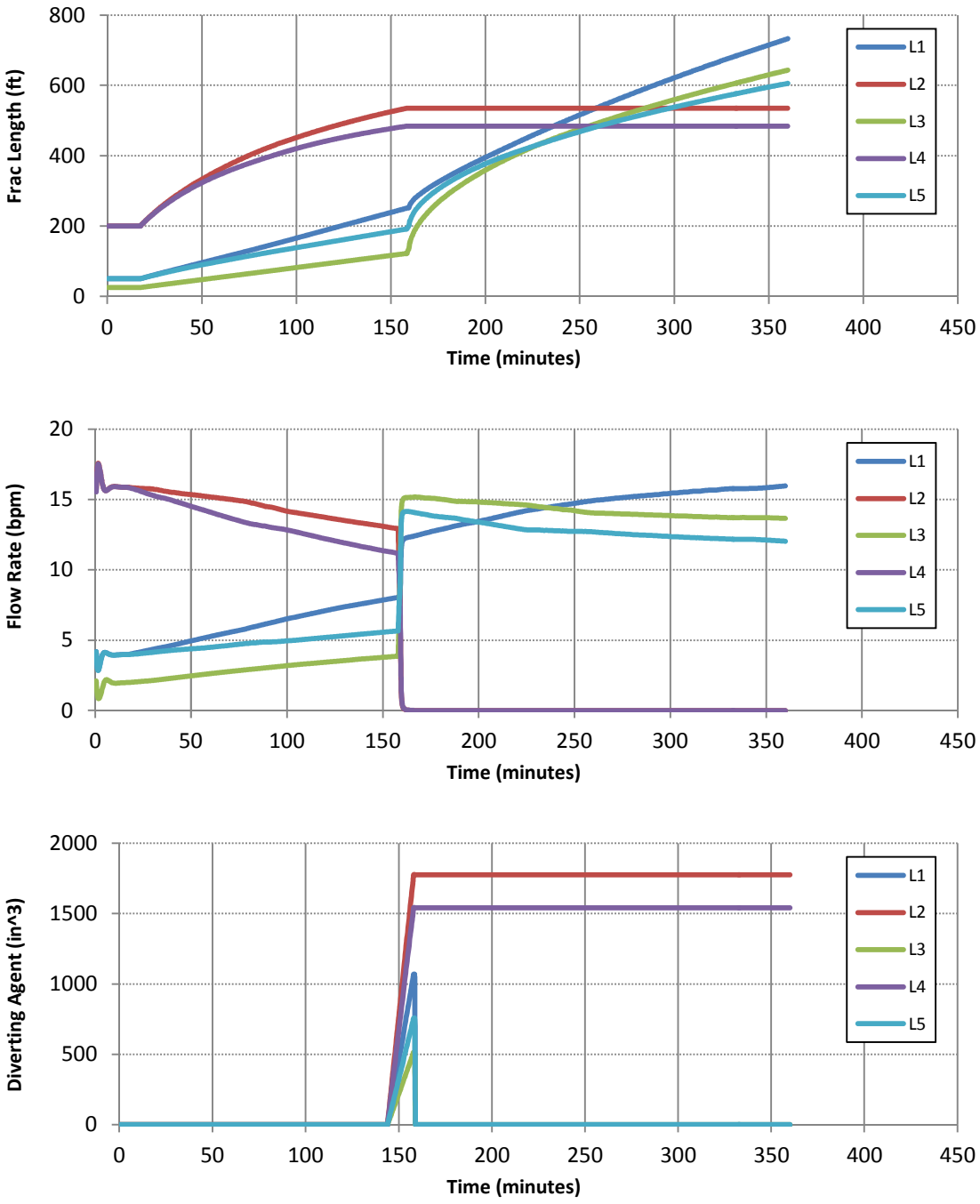

Figure 4-11 – Scenario IV, Case A. The fracture system is the same as in Scenario III Case B, except the permeability of the diverting agent cake is reduced to 100 mD.

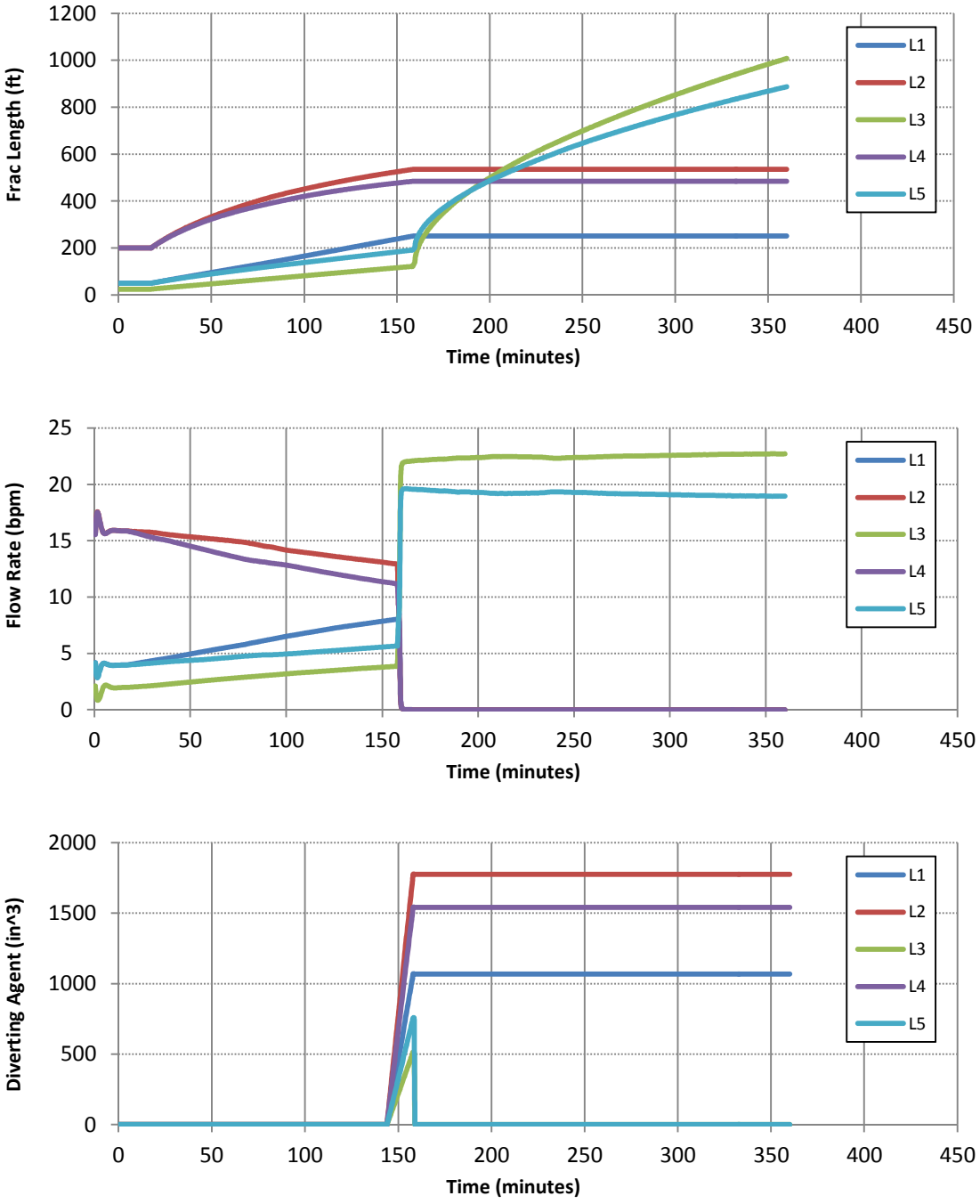

Figure 4-12 - Scenario IV, Case B. The fracture system is the same as in Scenario III Case B, except the permeability of the diverting agent cake is reduced to 50 mD.

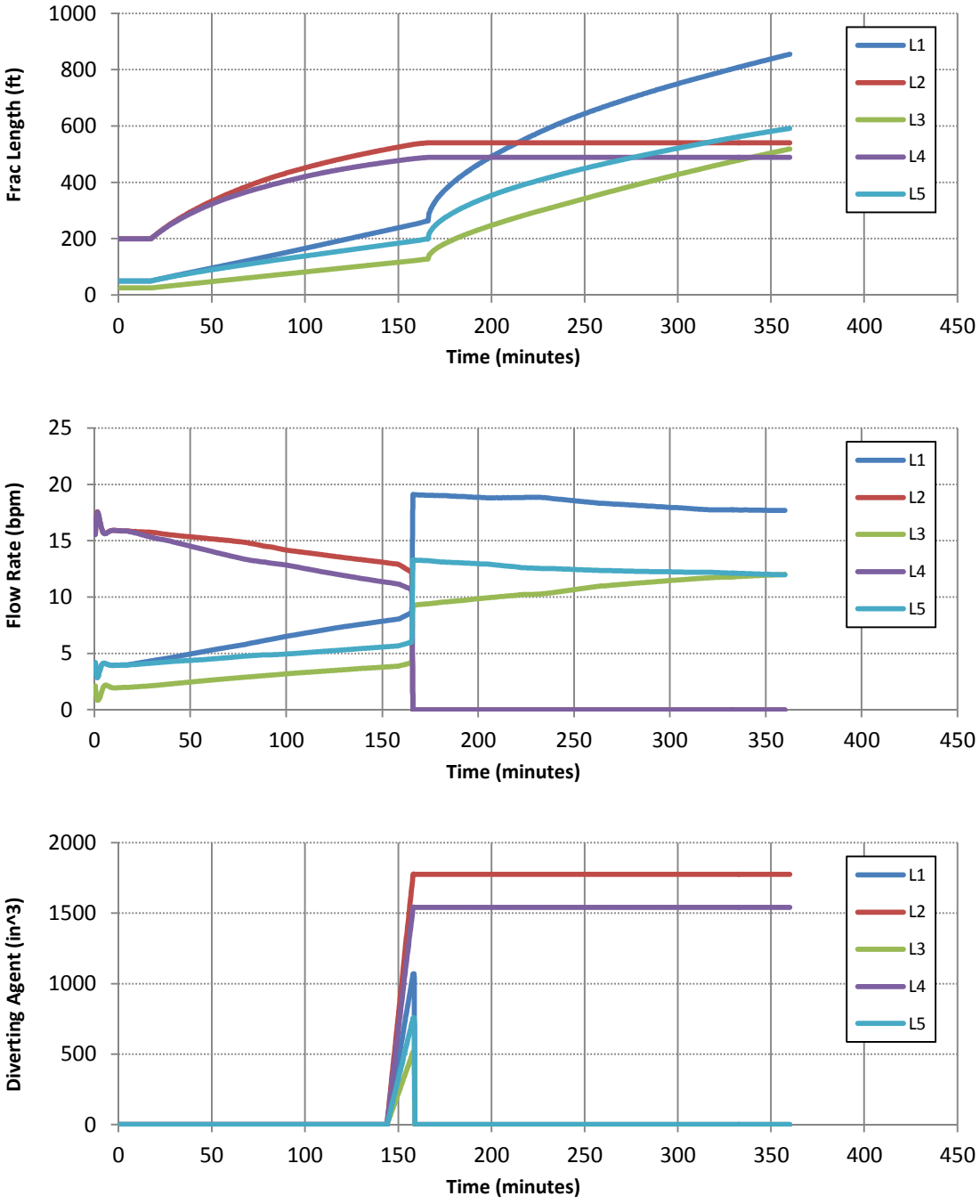

Figure 4-13 - Scenario IV, Case C. The fracture system is the same as in Scenario III Case B, except the permeability of the diverting agent cake is increased to 100 D.

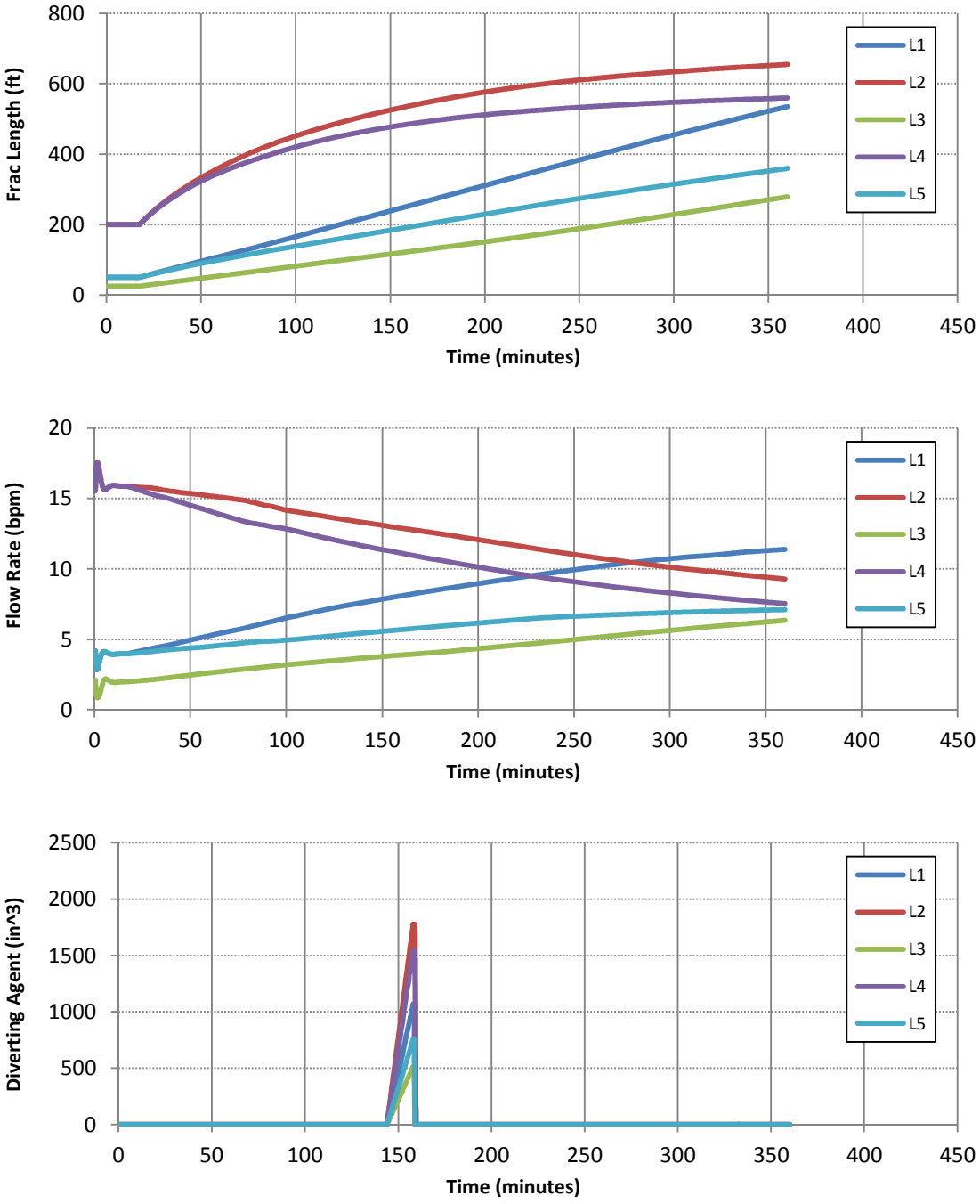

Figure 4-14 - Scenario IV, Case D. The fracture system is the same as in Scenario III Case B, except the permeability of the diverting agent cake is increased to 5E3D.

SCENARIO V – SENSITIVITY TO PUMPED DIVERTING AGENT VOLUME FRACTION

The underlying principles that apply in the previous scenario are again at work when the diverting agent volume fraction is adjusted. This is expected because adjusting the permeability or adjusting the volume fraction both causes a change in the pressure drop due to the diverting agent cake. As seen in Figure 4-15 reducing the diverting agent volume fraction to 1E-5 from the benchmark value of 1E-3 has little effect (again, the input values from Scenario III, case B are used; only the diverting agent volume fraction is adjusted). Diversion is reduced, and L1 grows at the expense of L5 and L3. Increasing the amount of diverting agent to 1E-2 (Case B – Figure 4-16) causes a larger change. The resulting increase in diversion causes the fracture with the lowest flow rate – L3 – to see the most gains in flow rate from the diversion. Immediately after the diverter stage, its flow rate is the highest, exceeding that of the fracture with the lowest amount of friction. As a result, fracture L3 is able to attain a greater length than fracture L5. In a sense, the order of the growing fractures is able to revert to a "preferred" position that is based on the amount of friction force the flow in each fracture experiences. That is, the order of the fractures is based on the length from the heel of the wellbore. This result is possible because the higher amount of diversion seen in Case B gives the L3 fracture the necessary amount of flow to overcome its initially reduced length.

As previously stated, this scenario is very similar to the last one. Case A below is nearly equivalent to Case C in the previous scenario where the diverting agent permeability is increased to 100 Darcies. Less diversion takes place, but the overall results are very similar to the baseline case. Case B below is very similar to Case A from the previous scenario where the diverting agent permeability is decreased to 100 mD. The resulting increase in diversion reorders the growth rates of the fractures to the preferred state. As expected, higher amounts of diversion, whether accomplished by pumping more

diverting agent or by decreasing the permeability of the cake, allows fractures to more quickly recover in length and flow rates from a reduced state.

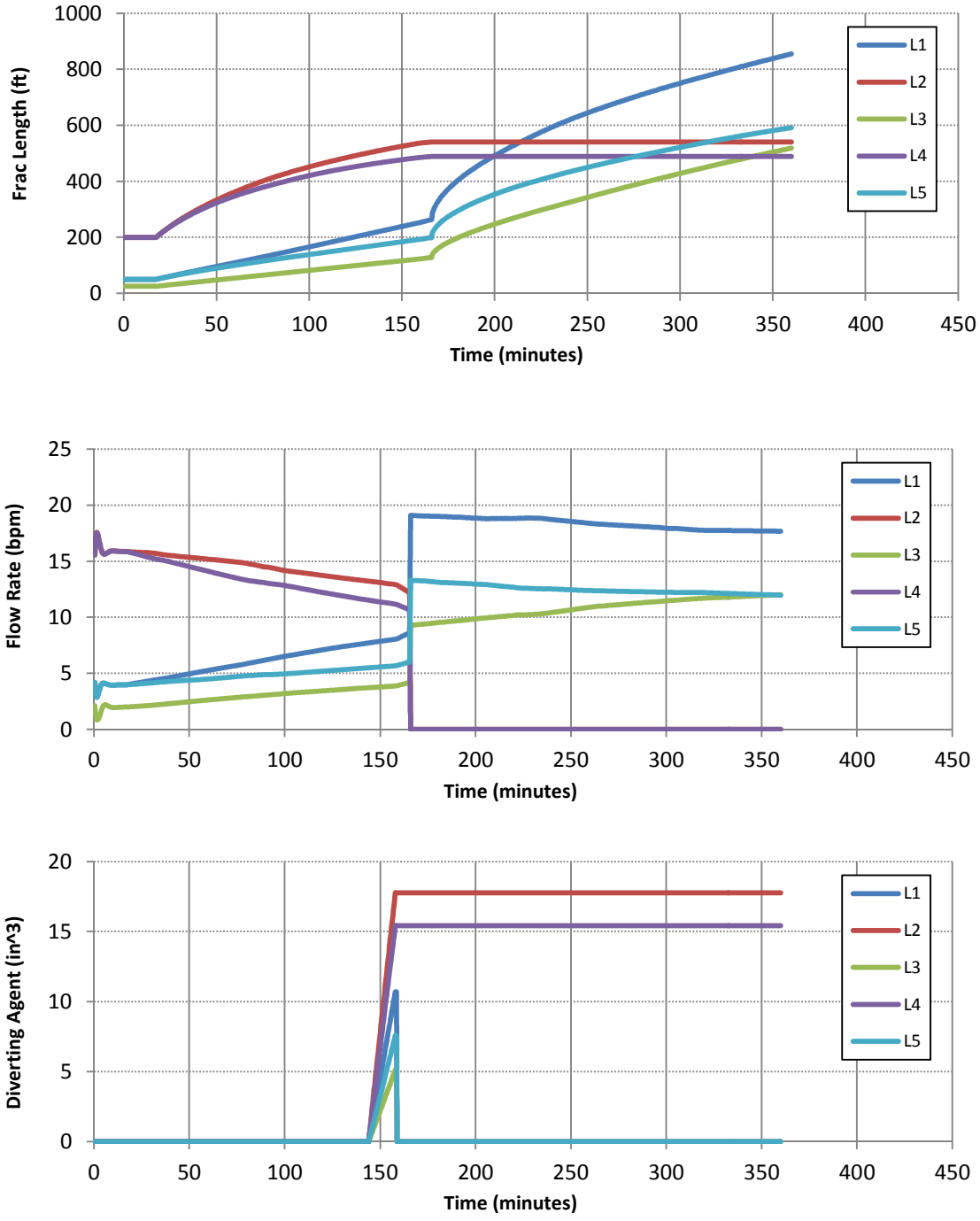

Figure 4-15 - Scenario V, Case A. The fracture system is identical to Scenario III, Case B, except the volume fraction of diverting agent is reduced to 1E-5.

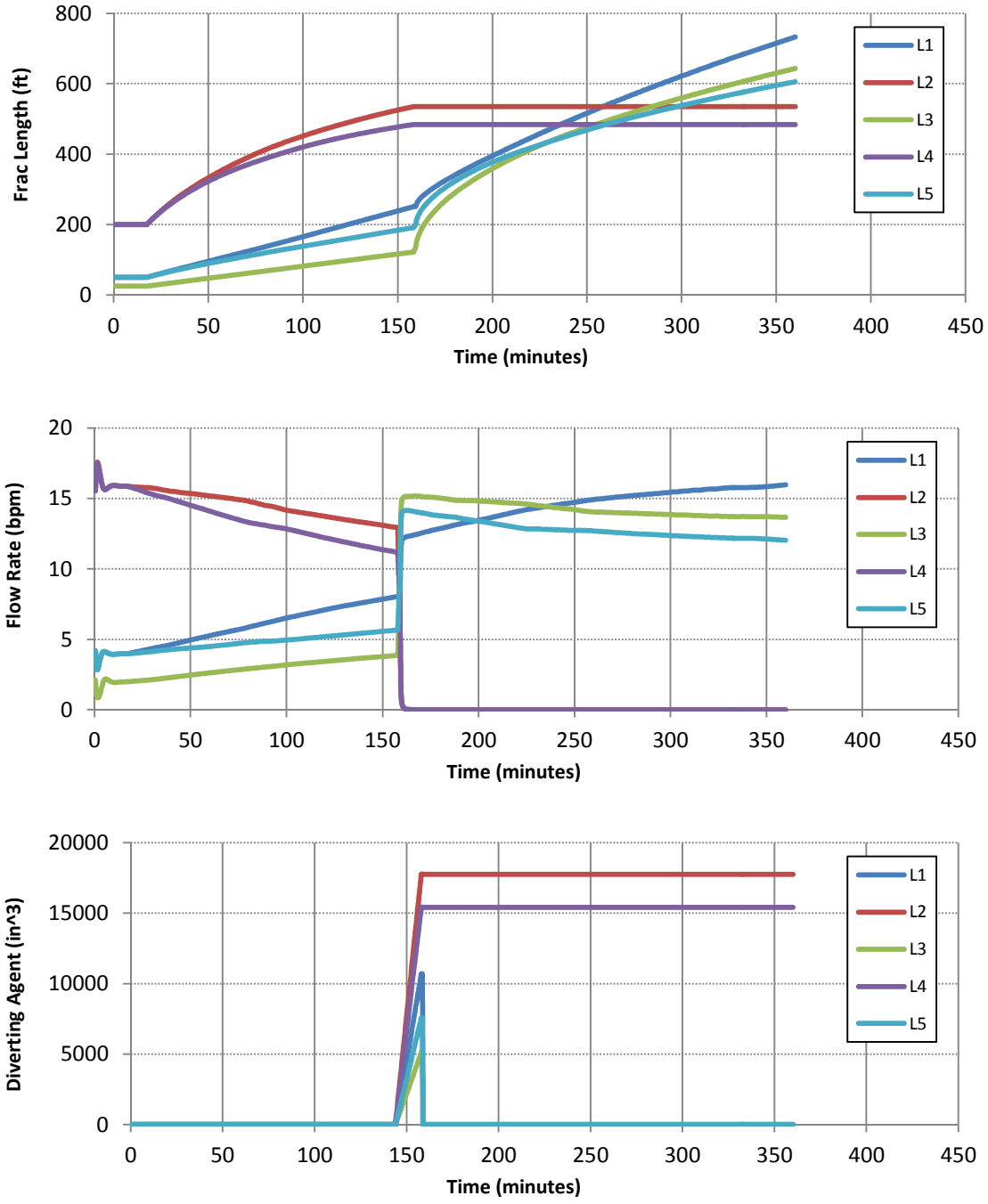

Figure 4-16 - Scenario V, Case B. The fracture system is identical to Scenario III, Case B, except the volume fraction of diverting agent is increased to 1E-2.

SCENARIO VI – SENSITIVITY TO PUMPING RATE OF INJECTED FLUID

In this scenario, the injection rate of the fracturing fluid is varied (again, the fracture system from Scenario III, Case B is used). The pattern found in Case A is similar to that found in Scenario IV – Case B: Fractures L1, L2, and L4 are plugged, and the length of fracture L3 overcomes its initial handicap to exceed the length of L5. However, the reasons for this occurrence differ between the two cases. In Scenario IV, the decrease in permeability resulted in a large amount of diversion in a short amount of time. The pressure drop due to the plug was sufficient enough to cause fracture L1 to plug. In this case, the increase in pumping rate has two primary effects. First, it increases the overall amount of diverting agent deposited, since deposition is based on flow rates. And second, the increase in flow rate increases the friction forces, which in turn act as a form of diversion – flow is diverted from fractures close to the toe toward fractures closer to the heel. When comparing the flow rate graphs between Figure 4-17 and Figure 4-12 in relative terms, fracture L1 catches up to L2 and L4 much more quickly with the higher pumping rate in Case A here than it did in Scenario IV. This is because friction diverts more of the flow to L1 from the other fractures. As a result, when the diverting agent stage begins, the flow rate in L1 is already near the flow rates in the top two fractures, and fracture L1 will receive a similar amount of diverting agent. The increase in diverting agent causes fracture L1 to remain plugged in this case.

Also, in both cases fracture L3 exceeds fracture L5 - however, they do so at different times in the two cases. In Scenario IV, the drop in permeability causes a sharp diversion that occurs in a short time span. The diversion resulting from friction, however, occurs over a longer period of time. As a result L3 surpasses L5 much later in the treatment in the current case than in Scenario IV.

An interesting result occurs in Case B where the flow rate is increased further to 83 bpm. Of course, absolute fracture lengths increase, but there are also significant changes in the relative differences between the fractures. As in the benchmark case, only two fractures are plugged; however, the initially reduced fracture L1 replaces L4 as the plugged fracture. This occurs even though L1 has a shorter fracture length at the time of the diverting agent stage. This is caused by the higher flow rate increasing the amount of diversion due to friction. As a result, fracture L1 greatly increases its flow rate at the expense of the other fractures. Its fracture growth rate increases as well, but, by the time diverting agent is pumped, its flow rate exceeds that of the other fractures despite its shorter fracture length. As a result, it receives more diverting agent than the other fractures (see Diverting Agent graph in Figure 4-18). Fracture L4, on the other hand, drops very quickly due to the increased level of friction and receives much less diverting agent than it did in the baseline case. As a result, fractures L1 and L2 remain plugged, and fracture L4 joins L3 and L5 as growing fractures. The higher level of friction diversion also influences the growing fractures, and the order of fracture lengths reverts back to one based on distance to the heel of the wellbore. Again, it is important to note that timing of the diverting agent plays a role. Had the diverting agent been pumped before the flow rate of L1 exceeded that of L4, then L1 may have remained unplugged.

In Case C, the injection rate is decreased to 28 bpm. At this very low flow rate, the effect of friction diversion is greatly reduced. As a result, the fractures with the largest initial lengths are the ones that get plugged. There is no relative change between the growing fractures, meaning the order is not based on distance from the heel, but rather based on the initial configuration. The main difference between the pattern seen in this case and the one from the benchmark case is that there is less disparity between the

fracture lengths of the three growing fractures – a result caused by the decrease in diversion due to friction.

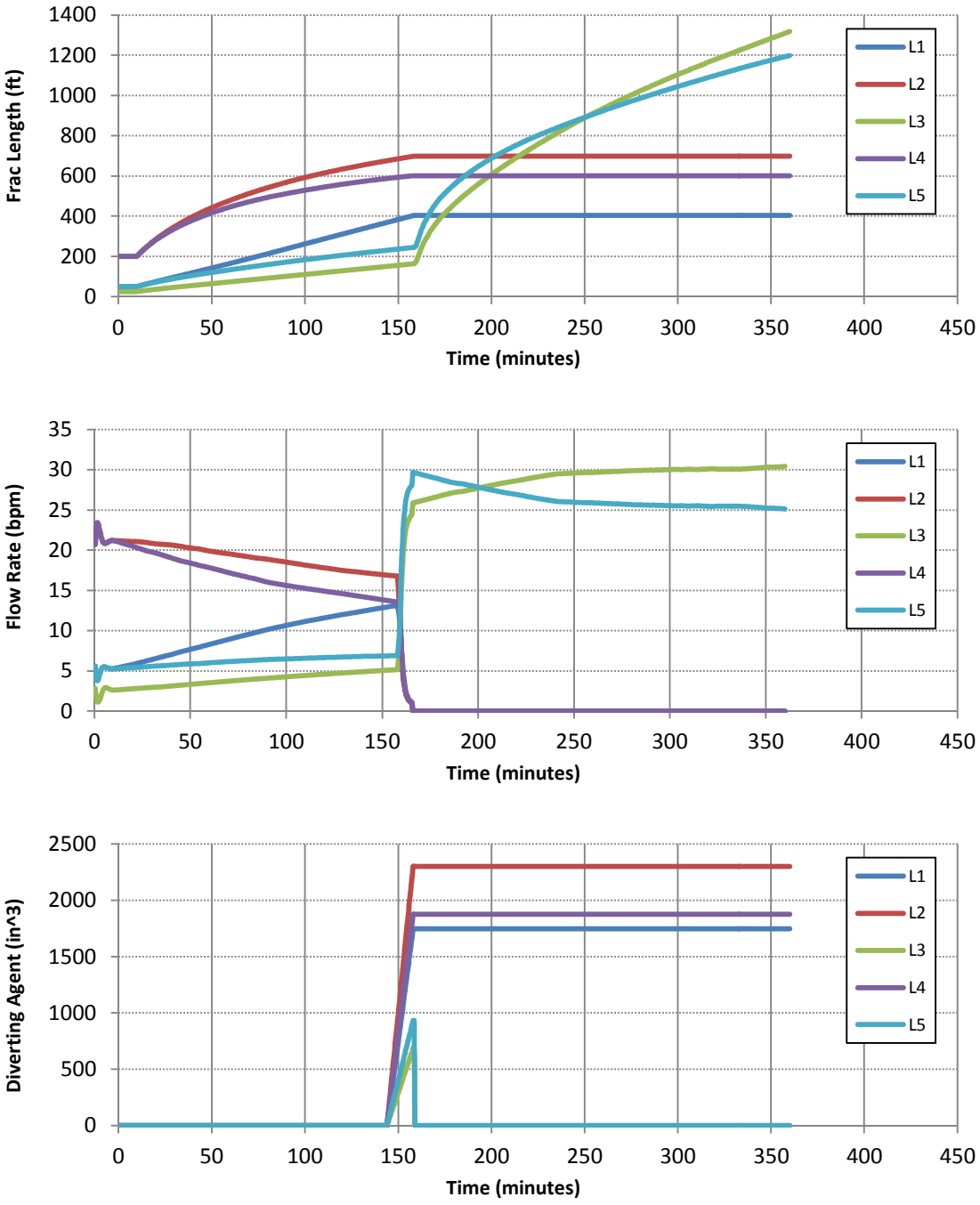

Figure 4-17 – Scenario VI, Case A. Fracture system is identical to Scenario III, Case B, except the pump rate of the injected fluid is increased to 56 bpm

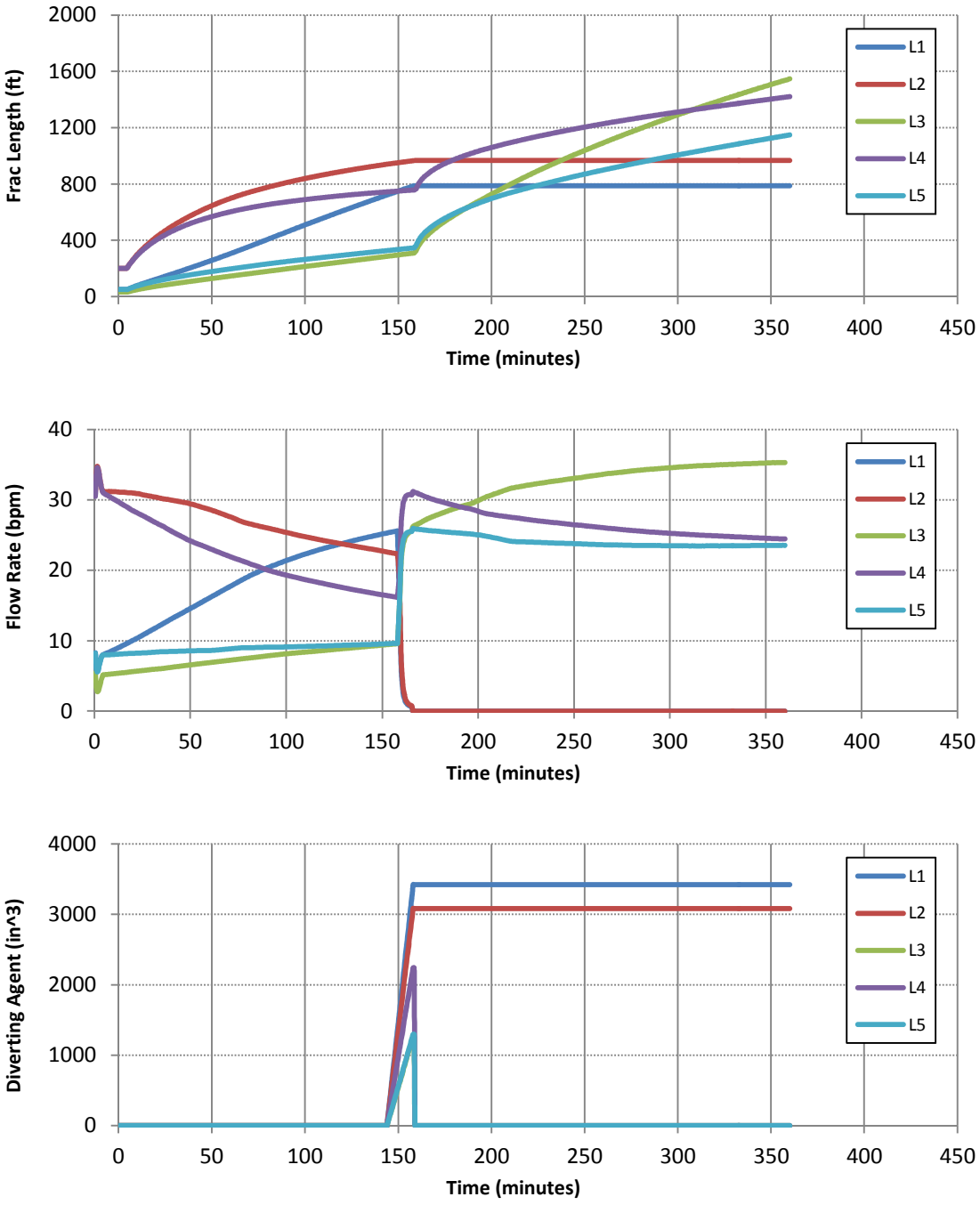

Figure 4-18 - Scenario VI, Case B. Fracture system is identical to Scenario III, Case B, except the pump rate of the injected fluid is increased to 83 bpm

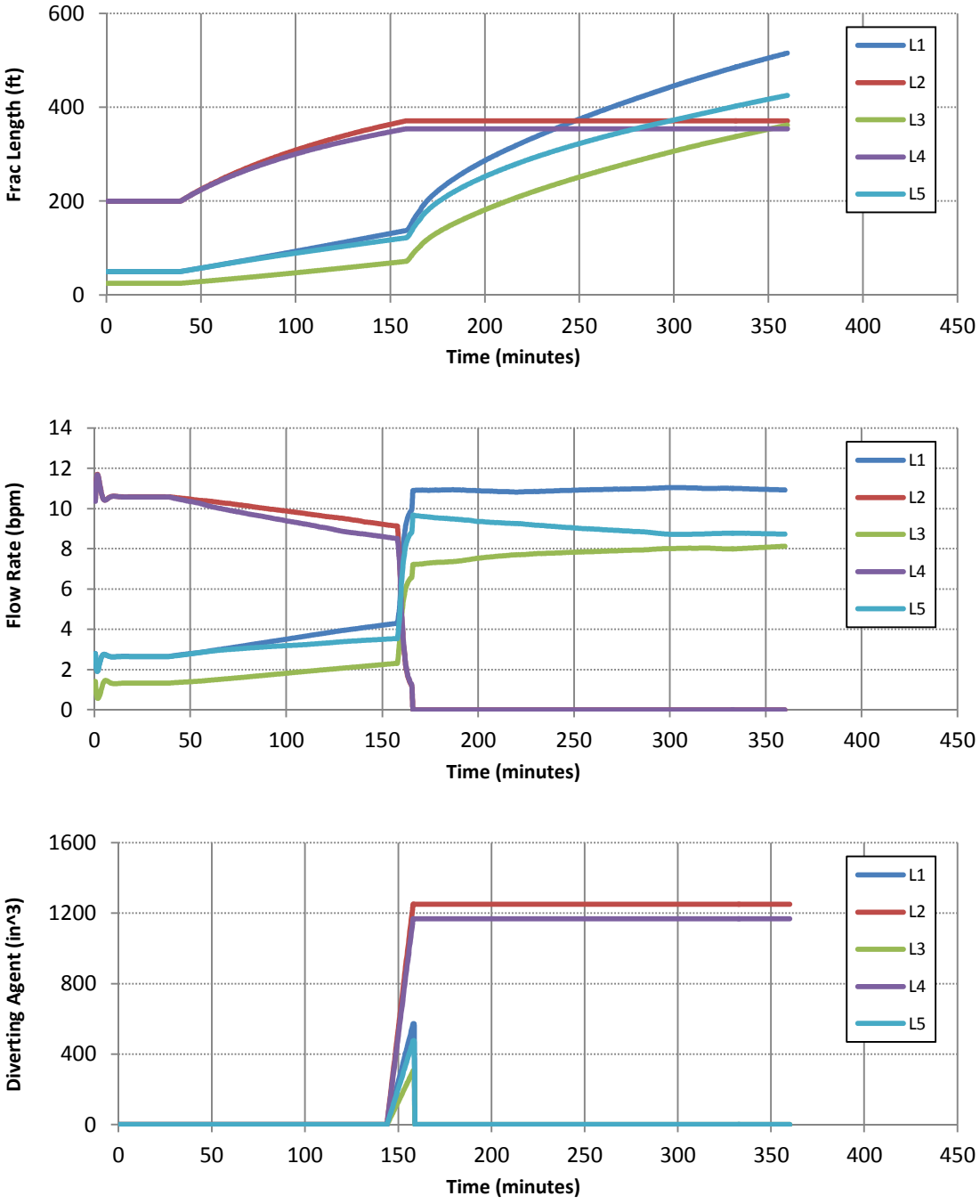

Figure 4-19 - Scenario VI, Case C. Fracture system is identical to Scenario III, Case B, except the pump rate of the injected fluid is decreased to 28 bpm

SCENARIO VII – SENSITIVITY TO ROCK FRACTURE PROPAGATION PRESSURE

One of the most opportune times to conduct a refracturing treatment is when there is a large disparity in fracture length along the wellbore. One cause for such a scenario is a variance of fracture propagation pressure. If the rock surrounding one portion of a well has a lower fracture propagation pressure, then it will grow faster and take more of the flow. As a result, other layers will be understimulated. This scenario simulates the process of adding diverting agent to a well that experiences diversity in propagation pressure (also called P_{frac} in this work) in order to equalize fracture lengths in a refracturing treatment. The difference between Case A and Case B is the selection of fractures that have a modified P_{frac}. In each case, results from a simulation without the application of diverting agent are presented first.

In Case A, the fracture propagation pressure for fractures L1 and L4 are reduced by 2%. As seen in Figure 4-20 when no diverting agent is added, the drop in P_{frac} is large enough to divert a significant majority of the flow to the fractures L1 and L4. The small flow rates in the other fractures are not sufficient to cause growth. When diverting agent is added (Figure 4-21), fractures L1 and L4 plug and flow is diverted to the fractures with higher values of $P_{frac.}$ The differences in growth rates in the growing fractures arise purely from friction forces. In this case, the application of diverting agent is timed so that at the conclusion of the treatment, the fracture lengths of all fractures are very similar.

Fractures L2, L3, and L4 are given lower fracture propagation pressures (also lowered by 2%) in Case B. The move to three fractures with lowered P_{frac} does not change the dynamics of the system. Without diverting agent, the fractures with lowered P_{frac} take the most flow and are the only ones to grow. When diverting agent is added, the growing fractures are plugged and the fractures with the higher values of P_{frac} start to grow. Control over the final pattern is dictated by the timing of the diverting agent stage.

In this case, the entire pumped fluid is split between only two fractures, causing them to grow at a faster pace than in Case A. As a result, the fracture lengths exceed those of the plugged fractures. The relative difference in fracture lengths between the plugged and unplugged fractures can thus be controlled by the timing of the diverting agent stage. The simulations presented here show the potential of using diverting agents to remedy situations where heterogeneity in fracture propagation pressures has caused an unequal distribution of treatment fluid.

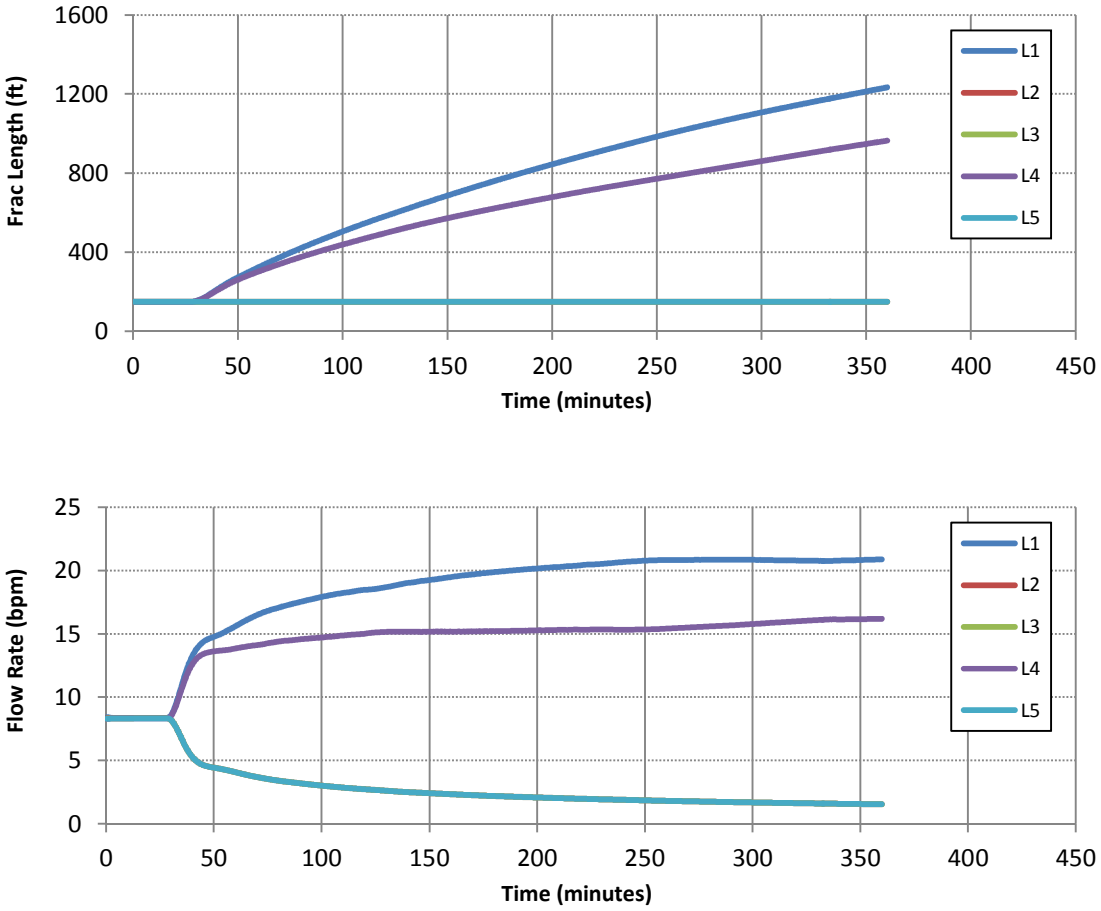

Figure 4-20 – Scenario VII, Case A with no diverting agent. All fractures are equal, except fractures L1 and L4 have lower fracture propagation pressures

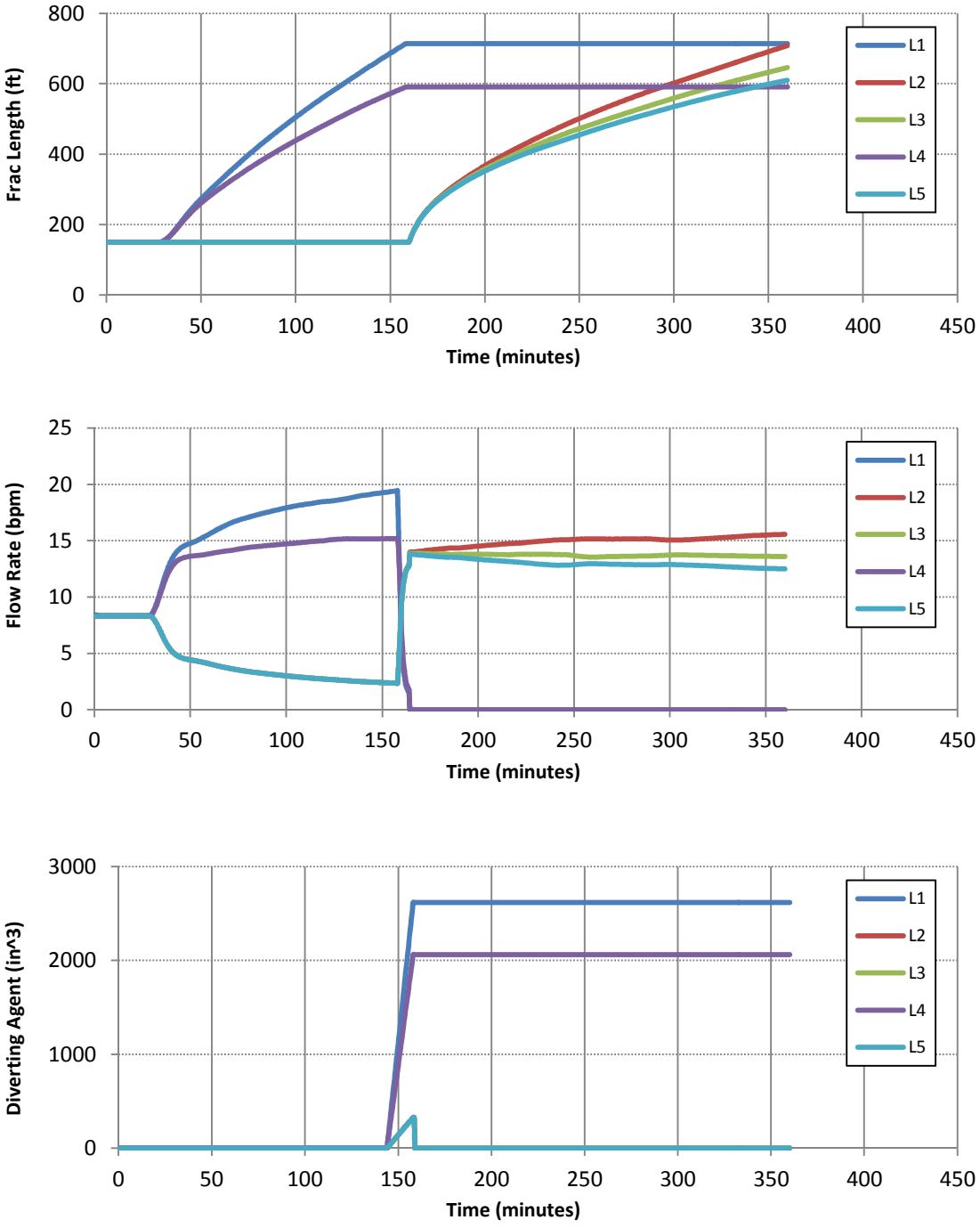

Figure 4-21 – Scenario VII, Case A with diverting agent. All fractures are equal, except fractures L1 and L4 have lower fracture propagation pressures

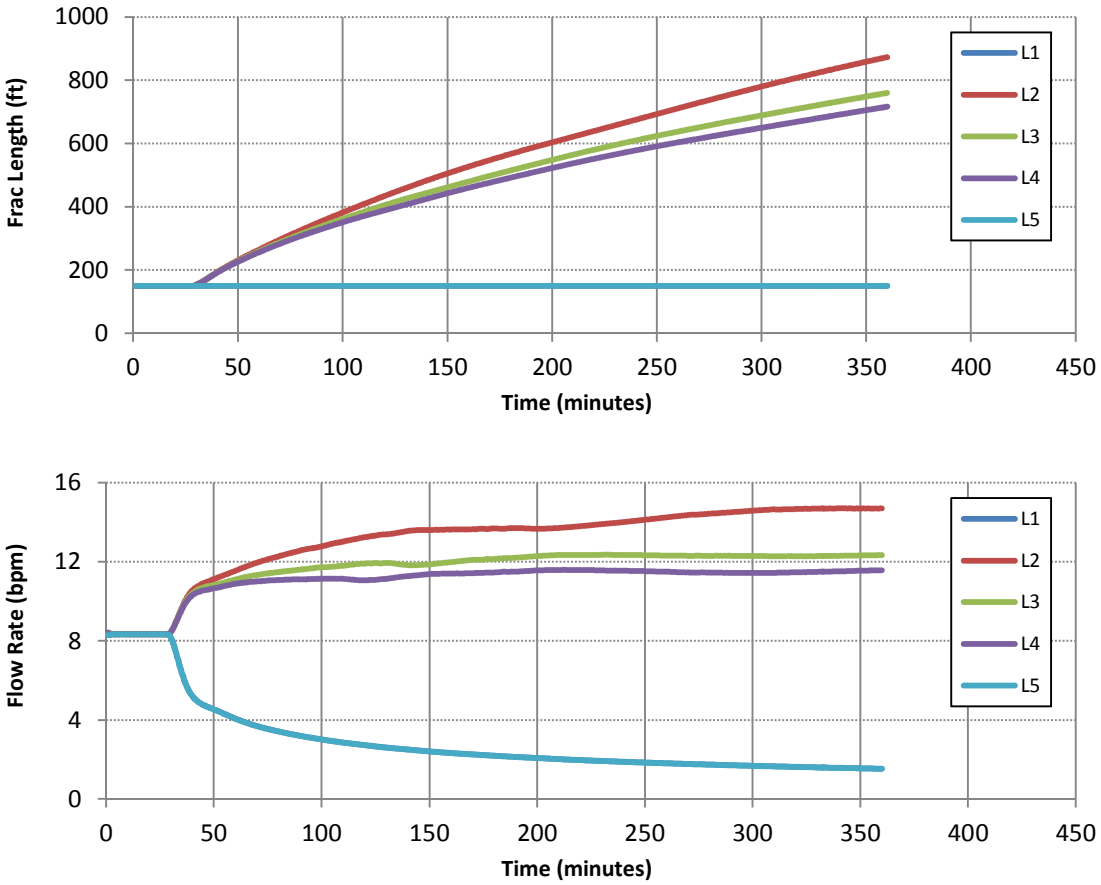

Figure 4-22 – Scenario VII, Case B without diverting agent. All fractures are equal, except fractures L2, L3, and L4 have a lower fracture propagation pressure

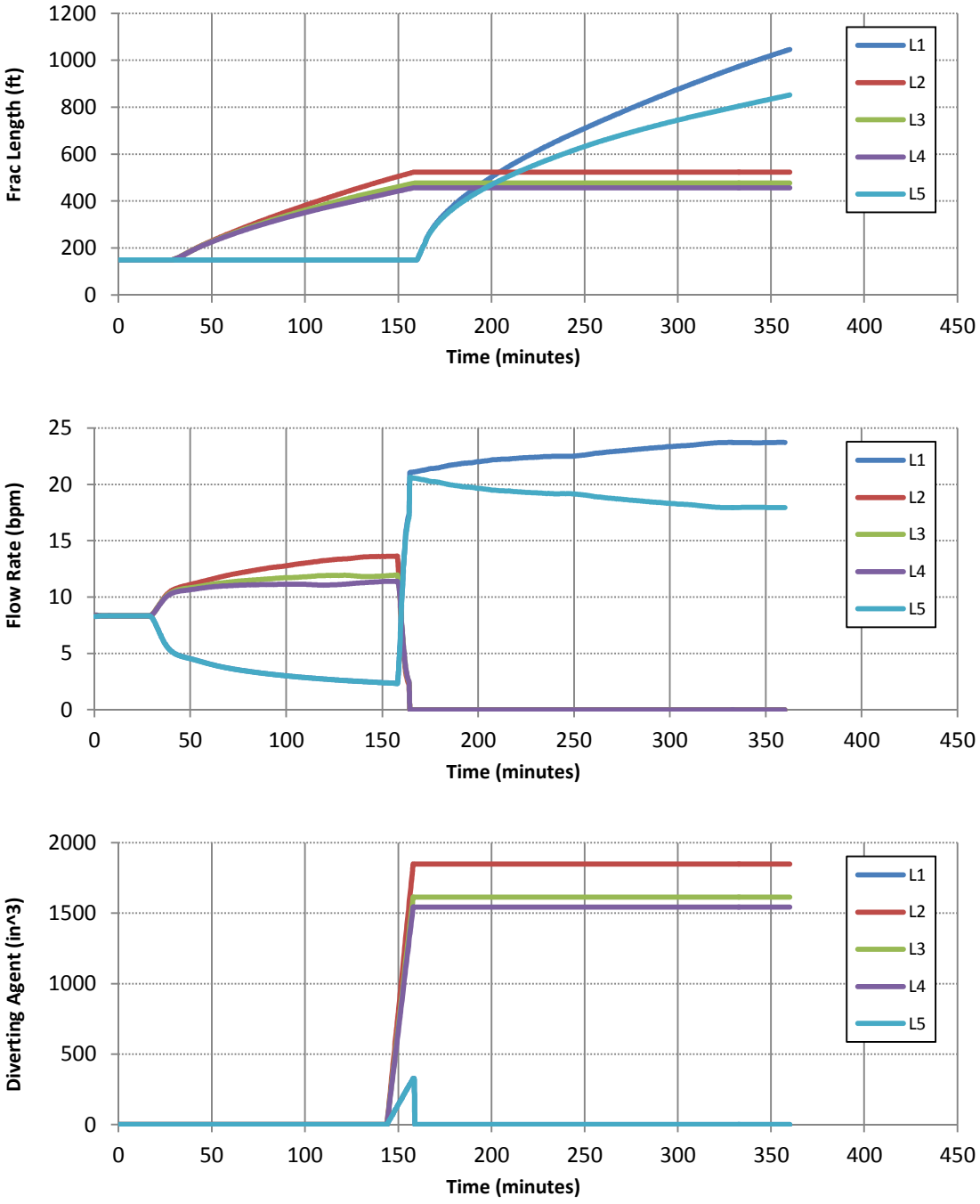

Figure 4-23 – Scenario VII, Case B with diverting agent. All fractures are equal, except fractures L2, L3, and L4 have a lower fracture propagation pressure

Chapter 5: Refrac Simulation Results and Discussion for Diverting Agent that Plugs in the Perforation Tunnel

This chapter discusses the results from simulations of a refracturing treatment with diverting agent that is modeled to plug the perforation tunnels. The simulations in this chapter are also divided into scenarios and cases, as done in Chapter 4. The parameters for the baseline case are presented in Table 5-1. Unless otherwise specified, these parameters are used in all of the simulations.

Scenario I – Baseline Case

Since the other scenarios generally utilize the parameter values used in the baseline case, this scenario serves as a foundation for the subsequent simulations. The most relevant parameters are summarized in Table 5-1.

Table 5-1 – Selection of Input Parameters

Permeability (μD)	100
Porosity	.15
Pore Pressure (psi)	10,000
Fluid Type	oil
Net Pay (ft)	250
Minimum Horizontal Stress (psi)	12,500
Injected Fluid Type	slickwater
Injected Fluid Rate (bpn	56
Diverting Agent Cake Permeability (D)	1
Volume Fraction of Diverting Agent Stage	5E-5

The baseline case is very similar to that used in Chapter 4. Five fractures are modeled along a horizontal wellbore, and all begin with a fracture length of 150 ft. This represents the length of the fracture that resulted from the previous treatment. The names L1 through L5 are assigned to each fracture, with L1 being the fracture closest to the heel of the well. The diverting agent stage is conducted from minute 144 to 173. Unlike the model from Ch. 4, none of the stages are designed to break or disassociate the diverting agent plug. Since the diverting agent collects in the perforation tunnel under this model, it remains in place for the duration of the treatment. One effect from this assumption is

equalization of flow and fracture propagation. In contrast to the model used in Ch. 4, the diverting agent in this chapter allows for the fracture lengths to equalize. Because equal fracture lengths likely indicate more efficient drainage along a lateral, the maximum distance between fracture lengths will be used as a performance metric for the refrac treatment.

For comparison purposes, the simulation results of the baseline case without the use of diverting agents are presented first (see Figure 5-1). Since the properties of each fracture are identical, the only difference is the position along the wellbore. L1 is closest to the heel and therefore experiences less of a pressure drop due to friction than the other fractures. The discrepancy seen in growth and flow rates is caused only by friction. As a result of this difference, the L1 and L2 fractures grow preferentially and take a larger share of the fracturing fluid.

When diverting agent is added, the disparity in both flow rates and fracture lengths between the fractures quickly dissipates (see Figure 5-2). As seen in the diverting agent plot, the fractures closest to the heel take more diverting agent. This causes the flow rates in those fractures to drop, and the flow rates in the other fractures to rise. Even small differences in diverting agent volume are sufficient to cause diversion. The effect of diverting agent is strong because all of the fluid entering a particular fracture flows through the diverting agent cake. At the end of the treatment, the fractures have roughly the same fracture half-length.

One interesting characteristic of the response can be seen in a zoomed in plot of the flow rate graph (Figure 5-3). Initially, the diverting agent causes a sharp change in flow rates where the rate of the first fracture actually drops below the rate of the last fracture. However, as the diverting agent stage continues, the last fracture is now the one receiving diverting agent at the fastest rate. As a result, its flow rate drops, and eventually

the flow rates between the fractures equalize. In this process, the diverting agent acts as a feedback mechanism. When the flow rates are off target (i.e., not equal), the diverting agent will move them towards equilibrium. Results from later scenarios will show the importance of this principle to the accurate tuning of diverting agent parameters.

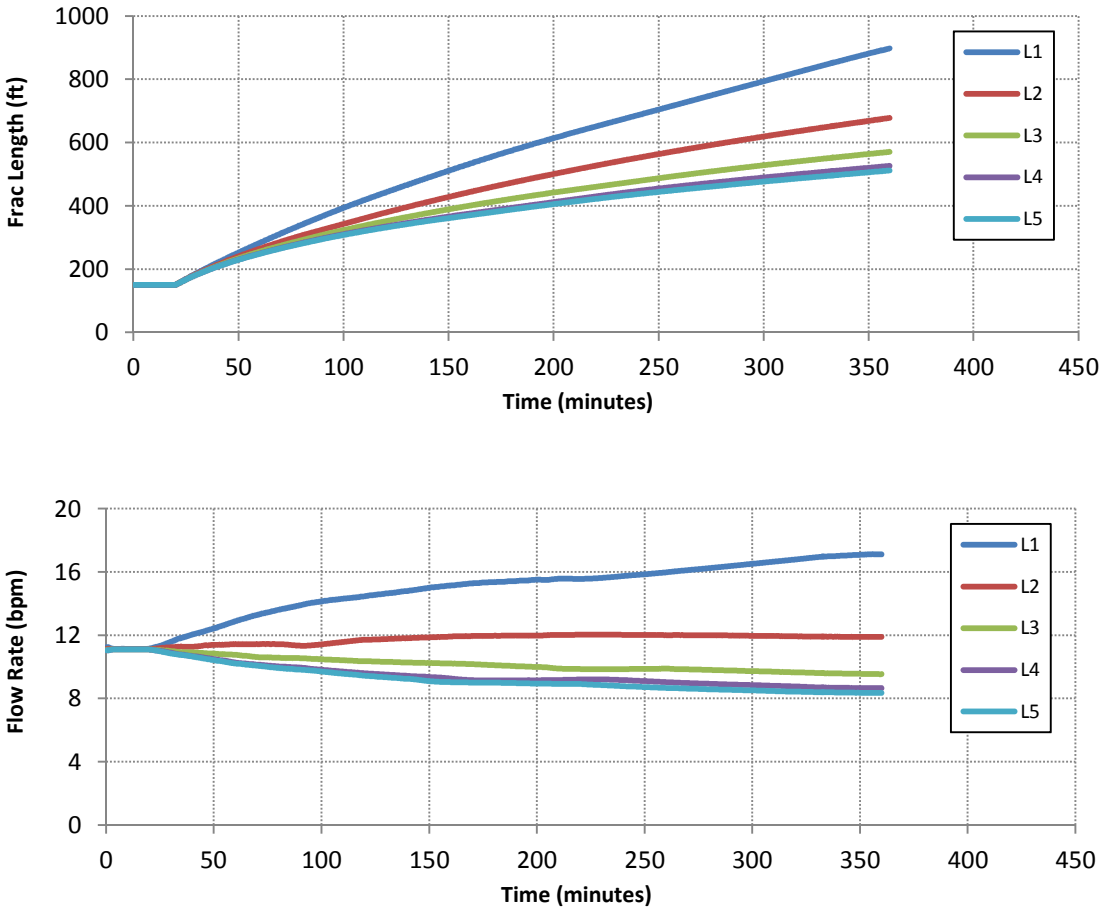

Figure 5-1 – Scenario I: Baseline case without the use of diverting agent. All fractures are identical, except their position along the wellbore and consequently their frictional pressure drop. Select properties are given in Table 5-1.

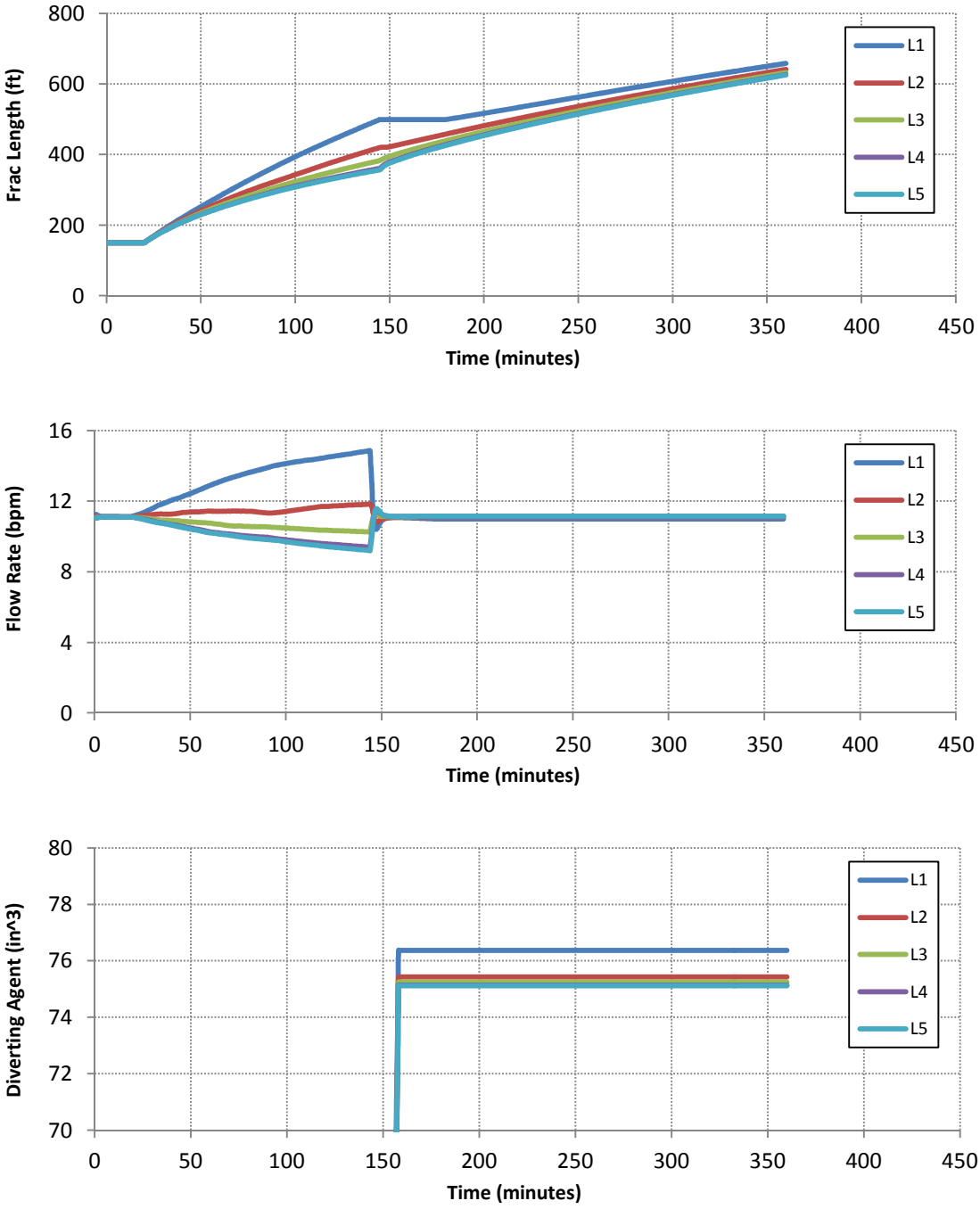

Figure 5-2 – Scenario I: Baseline case with the standard diverting agent stage included. All fractures are identical, except their position along the wellbore. The fractures closest to the heel initially grow the fastest due to less friction, but also take more diverting agent.

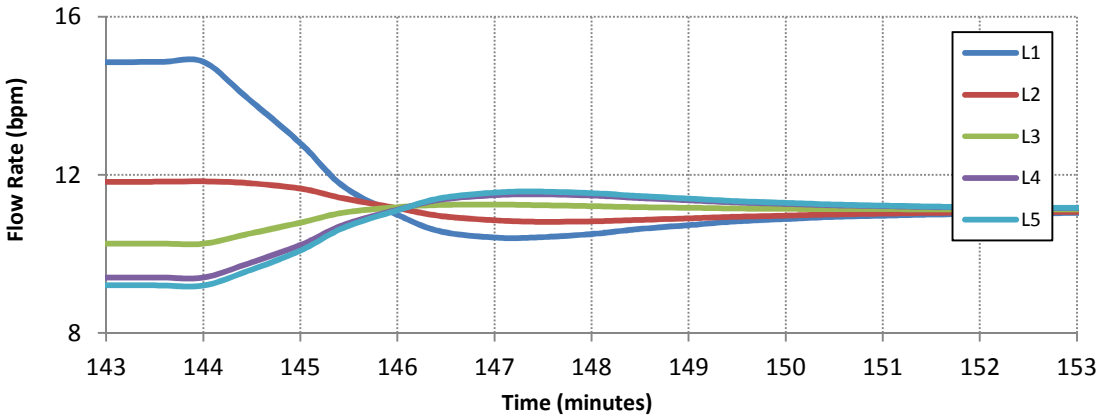

Figure 5-3 – Zoomed in flow rate plot for Scenario I with diverting agent. The diverting agent acts as a feedback mechanism to equalize flow between the fractures.

Scenario II – One Fracture with Reduced Length

This scenario is identical to the baseline case, except one of the fractures begins the treatment with a shorter fracture length. In Case A (Figure 5-4 and Figure 5-5), fracture L3 begins with a 50 ft. length and in Case B (Figure 5-6 and Figure 5-7) fracture L1 begins with a 50 ft. length. Shorter fractures start the treatment with less flow; however, their flow rates and fracture lengths begin to recover to the relative position held in the baseline case. For the situation in which no diverting agent is pumped in Case A, fracture L3 does not surpass the bottom two fractures in length. However, in case B (also with no diverting agent), the higher flow rate caused by its position closest to the heel allows fracture L1 to end the treatment with the longest length. In both cases, the application of diverting agent equalizes flow rates and greatly reduces the differences between fracture lengths. In Case A, L3 remains the smallest fracture despite successful diversion. Since flow is equalized between the fractures after diversion, the growth rates between fractures are roughly equal, and L3 is not able to recover from its original shorter length.

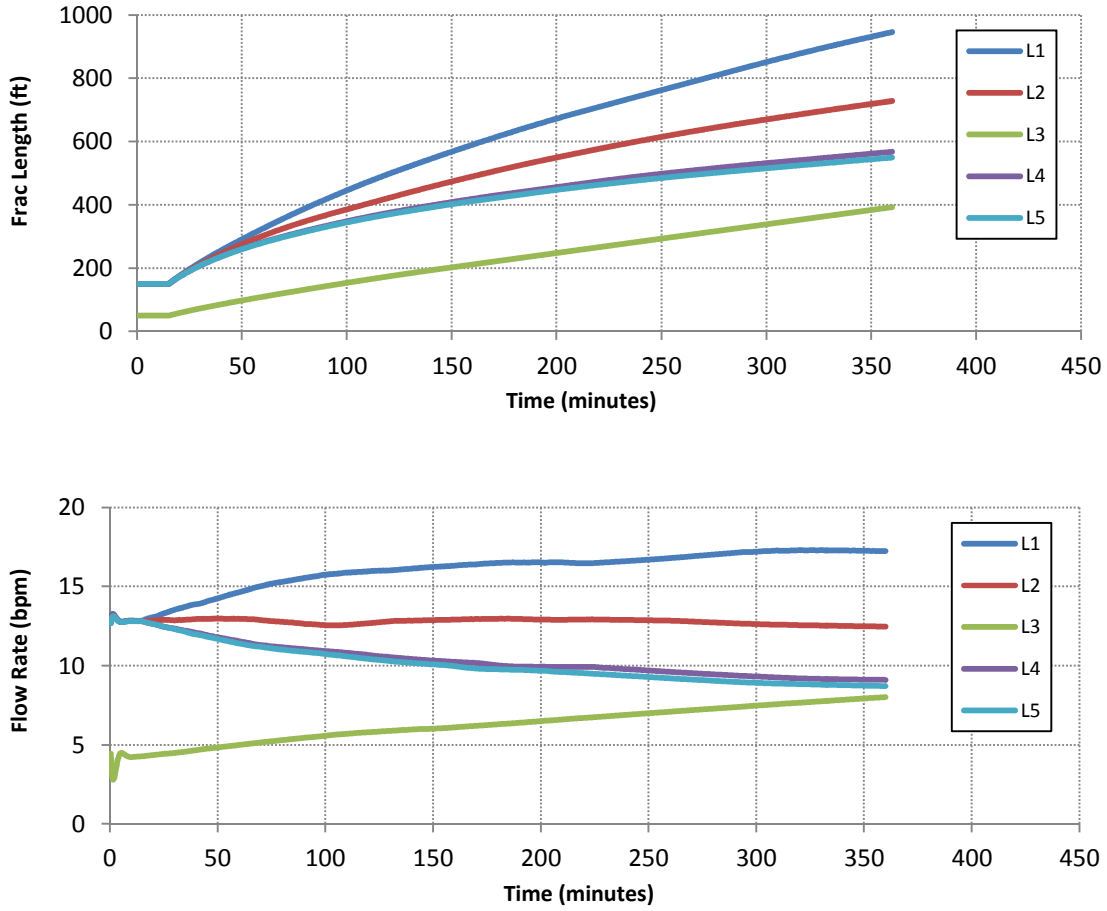

Figure 5-4 – Scenario II, Case A without diverting agent. All fractures are identical except fracture L3 begins the treatment with a shorter fracture length

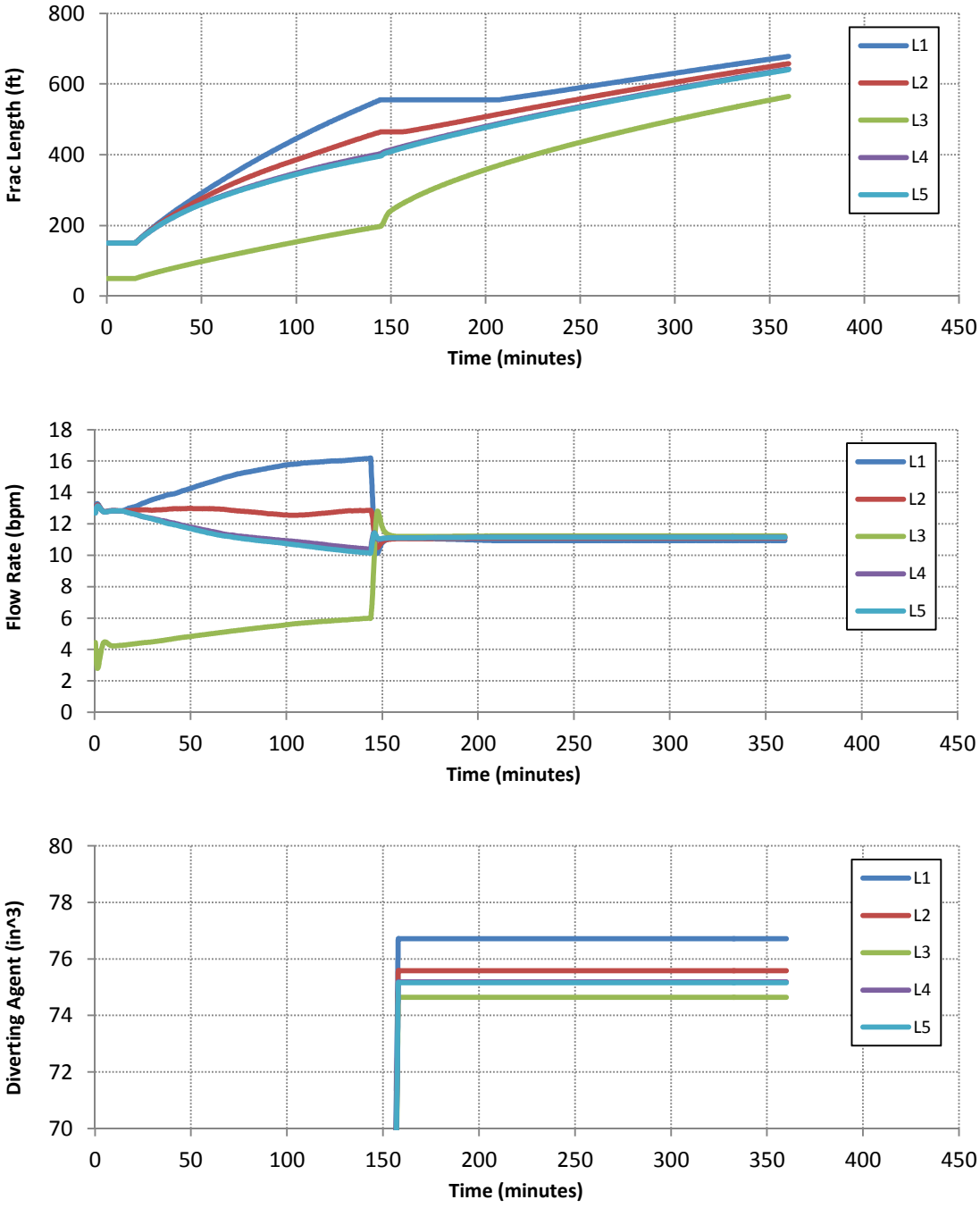

Figure 5-5 – Scenario II, Case A with diverting agent. All fractures are identical except fracture L3 begins the treatment with a shorter fracture length

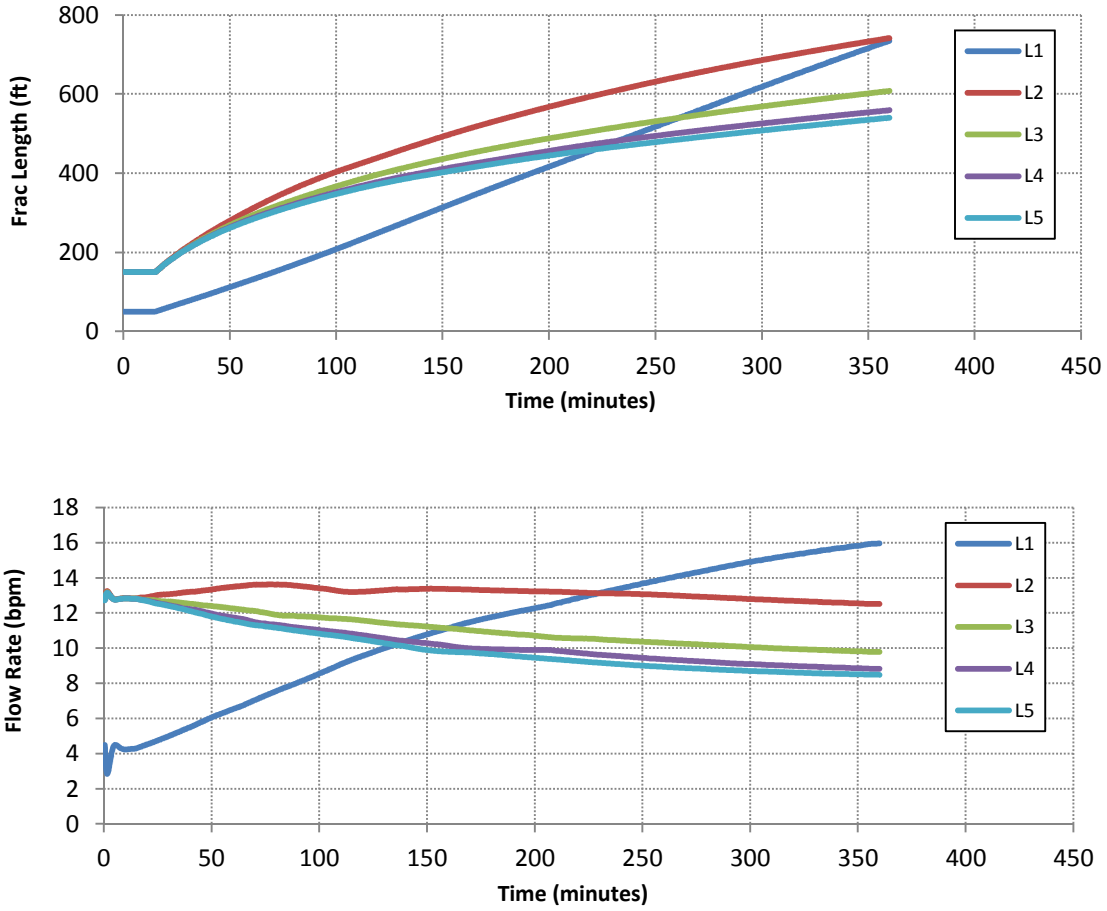

Figure 5-6 – Scenario II, Case B without diverting agent. All of the fractures are identical, except fracture L1 begins the treatment with a shorter fracture length

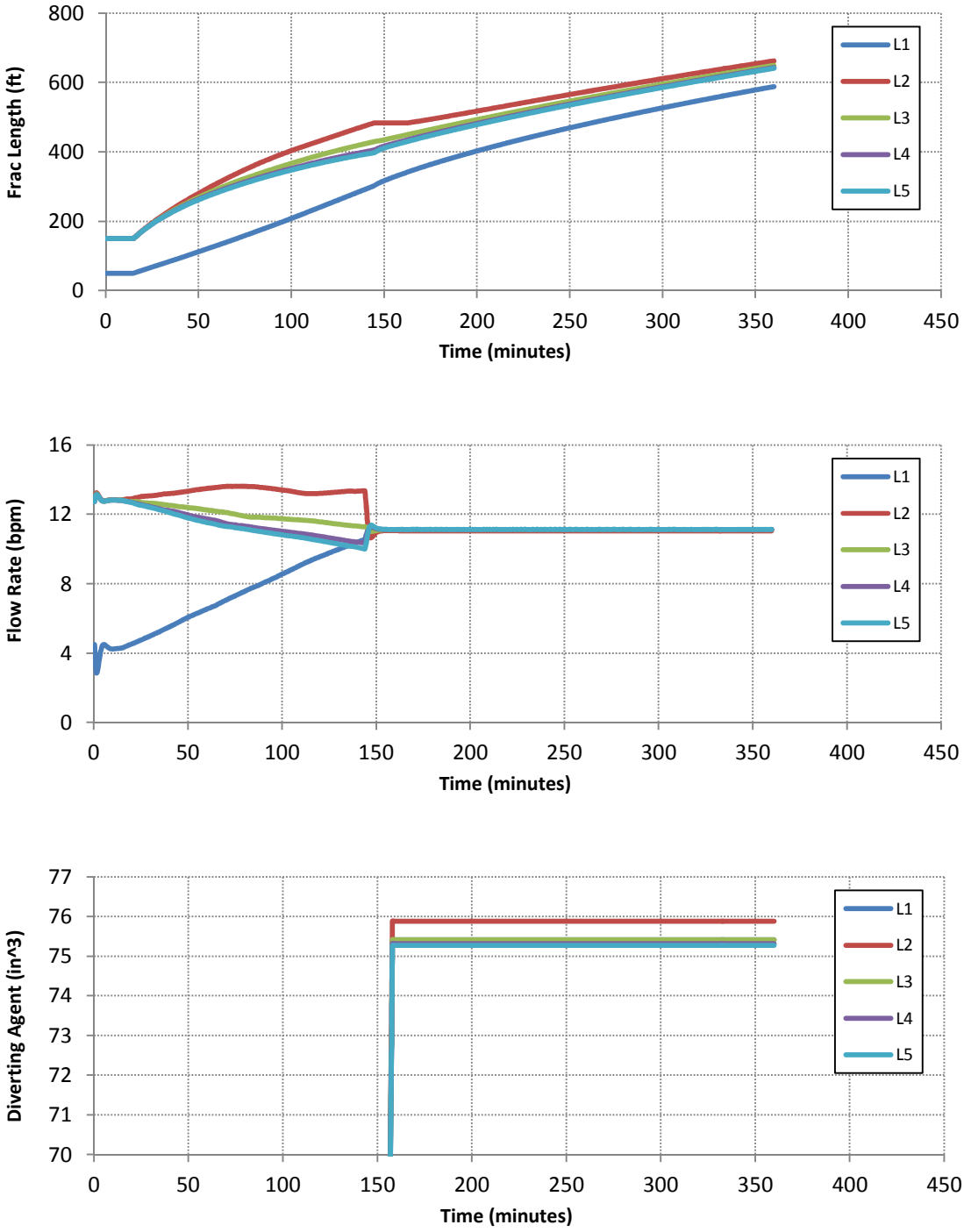

Figure 5-7 – Scenario II, Case B with diverting agent. All fractures are identical, except fracture L4 begins the treatment with a shorter fracture length

Scenario III – Mix of Frac Lengths

In this scenario, the half-lengths of each fracture are varied. Case A (Figure 5-8 and Figure 5-9) and Case B (Figure 5-10 and Figure 5-11) represent different combinations of initial lengths. In Case A, the lengths of the fractures roughly correspond to their position along the wellbore (i.e., fractures closest to the heel have the largest beginning fracture length). The only exception is that fracture L3 is assigned the lowest half length. When no diverting agent is used, the differences between fracture lengths increases since the longer fractures are also closer to the heel and experience less friction. As a result, by the end of the treatment there is a large difference between the longest fracture and the shortest one (about 700 ft).

When diverting agent is applied, the flow rates in the fractures quickly align. The growth rates at the end of the treatment are roughly equal as well. It should be noted that for fracture L1, L2, and L4, the growth rates become 0 for a period of time after the diversion stage. At this point in the treatment, all of the fractures have the same flow rate, but they do not have the same length. For a given flow rate, smaller fractures grow preferentially. In addition, L1, L2, and L4 have higher amounts of diverting agent than the other two fractures. At the end of the treatment, the difference between fracture lengths is much less than in the case without diverting agent, but a distance of roughly 200 feet still exists between the longest and shortest fractures.

In Case B, the fractures closer to the toe have the larger lengths, and so friction forces naturally direct the flow rates and half-lengths to move together. The shorter L1 and L2 fractures end up growing faster than the initially longer L3 and L5 fractures. As a result, the difference between fracture lengths in the case without diverting agent is less than 500 feet, much less than the distance in Case A. When diverting agent is added, the

flow and growth rates quickly equalize, and the maximum distance between the fractures at the end of the treatment is only 154 feet.

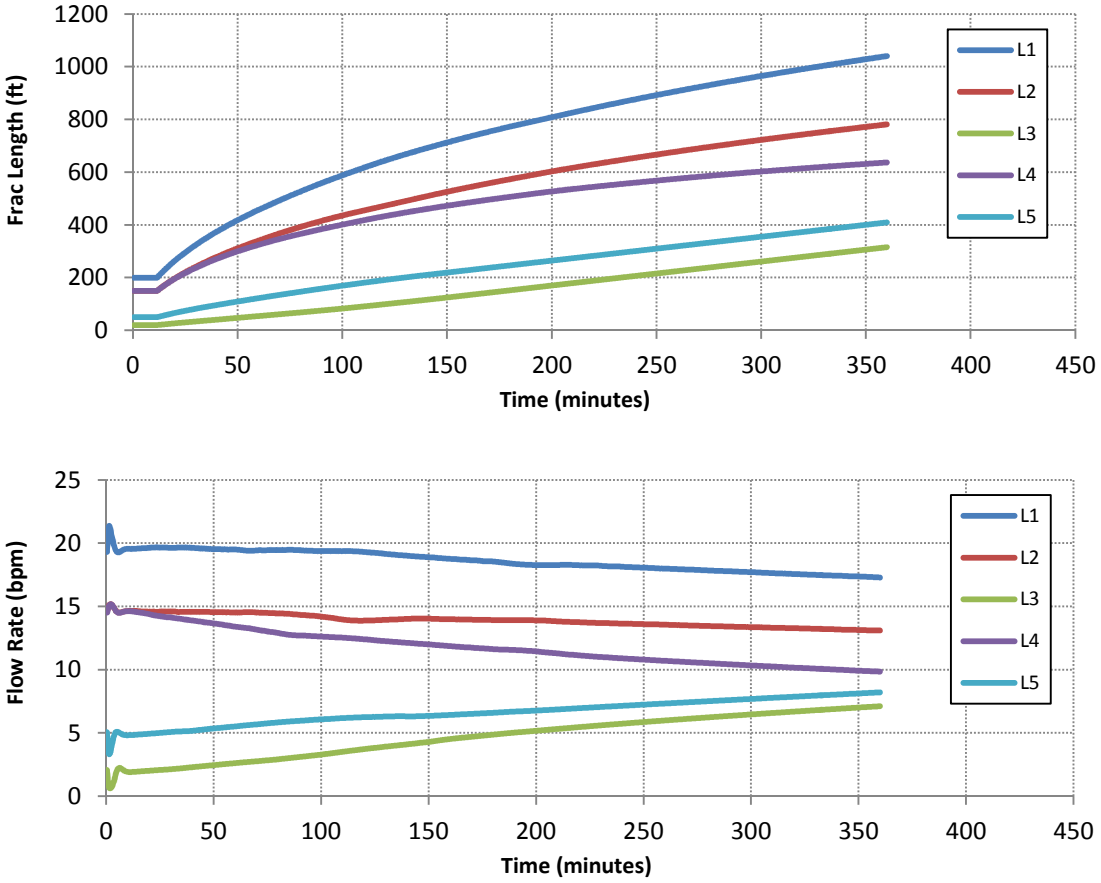

Figure 5-8 – Scenario III, Case A without diverting agent. The fractures begin the treatment with a mix of fracture lengths

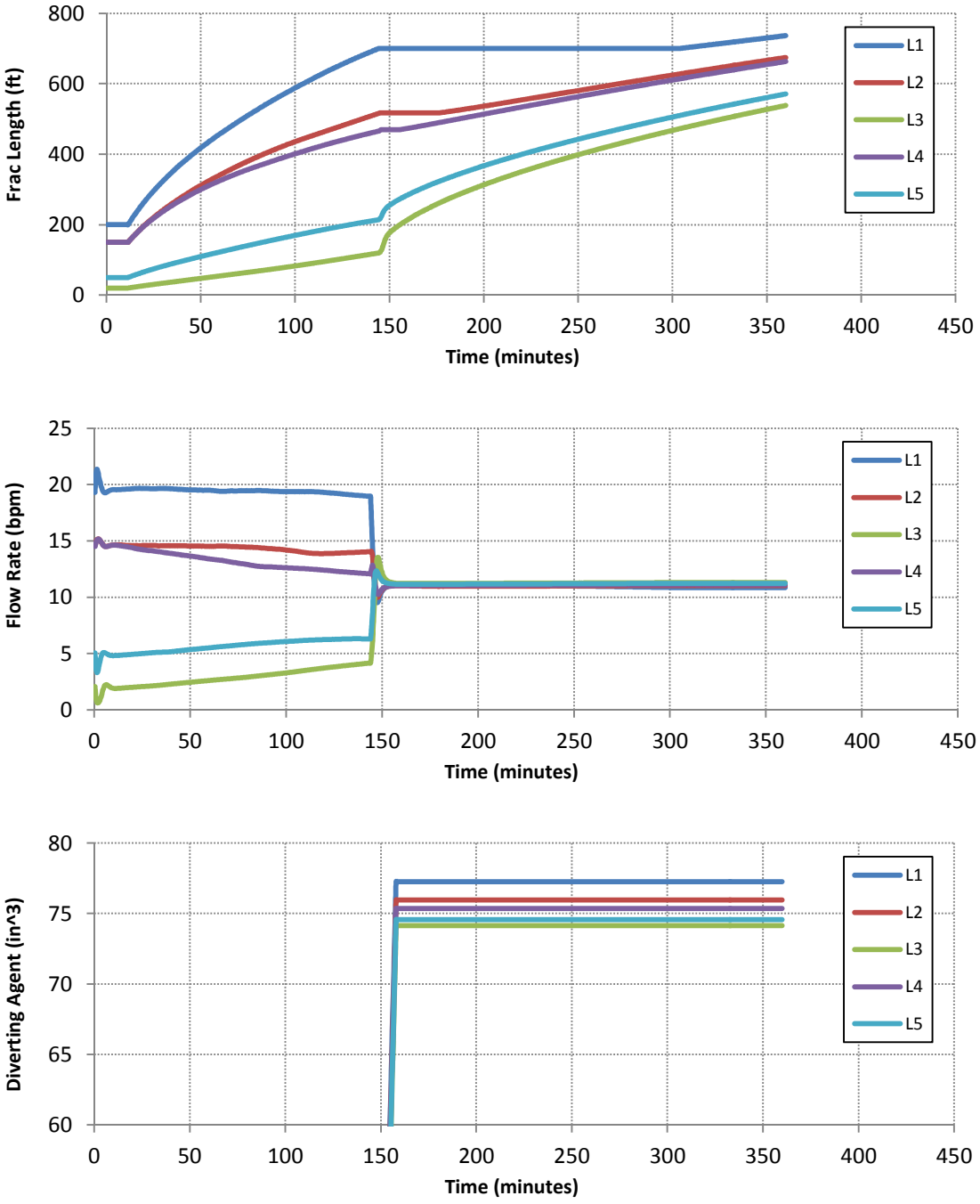

Figure 5-9 - Scenario III, Case A with diverting agent. The fractures begin the treatment with a mix of fracture lengths

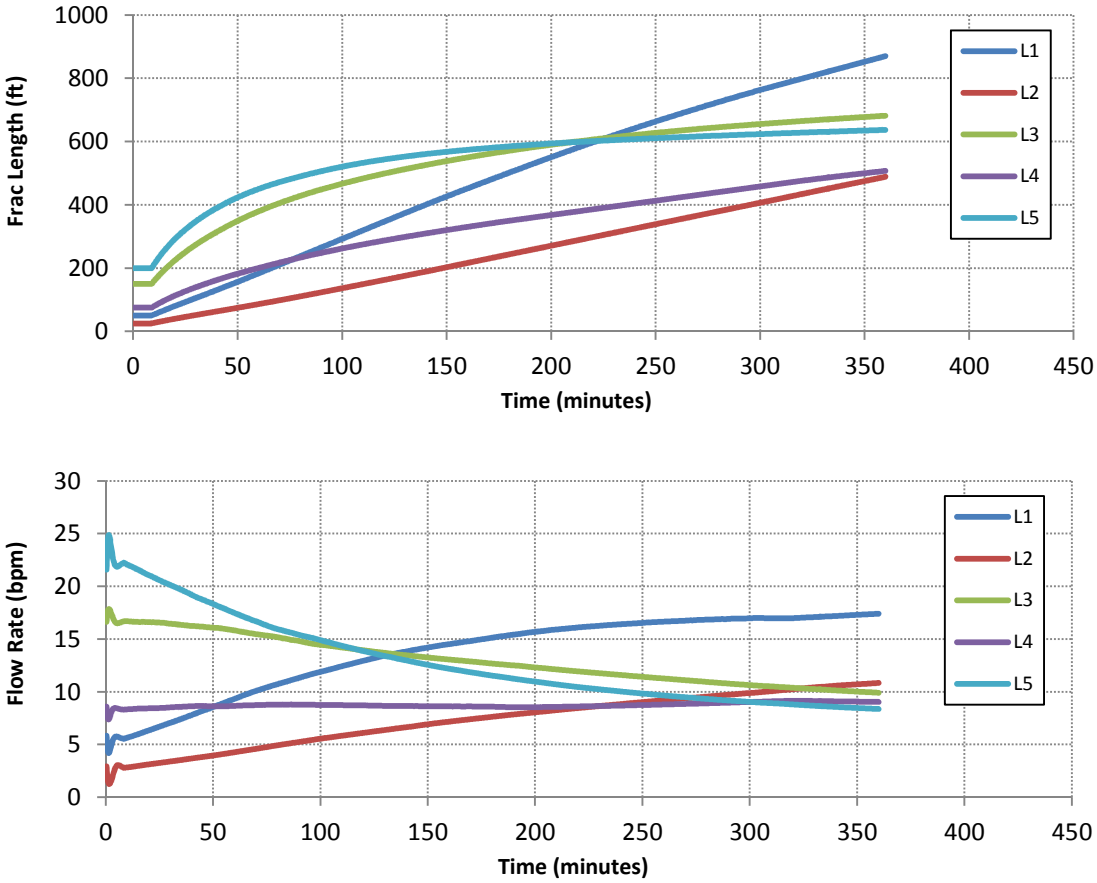

Figure 5-10 - Scenario III, Case B without diverting agent. The fractures begin the treatment with a different mix of fracture lengths than those in Case A

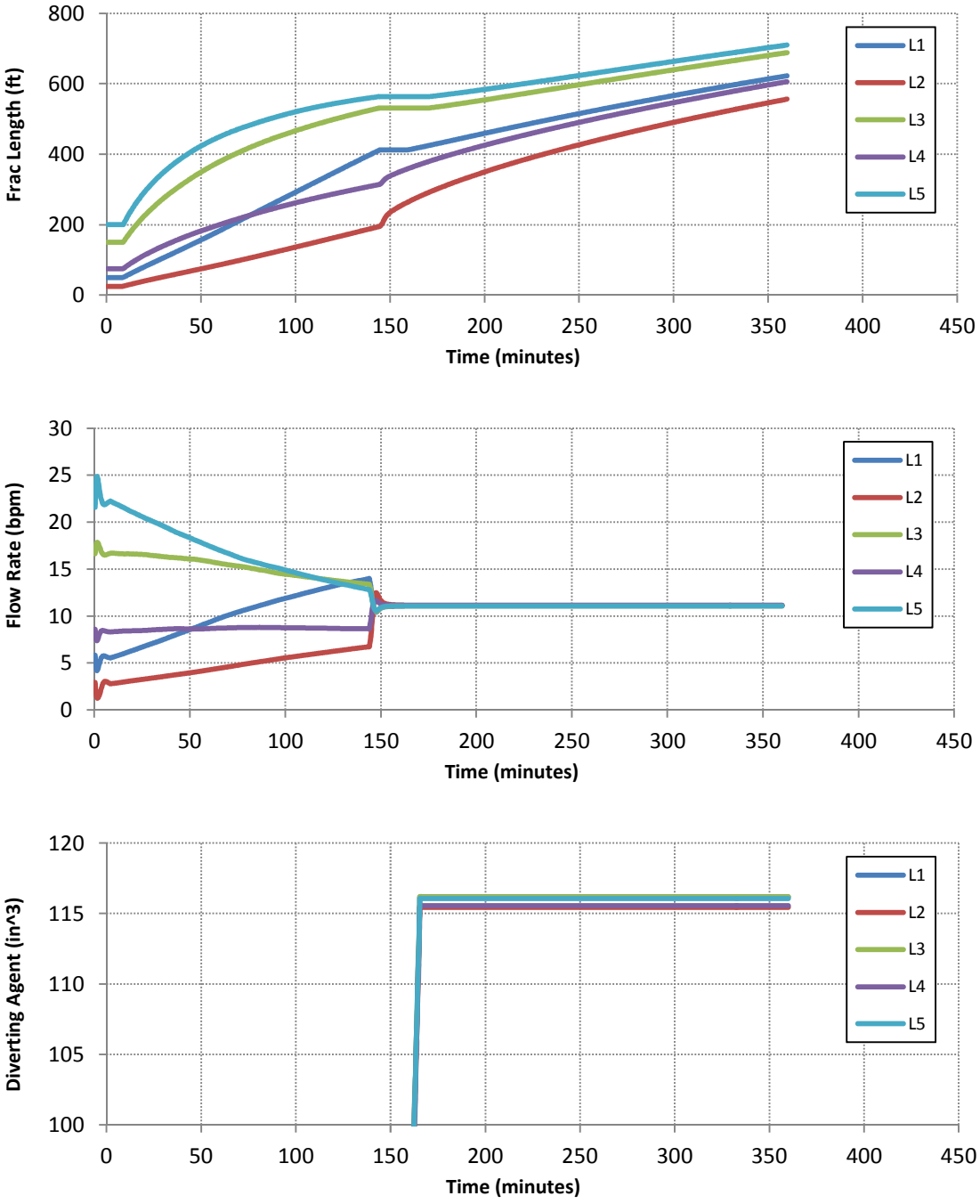

Figure 5-11 - Scenario III, Case B with diverting agent. The fractures begin the treatment with a different mix of fracture lengths than those in Case A

Scenario IV – Diverting Agent Stage Duration

This scenario demonstrates the effect of changing the duration of the diverting agent stage. Using the input file from Scenario III, the length of the diverting agent stage is changed from 29 minutes to 2.9 minutes (the stage still begins at 144 minutes). Interestingly, the change produces a very pronounced effect. The fractures that began the treatment with shorter lengths end with much higher lengths than they did in Scenario III. Essentially, reducing the length of the diverting agent stage paradoxically resulted in a higher degree of diversion. This effect occurred in both cases.

The explanation for this result can most easily be seen when comparing the zoomed in graph of Figure 5-3 with the flow rate graphs of Figure 5-12 and Figure 5-13. In the first graph, the sudden flipping of the relative order of fractures with respect to flow rates is only transient, and the flow rates of the fractures eventually equalize. Whereas, in Figure 5-12 and Figure 5-13, a permanent disparity between flow rates of the fractures holds in which the fractures that started out with the lowest flow rates now have the highest rates. The shortened length of the diverting agent stage allows this disparity to remain. Figure 5-3 shows the same disparity between flow rates immediately after the application of diverting agent. However, as diverting agent continued to be deposited, the disparity in flow rates quickly diminishes. Limiting the application of diverting agent allows the inequality in flow rates to remain.

The end result of the adjustment made in this scenario is that the previously shorter fractures attain a much higher fracture length. The maximum distance between the fractures for Case A is 218 feet, roughly the same as in Scenario III. In Case B, the maximum distance is 130 feet, a slight reduction from Scenario III.

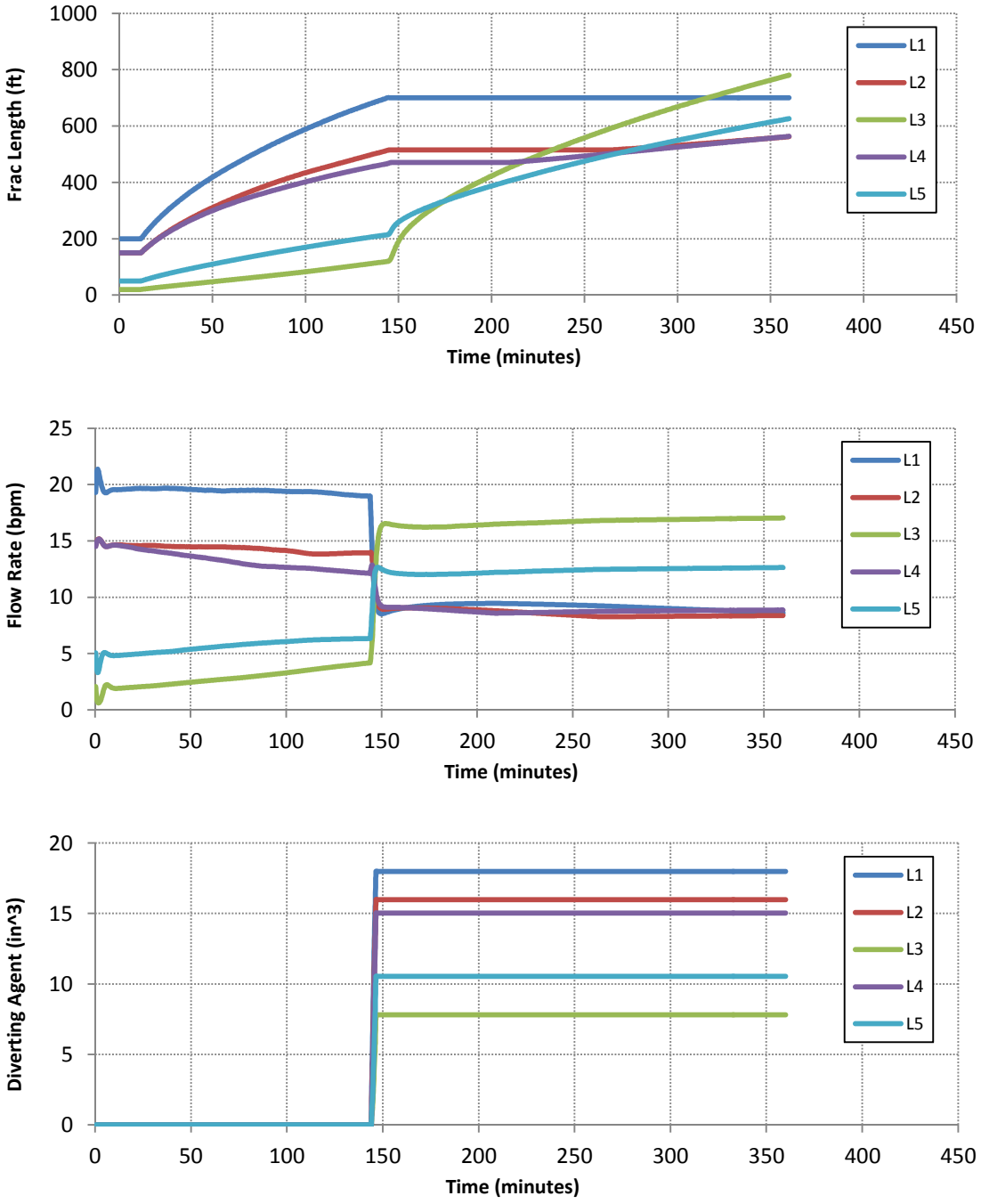

Figure 5-12 – Scenario IV, Case A. The fracture system is the same as in Scenario III Case A, except the duration of the diverting agent stage is reduced from 29 minutes to 2.9 minutes. The reduced length results in a permanent disparity in flow rates between the fractures after the diverting agent stage

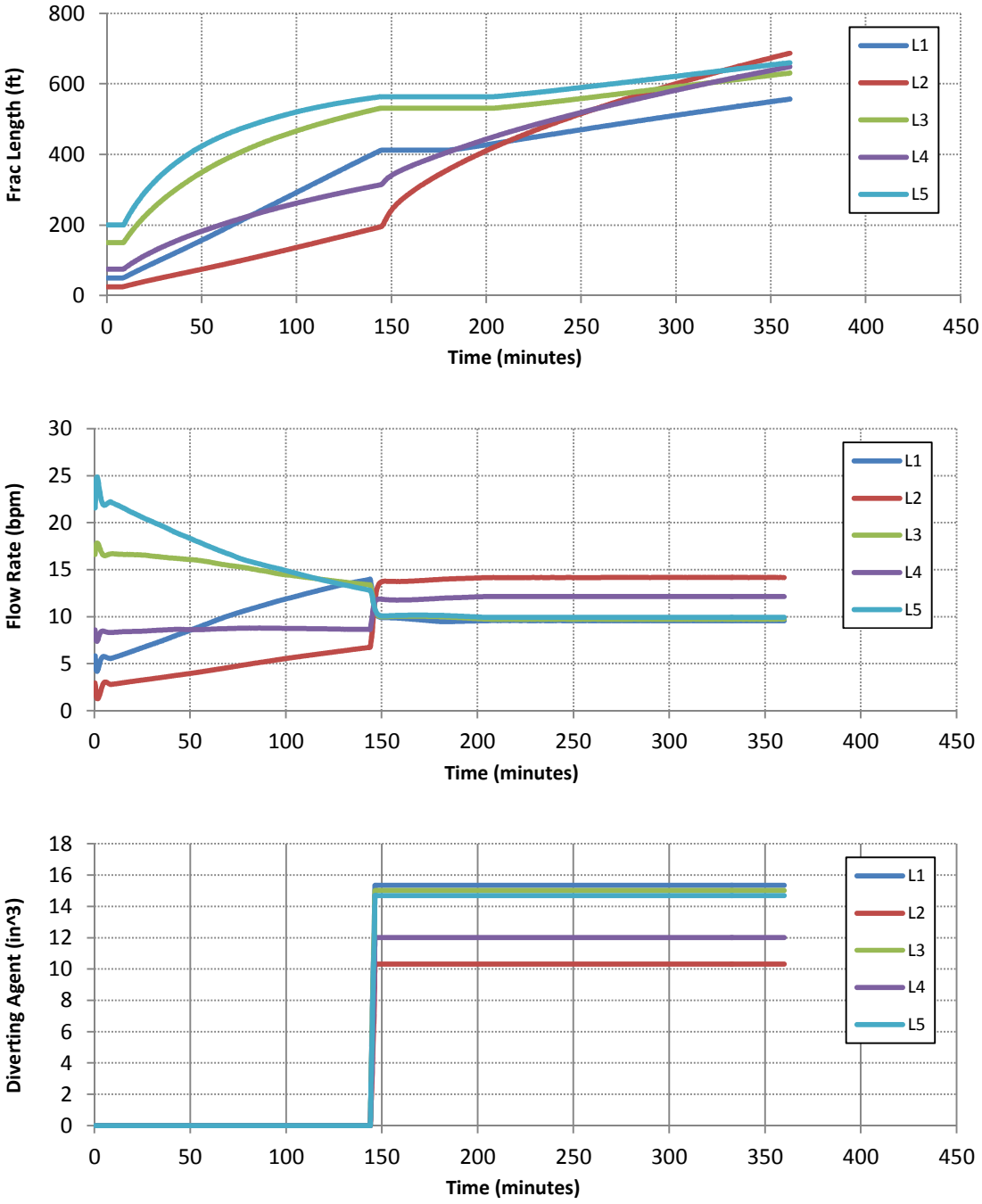

Figure 5-13 - Scenario IV, Case B. The fracture system is the same as in Scenario III Case B, except the duration of the diverting agent stage is reduced from 29 minutes to 2.9 minutes. The reduced length results in a permanent disparity in flow rates between the fractures after the diverting agent stage

Scenario V – Addition of a Second Diverting Agent Stage

In the previous scenario, the reduction in the timing of the diverting agent stage significantly changed fracture propagation, but the change did not result in more equal fracture lengths. As demonstrated by the figures in the previous scenario, the growth rates are not equivalent near the end of the fracture. This scenario adds a second diverting agent to equalize these growth rates near the end of the treatment in order to achieve a higher degree of similarity in lengths between the fractures. The second diverting agent stage is added from 274 minutes to 288 minutes, and the volume fraction of the stage is also 5×10^{-5}. In addition, the treatment is extended to 500 minutes so that the full effect of the second stage can be seen. All other parameters are identical to those used in Scenario IV.

The first part of the treatment is the same as that from Scenario IV. The shortened length of the first diversion stage causes a higher flow rate and faster growth in the shorter fractures. The second diverting agent stage is longer than the first (the diverting agent plots of Figure 5-14 and Figure 5-15 show that the second stage deposits the majority of the diverting agent). The effect is that the flow rates between the fractures immediately equalize after the second diverter stage. This leads the growth rates to also equalize. Since the second diverting agent stage is timed when the fracture lengths are already close, the equalization of the growth rates keeps the disparity in fracture lengths small. The addition of a second stage significantly reduces the maximum distance between the fractures. In Case A, the distance is reduced from 218 feet to 97 feet, and in Case B it is reduced from 130 feet to 82 feet.

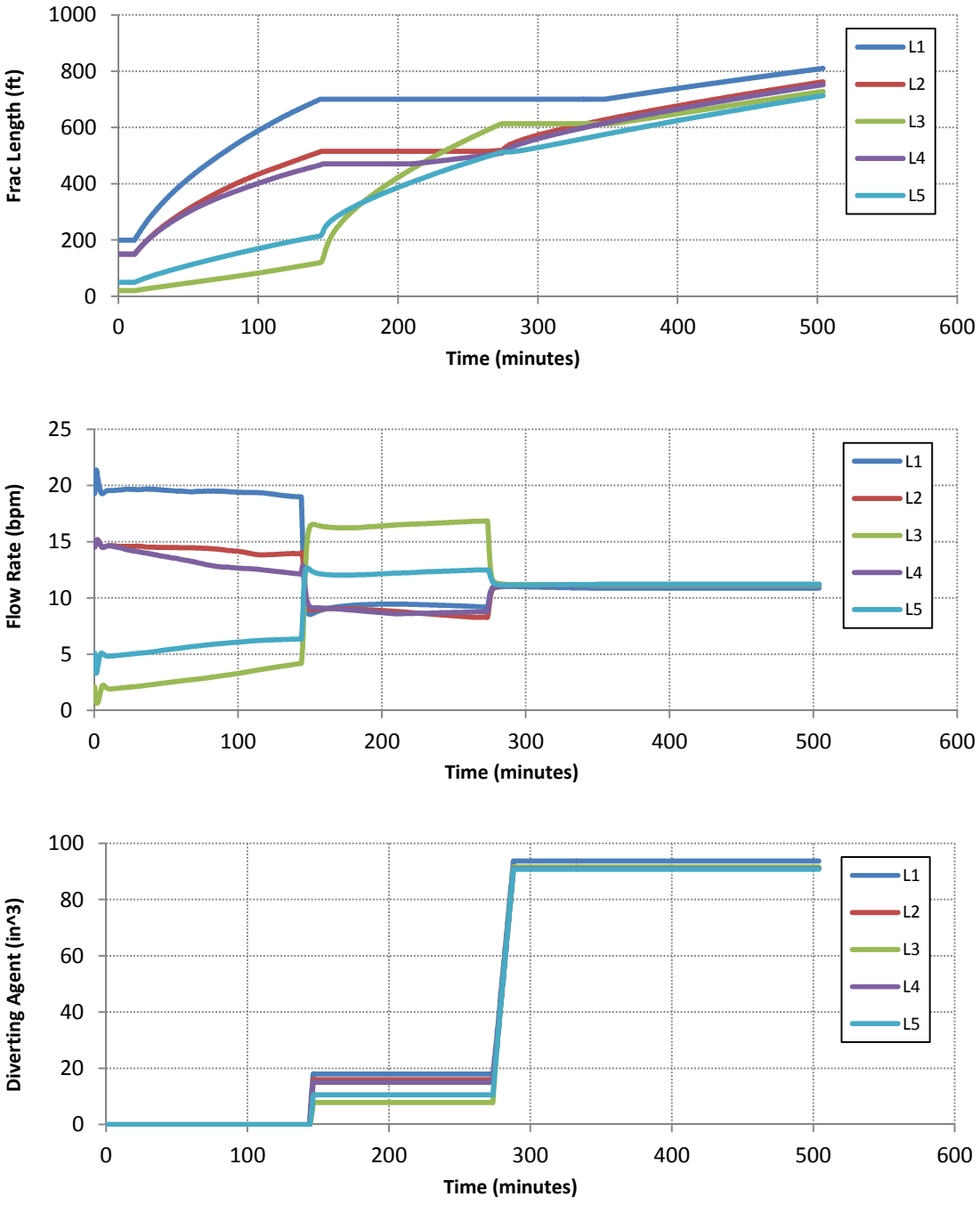

Figure 5-14 - Scenario V, Case A. The fracture system is the same as in Scenario IV Case A, except a second diverting agent stage is added from minute 274 to 288. The second stage equalizes growth and flow rates between the fractures, leading to more similar fracture lengths

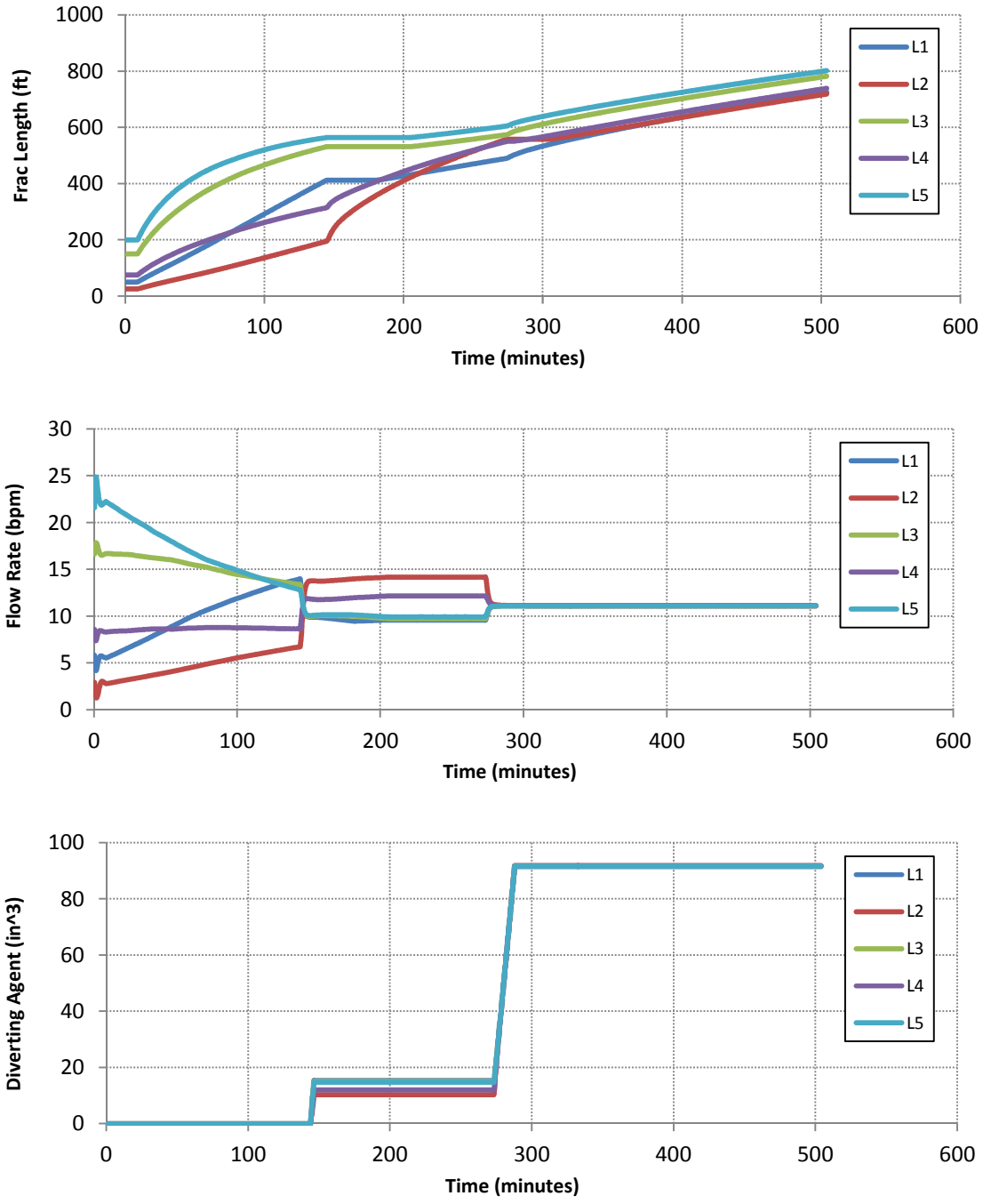

Figure 5-15 - Scenario V – Case B. The fracture system is the same as in Scenario IV Case B, except a second diverting agent stage is added from minute 274 to 288. The second stage equalizes growth and flow rates between the fractures, leading to more similar fracture lengths

Scenario VI – Sensitivity to Diverting Agent Cake Permeability

In Scenario VI, the sensitivity of the system to the permeability of the diverting agent cake is investigated by using three different values of permeability. All other parameters are identical to those in Scenario V, Case A. In Case A (Figure 5-16), the permeability is increased from 1 Darcy to 10 Darcies. The only obvious impact is the change in the flow rate graph. If the diverting agent is thought of as a feedback mechanism, then the increase in permeability results in a much "softer" feedback response. Unlike the behavior seen in Scenario V, the flow rate in L3 continues to build after the first diverting agent stage. Changes in flow rates are also observed in the other fractures during the period between the two diverting agent stages. Essentially, the higher permeability of the diverting agent cake redirects flow at a slower pace.

The difference in the flow rates is insufficient to cause a significant impact on the fracture length plot. The only change is a slight reduction in the growth of fracture L3. This occurs because the higher permeability causes the flow rate to drop to the bottom of the pack after the second diverting agent stage.

A more significant change is seen when the diverting agent permeability is greatly increased from 10 Darcies to 100 Darcies (Case B, Figure 5-17). Such a high permeability value is shown to limit the extent of diversion. A very slow response is seen in the flow rate graph after the first diverting agent stage. As a result, fracture growth for L3 and L5 is much lower than in the previous scenario and fractures L2 and L4 grow at their expense. The maximum distance between the fracture half lengths at the end of the treatment is 234 feet, much greater than in the previous scenario but still much better than the case without diverting agent (Figure 5-8).

The reduction in permeability to 100 mD in Case C (Figure 5-18) also has a large impact on the behavior of the system. The benefits of reducing the duration of the

first diverting agent stage are largely nullified by the decrease in permeability. The flow rate graph shows that only a very small disparity in flow rates persists after the application of diverting agent. As a result, there is also little disparity between the growth rates, and fractures L3 and L5 remain much shorter than the other fractures. The second stage equalizes the flow rates, but since the disparity is already so small, little effect is seen and the fractures continue on the same path as before. Just as in the instance when the diverting agent stage was longer, the lower permeability diverting agent results in a very strong response that minimizes the amount of diversion that can take place. The maximum distance between the fracture half-lengths for this case is 161 feet.

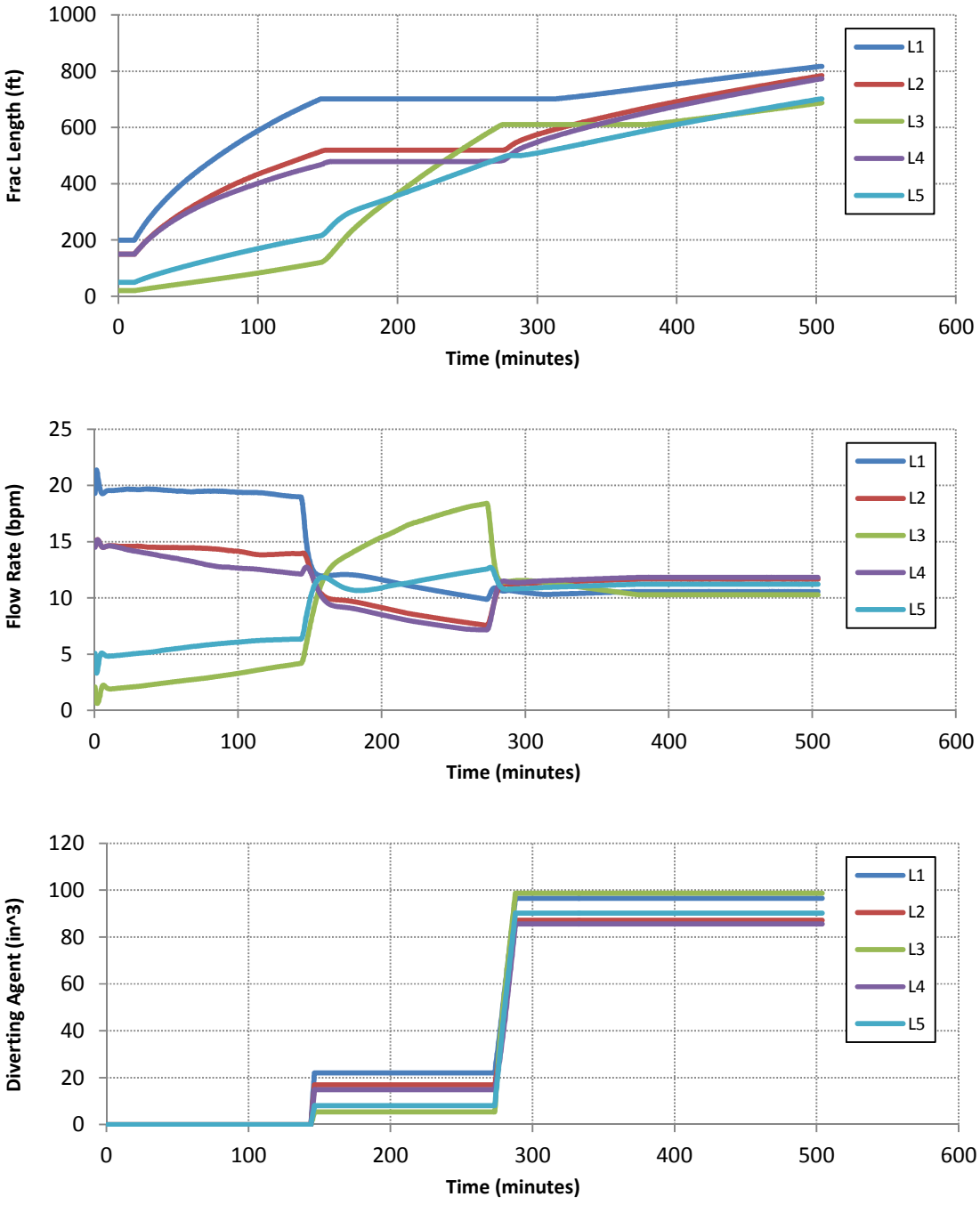

Figure 5-16 – Scenario VI – Case A. Fracture system is identical to Scenario V, Case A, except the permeability of the diverting agent cake is changed from 1 Darcy to 10 Darcies

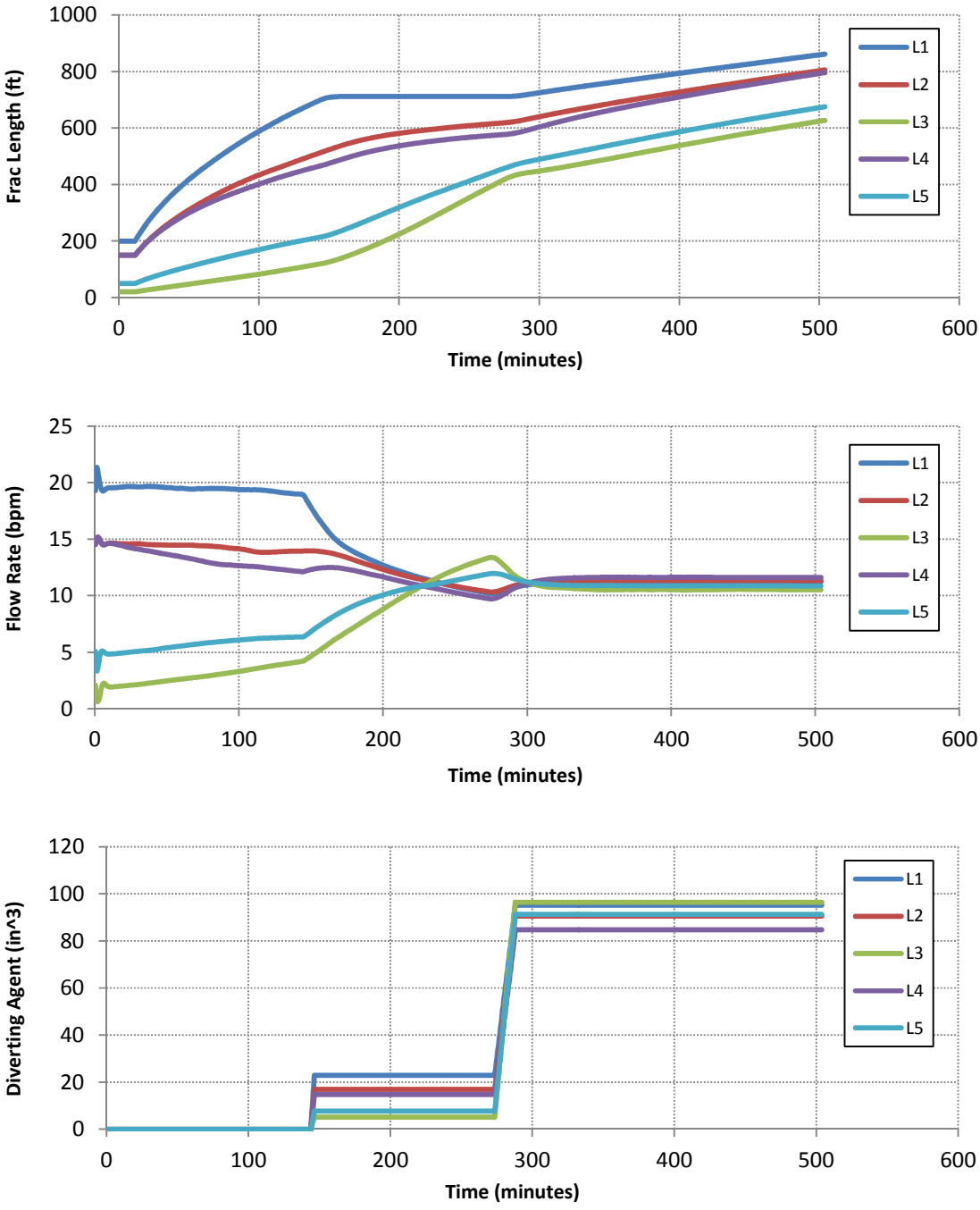

Figure 5-17 - Scenario VI – Case B. Fracture system is identical to Scenario V, Case A, except the diverting agent cake is increased from 1 Darcy to 100 Darcies

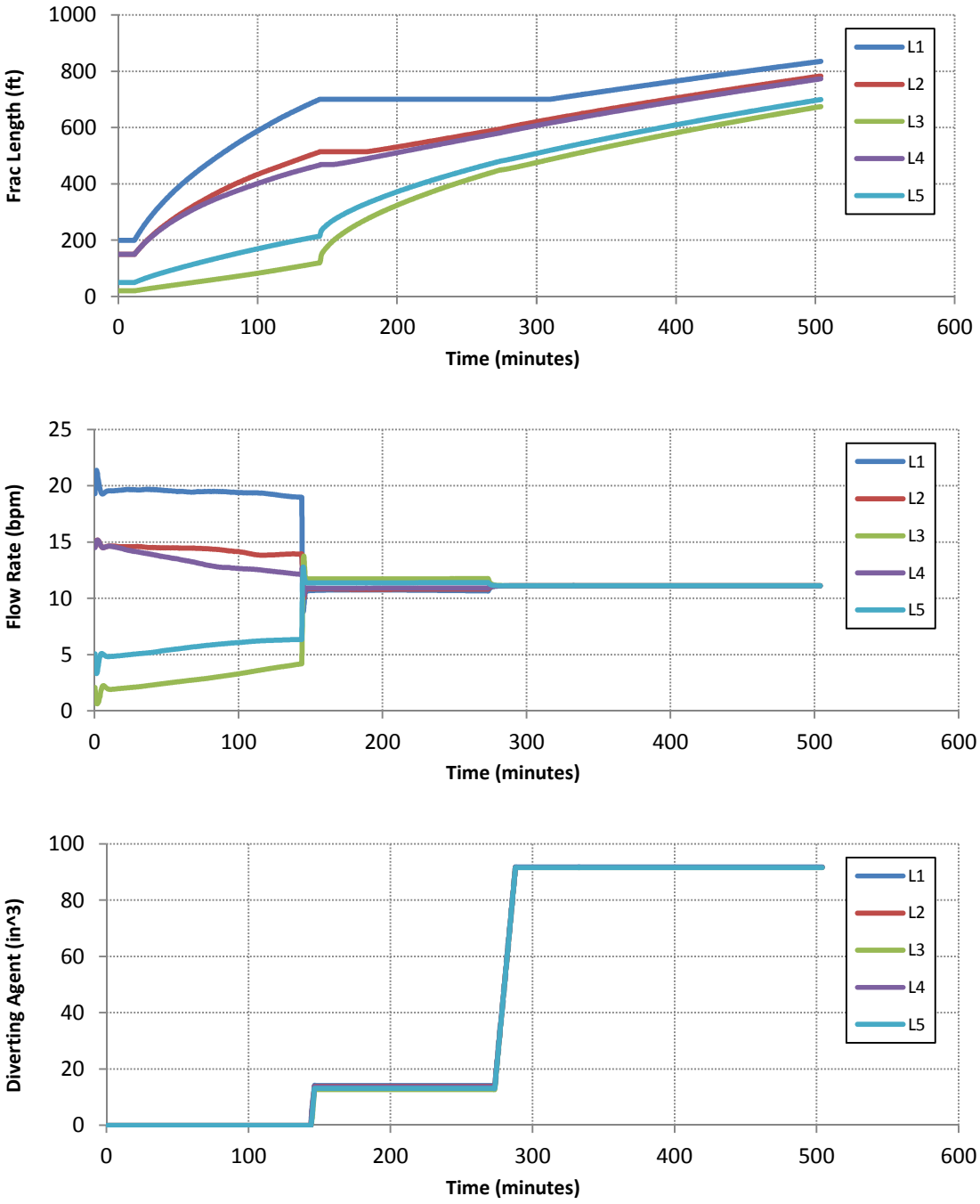

Figure 5-18 - Scenario VI – Case C. Fracture system is identical to Scenario V, Case A, except the permeability of the diverting agent cake is decreased from 1 Darcy to 100 mD

Scenario VII – Sensitivity to Volume Fraction of Diverting Agent

In Scenario VII the sensitivity of the system to diverting agent volume fraction is investigated. The direct result of changing the volume fraction is a change in the pressure drop due to the diverting agent, so the responses seen here are similar to those for a change in diverting agent permeability. However, the diverting agent volume is constrained by the volume of the perforations, so a large range of volume fractions is not investigated.

Both cases show very little change from the results of Scenario V. The reduction in diverting agent volume from Case A shows a similar response to that from the increase in diverting agent permeability. The response is softer, and the flow rates are still changing after the application of the diverting agent. In Case B, the increase in diverting agent results in a stronger response, and the disparity between flow rates is reduced. As a result, there is a smaller difference in fracture growth rates, and the maximum distance between fractures increases from 82 feet to 111 feet. In Case A, the maximum distance between the fractures is 129 feet, almost identical to that from Scenario V.

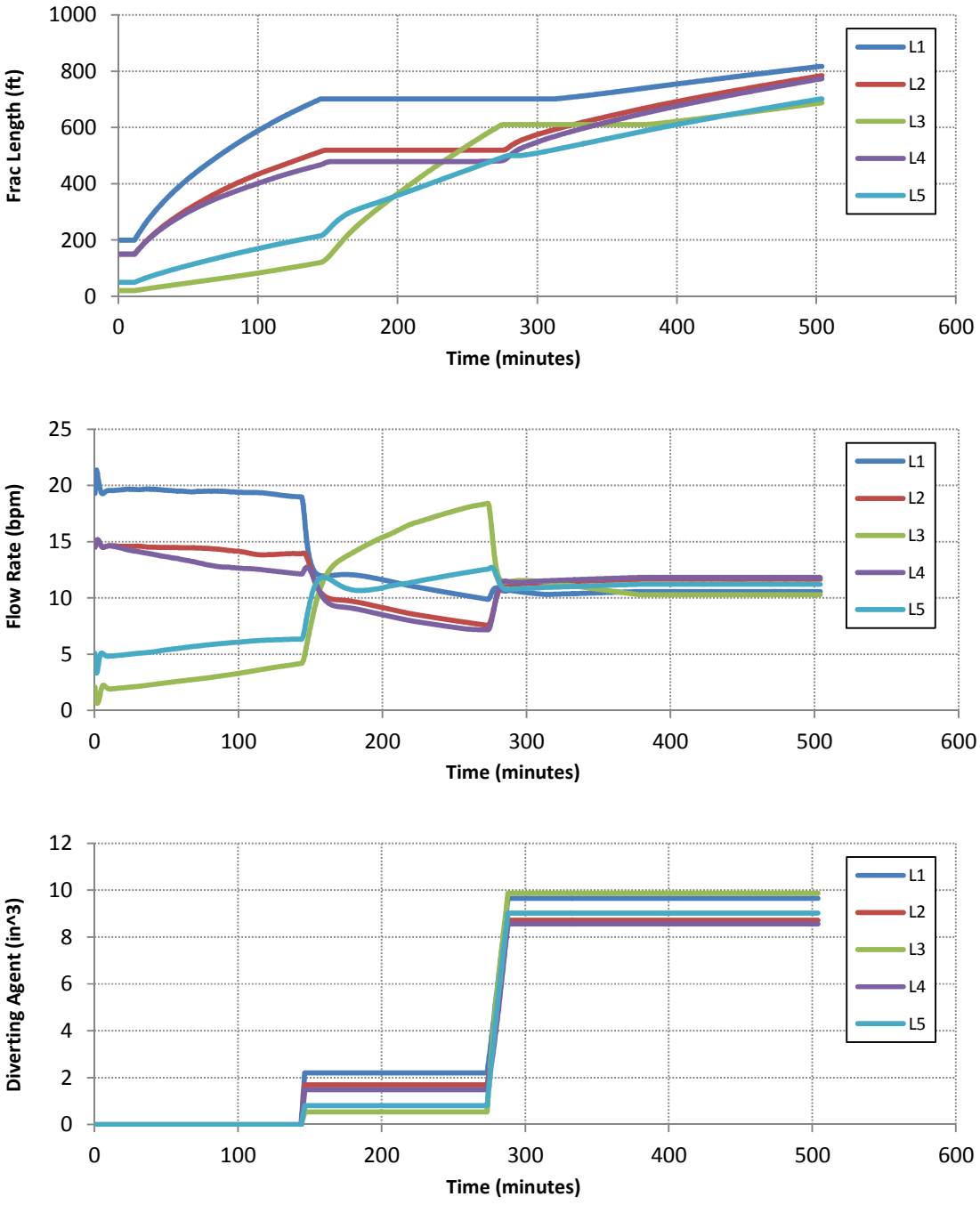

Figure 5-19 – Scenario VII – Case A. Fracture system is identical to Scenario V, Case A, except the volume fraction of the injected diverting agent is decreased from 5E-5 to 5E-6.

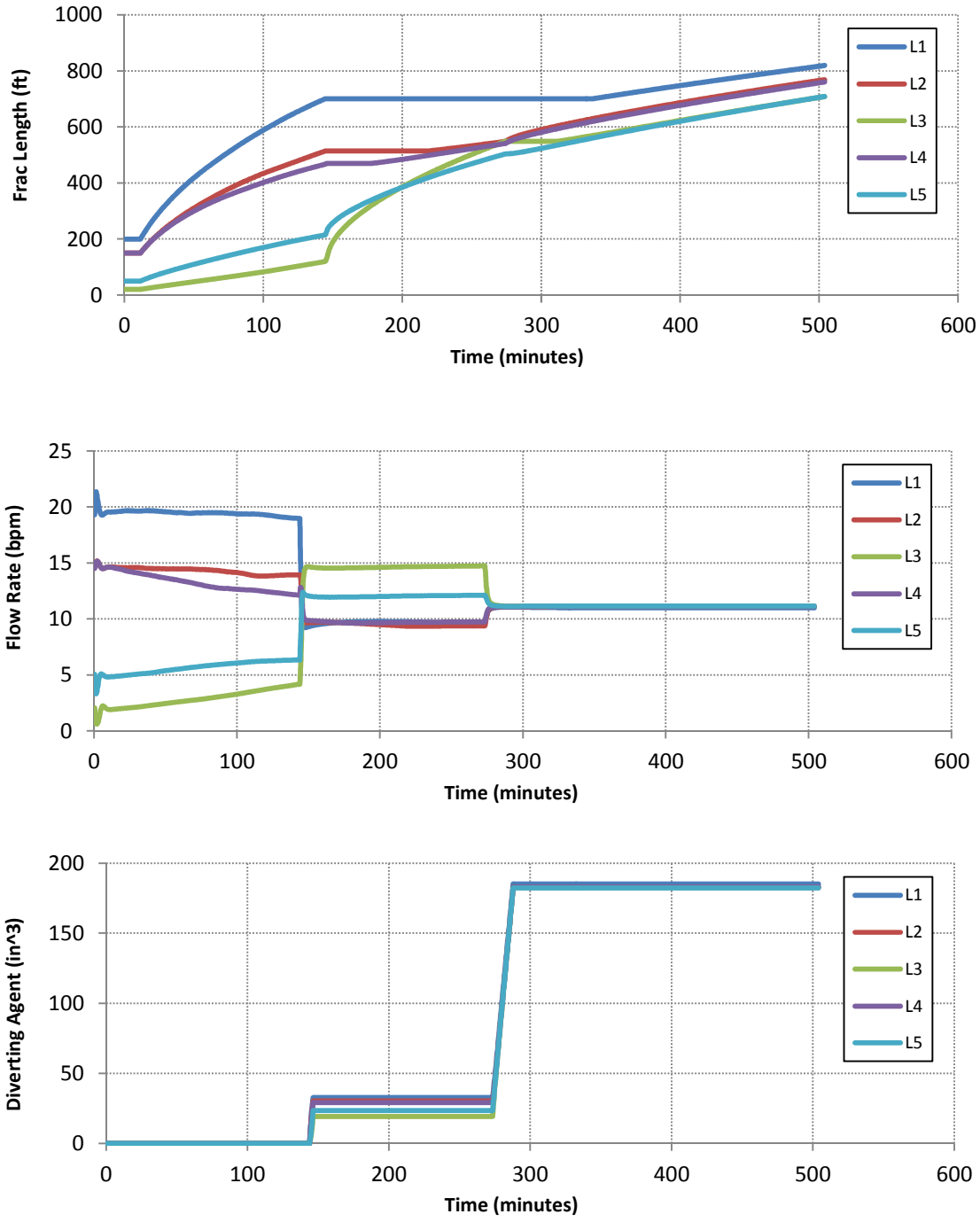

Figure 5-20 – Scenario VII – Case B with diverting agent. Fracture system is identical to Scenario V, Case A, except the volume fraction of the injected diverting agent is increased from 5E-5 to 1E-4.

Scenario VIII – Importance of Tuning Parameters for Successful Diversion

The simulations in Scenario VIII (Figure 5-21) demonstrate that the success of the refracture treatment is dependent upon the combination of diverting agent parameters. In the previous scenarios, only one parameter was adjusted and the resulting performance discussed. However, the analysis should not lead the reader to believe that the values that resulted in success are the only optimum values for that parameter. Instead, the optimum value for a particular parameter is dependent upon the values used for the other parameters. As a result, the parameters of a refracture treatment must be tuned to each other and to the environment in which the treatment will be used.

In this scenario, the diverting agent cake permeability was reduced to 100 miliDarcies, and the volume fraction was reduced to 5×10^{-6}. All other parameters are identical to Scenario V, Case A. Scenario VI demonstrated that the reduction of permeability increased the maximum distance between the fractures. However, the simulations in this scenario show that a permeability of 100 miliDarcies can result in just as successful of a diversion when coupled with a reduction in diverting agent volume, as these two changes oppose one another. The decrease in permeability raises the pressure drop, while the reduction in diverting agent decreases the pressure drop. As a result, the results are very similar to those for Scenario V Case A, and the maximum distance between the fractures remains at 97 feet.

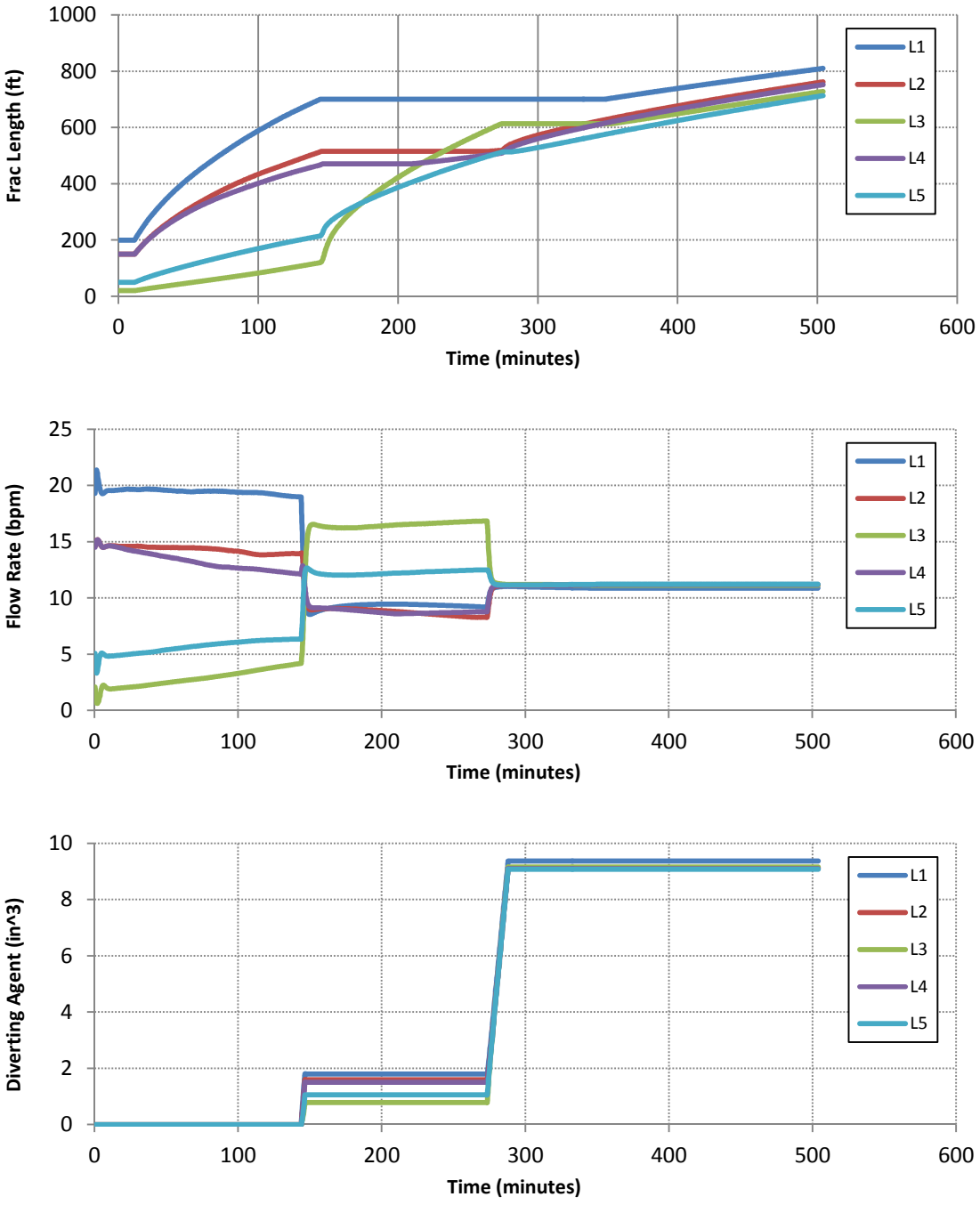

Figure 5-21 - Scenario VIII with diverting agent. Fracture system is identical to Scenario V, Case A, except the permeability of the diverting agent cake is reduced from 1 Darcy to 100 mD and the volume fraction of the injected diverting agent is reduced from 5E-5 to 5E-6.

Scenario IX – Sensitivity to Pumping Rates

In Scenario IX, the sensitivity of the system to the injection rate of the fracturing fluid is investigated. Case A increases the pumping rate from 56 bpm to 69 bpm, and Case B decreases it to 28 bpm. In Case A (Figure 5-22), as expected, the increase in pumping rate results in faster fracture propagation for all fractures. Apart from this occurrence, little change is seen in the overall pattern, aside from a slight reduction in the position of fracture L3 (it moves away from fracture L4 and closer to L5).

In Case B, the large drop in pumping rate has a significant impact on the system. As expected, the fracture lengths are smaller; but additionally, the overall pattern of the system has shifted. The first diverting agent stage diverts much more flow to fracture L3, and its growth rate accelerates accordingly. As a result, it becomes the longest fracture for a portion of the treatment. This result can be explained by the relative increase or decrease in the importance of friction. The flow into a fracture is governed by the relation of its resistance to that of the other fractures. The effects from both friction and diverting agent are incorporated into this resistance. The pressure drop due to friction is related to the flow rate, so as the flow rate is adjusted, so too is the magnitude of the friction forces. As a result, when the pumping rate is decreased, the fraction of the resistance due to friction decreases, and that due to diverting agent increases. This explains why more diversion occurs in Figure 5-23. As the pumping rate drops, the diverting agent has a larger effect on the relative differences between the resistances of the fractures. The change in pumping rate is smaller in Case A, and so the effect is smaller. However, this principle can also explain why fracture L3 has slightly less fracture growth than in Scenario V.

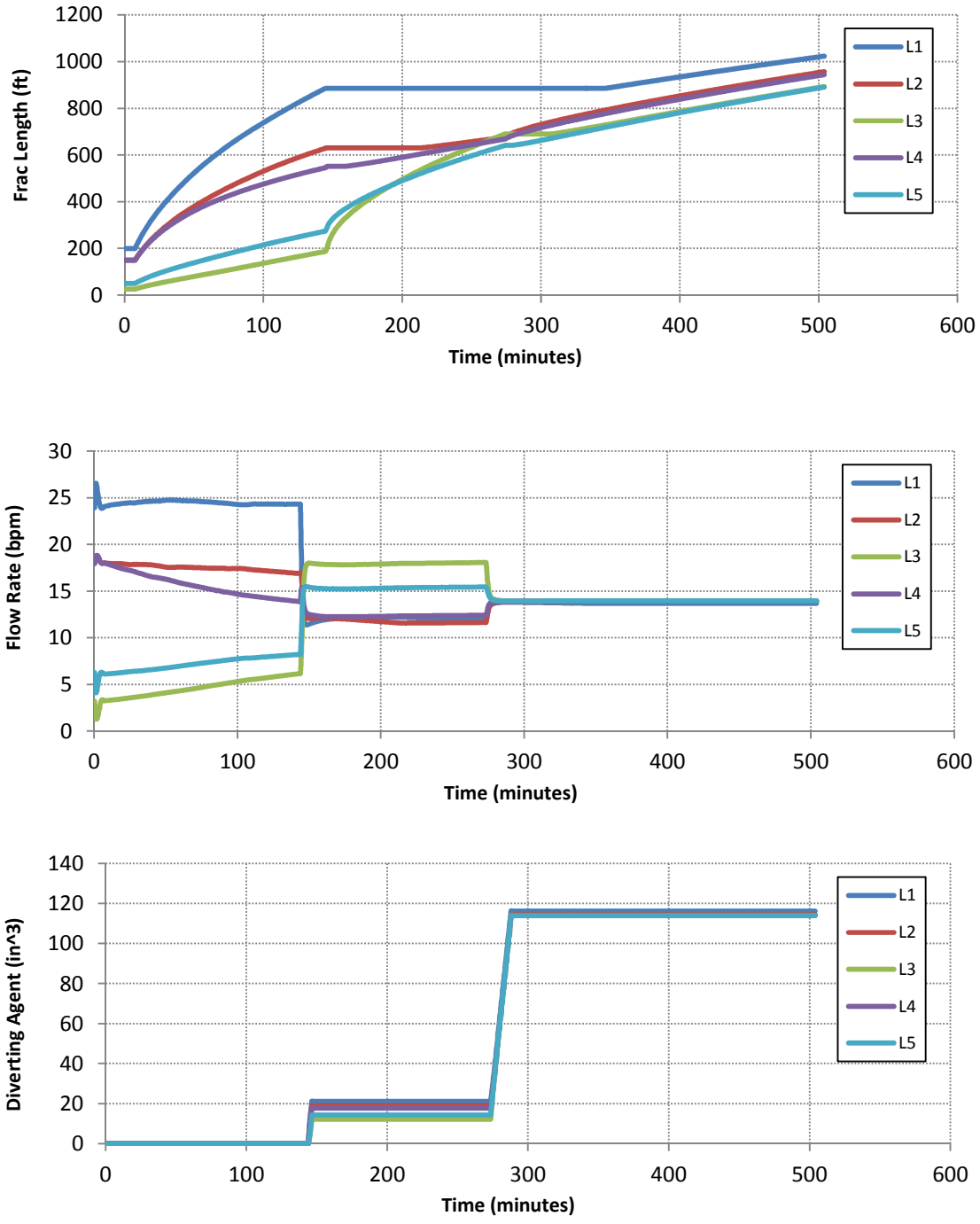

Figure 5-22 - Scenario IX, Case A with diverting agent. Fracture system is identical to Scenario V, Case A, except the pumping rate is increased from 56 bpm to 69 bpm.

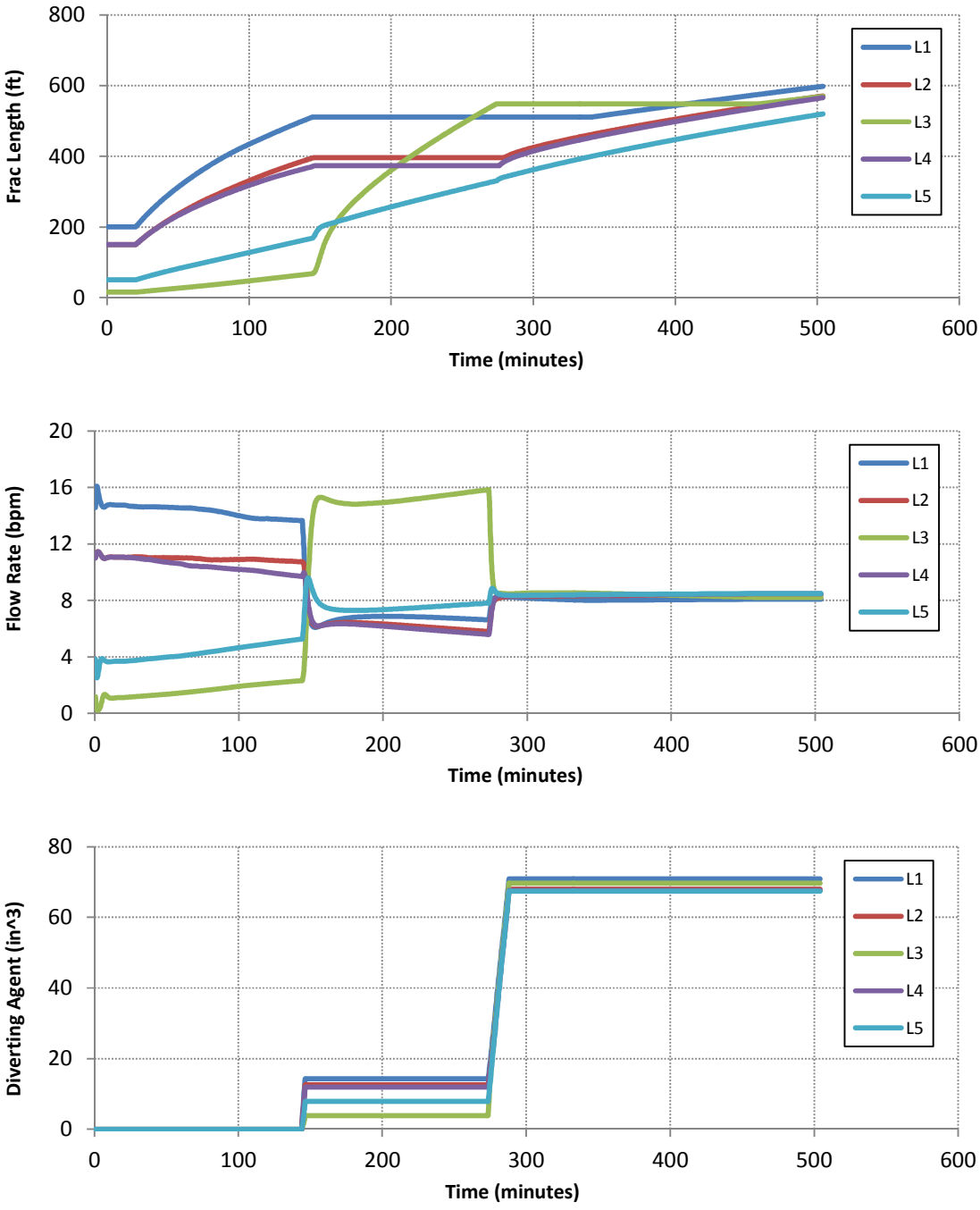

Figure 5-23 - Scenario IX, Case B with diverting agent. Fracture system is identical to Scenario V, Case A, except the pumping rate is decreased from 56 bpm to 28 bpm.

Scenario X – Sensitivity to Fracture Propagation Pressure

In Scenario X, the sensitivity of the system to fracture propagation pressure is investigated. All other parameters are identical to Scenario V. The effects are significant. In each case, just a 1% reduction in the fracture propagation pressure of the rock diverts a large majority of flow to the fractures with lower P_{frac} values and shuts off growth in the other fractures (Figure 5-24 and Figure 5-26). Such cases are very problematic in field scenarios, as portions of the reservoir will never be accessed. As a result, these are great candidates for refracturing with diverting agents.

As seen in Figure 5-25 and Figure 5-27, the diverting agent successfully diverts flow and growth to the underperforming fractures with the stronger rock. The same principle applies in this scenario as in previous ones: the faster growing fractures receive more diverting agent and flow subsequently moves to the slower growing fractures. The application of the second diverting agent stage does not have as strong of an effect because there is little disparity in flow rates after the first diverting agent stage. The maximum distances between fractures at the end of the treatment is large compared to the other scenarios, but much smaller than the case without diverting agent. In Case A, the maximum distance is 180 feet, while it is 1197 feet when no diverting agent is used. In Case B, the maximum distance is 230 feet, while it is 1428 feet when no diverting agent is used. These simulations indicate that, without diverting agent, only the fractures with the lowest fracture propagation pressures will be stimulated, and that diverting agent allows the fracturing fluid to be more equitably distributed across the length of the lateral.

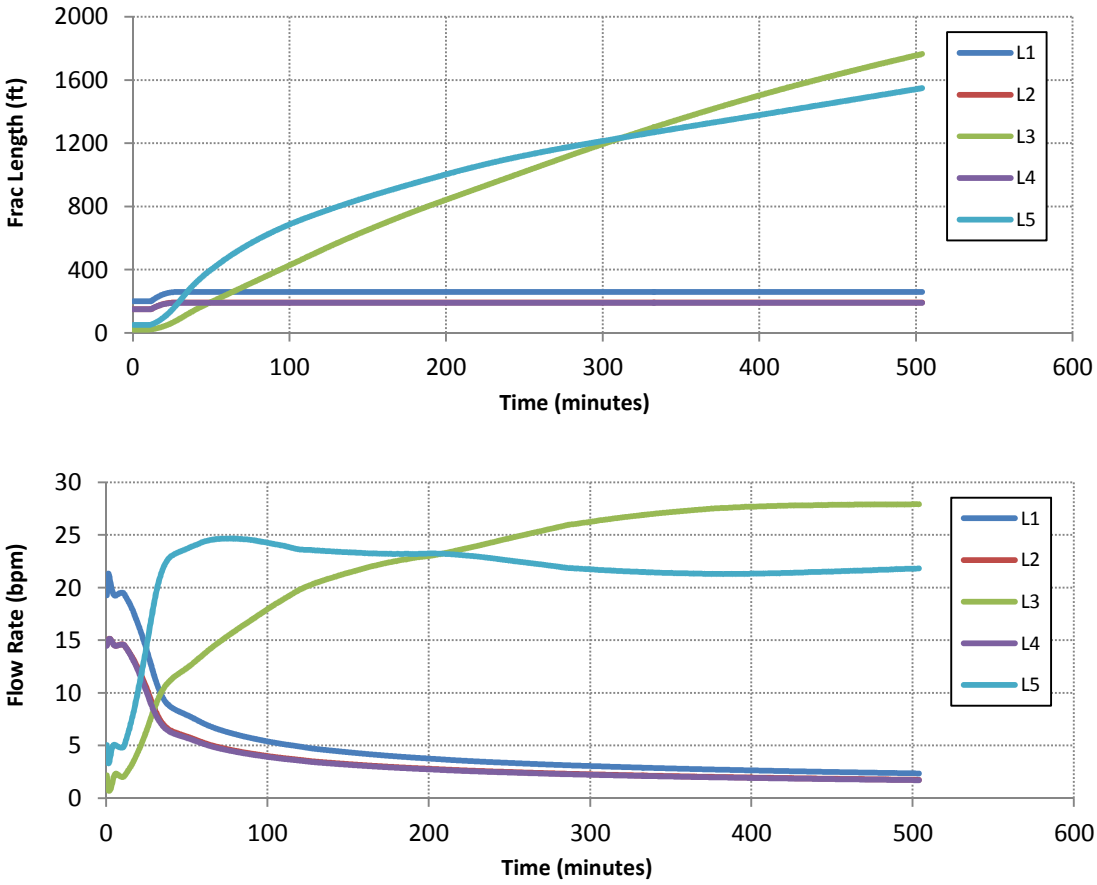

Figure 5-24 - Scenario X, Case A without diverting agent. Fracture system is identical to Scenario V, Case A, except the fracture propagation pressure is decreased for fractures L3 and L5.

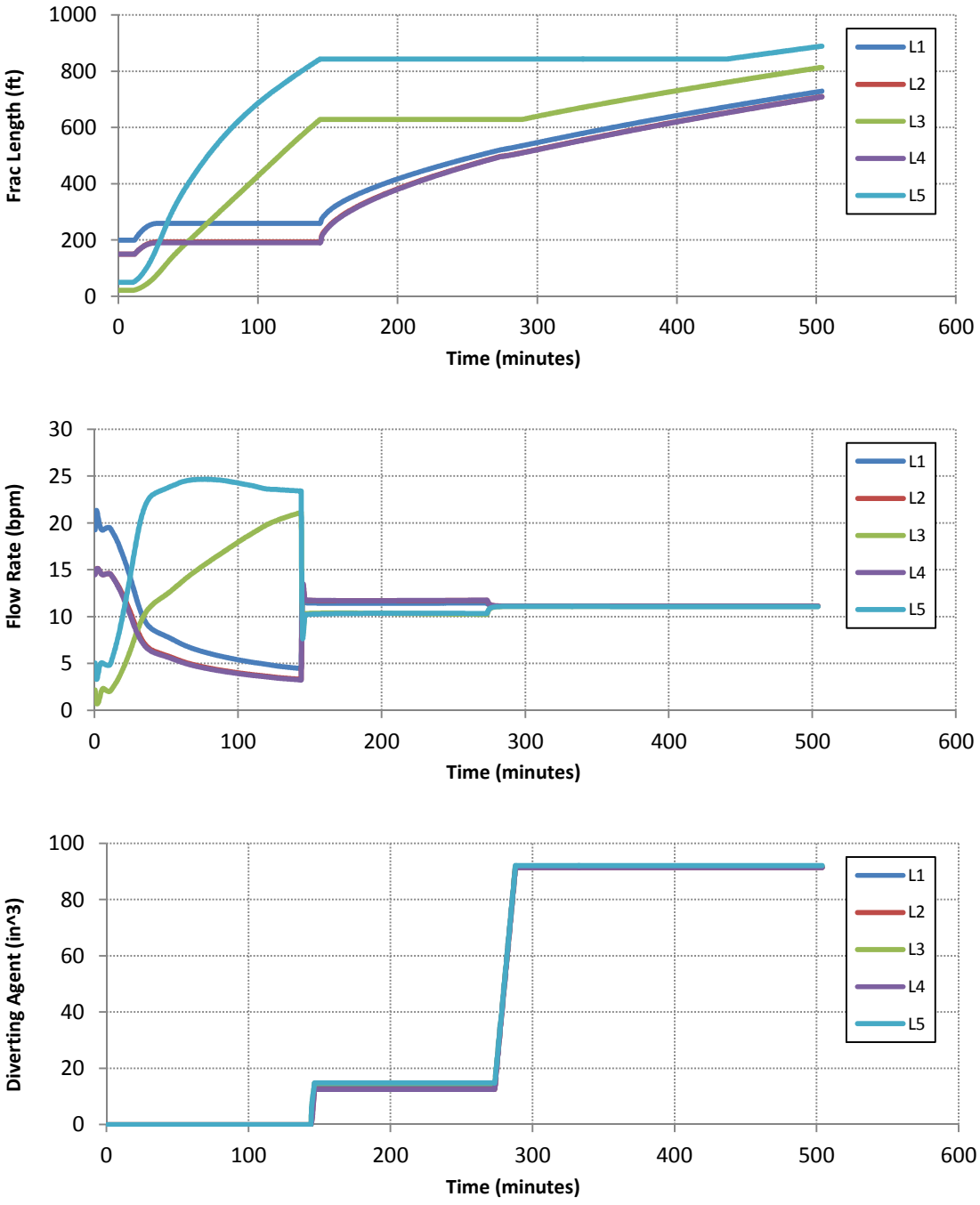

Figure 5-25 - Scenario X, Case A with diverting agent. Fracture system is identical to Scenario V, Case A, except the fracture propagation pressure is decreased for fractures L3 and L5.

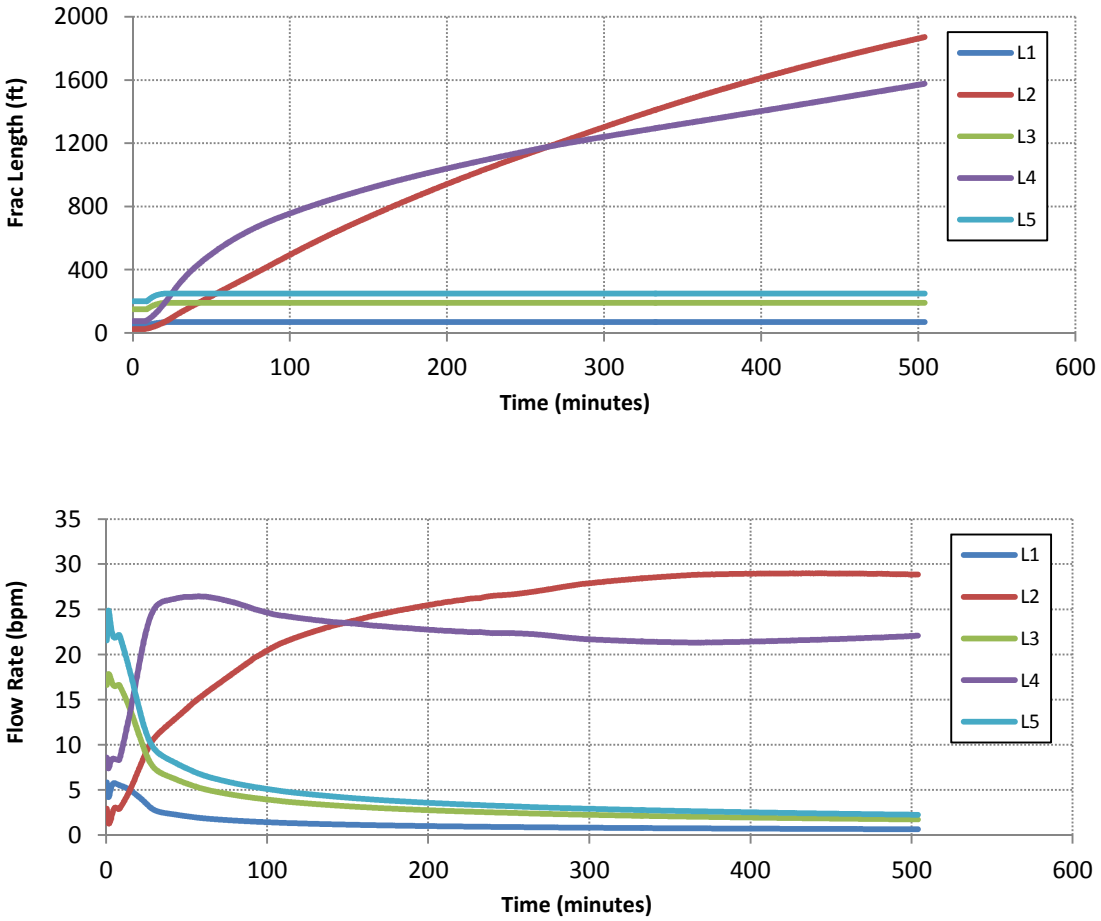

Figure 5-26 - Scenario X, Case B without diverting agent. Fracture system is identical to Scenario V, Case B, except the fracture propagation pressure is decreased for fractures L2 and L4.

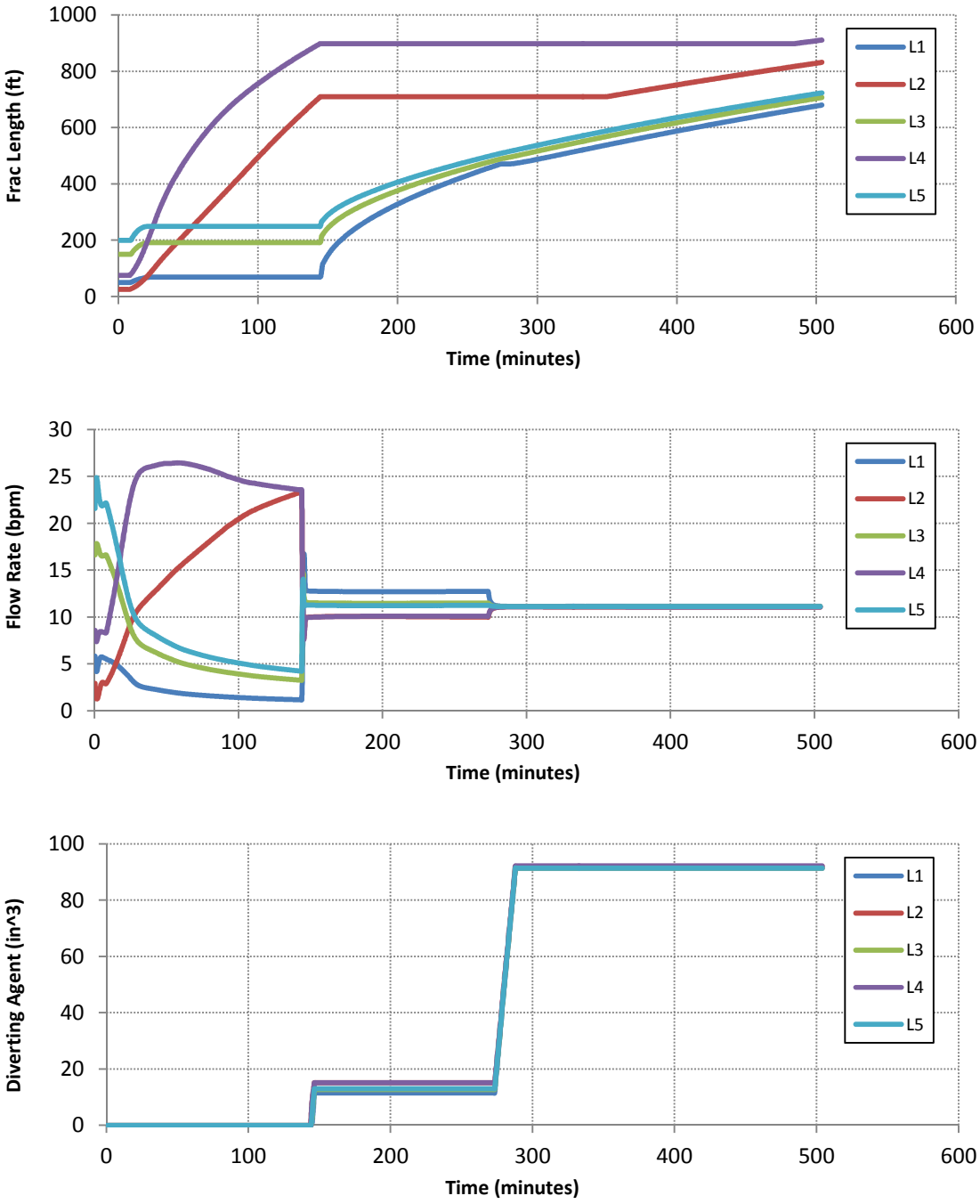

Figure 5-27 - Scenario X, Case B with diverting agent. Fracture system is identical to Scenario V, Case A, except the fracture propagation pressure is decreased for fractures L2 and L4.

Chapter 6: Summary and Conclusions

This thesis describes the simulation of refracturing treatments with the use of diverting agents designed to divert fracturing fluid to different sections along a wellbore. Propagation of competing fractures was calculated using the computer program UTWID. Two models were added to this program to account for the application of diverting agent – one that models the diverting agent to form a plug in the fracture, and another that models to plug to form in the perforation tunnel. The choice of model depends on the type of diverting agent used. However, the model for plugging in the perforations does not currently allow for the pumping of proppant after a diversion stage. As a result, the model for plugging in the fractures should be used to simulate realistic refracturing treatments. While the dynamics of each model differ, both resulted in successful diversion of flow to the fractures that were previously growing less preferentially.

PLUGGING IN THE FRACTURE

Seven scenarios were simulated for the model where plugging occurs in the fracture. In the baseline case, the diverting agent fully diverted flow from the two fastest growing fractures to the other three. When the initial lengths of the fractures were varied in Scenarios II and III, flow was diverted to the shorter fractures. The result is a more equal distribution of stimulated reservoir volume along the length of the wellbore. In Scenario IV, the permeability of the diverting agent cake was varied from the baseline value of 1 Darcy. In order to accomplish a significant change in the growth pattern of the fractures, large permeability changes were necessary. The reduction in permeability to 100 mD results in a stronger response from the diverting agent and, as a result, more equal growth rates after diversion. However, the relative order of the fractures remains the same. A further reduction to 50 mD has a more noticeable effect: three fractures are

plugged as opposed to two in the baseline case. Since the total flow rate is divided between fewer fractures, these fractures grow faster than they did previously. Very little difference in the system occurred when the permeability was increased to 100 Darcies from the baseline value of 1 Darcy. The average difference in fracture lengths of the growing fractures between this case and the baseline case is only 1.5%.

Similar results are seen when the diverting agent volume fraction was altered in Scenario V. The volume fraction was increased to 1E-2 and decreased to 1E-5, from a baseline value of 1E-3. In both cases, the overall fracture growth pattern remained the same. Increasing the volume fraction had a similar result as decreasing the permeability. Diversion of flow increased and the growing fractures had more equal growth rates. Overall, the fracture lengths at the conclusion of the treatment for these two cases stayed within 15% of that from the baseline case. In Scenario VI, the injection rate of the fracturing fluid is varied. In addition to the expected net change in fracture lengths, relative differences between the fractures are seen. When the rate is increased to 56 bpm from the baseline case of 42 bpm, an additional fracture remains plugged due to the diverting agent. This is caused by the increased importance of frictional forces caused by the increase in pump rate. This effect is more pronounced when the flow rate is again increased to 83 bpm. One of the fractures that normally would be plugged is not. When the flow rate is reduced to 28 bpm, the same overall pattern from the baseline case is seen. The fracture lengths are, as expected, much shorter. In the last scenario, large impacts are observed when the fracture propagation pressure is adjusted. Fractures that have lower propagation pressures receive a much larger proportion of the injected fluid. In this case, the diverting agents successfully stop the growth of the preferentially growing fractures, and allow growth in the fractures with higher propagation pressures.

Taken together, the different scenarios demonstrate the successful diversion of flow to fractures that would otherwise grow less preferentially. Additionally, adjustment of the refracturing parameters typically does not affect the success of the diversion stage, but it does impact the dynamics of the system. The timing of the diverting agent stage was shown to have an important impact on the fracture plugging and subsequent propagation.

PLUGGING IN THE PERFORATIONS

In the second model, the diverting agent plugs in the perforation tunnel itself. In this model, the simulations were compared based on the maximum distance between the fracture lengths of the five fractures. Treatments with small differences between final lengths indicate that the wellbore is stimulated more evenly along its length, and these treatments are therefore considered to be more successful. The first five scenarios develop a treatment design that greatly reduces the difference between fracture lengths. The baseline case is shown to cause successful diversion under a variety of conditions in the first three scenarios. In Scenario IV, an adjustment to the timing of the diverting agent stage improves diversion. In the previous scenarios, the diverting agent caused a strong response and flow rates were roughly equal after the diverting agent stage. In Scenario IV, the response was reduced by limiting the duration of the diverting agent stage. This adjustment resulted in a permanent disparity in both flow and growth rates after the diverting agent stage. The treatment design was improved further in Scenario V by adding a second diverting agent stage. This stage, which is timed so that the fractures have similar lengths, equalizes the flow and growth rates. The result is that the distance between the fractures at the end of the treatment is smaller than in the previous scenarios.

In the remaining scenarios, the treatment design is held constant while the sensitivity to other parameters is determined. In Scenario VI, the permeability is varied from 100 miliDarcies to 100 Darcies (the permeability in the baseline case is 1 Darcy), and the results show that the system is fairly sensitive to permeability. The increase to 10 Darcies does not have a large impact: the maximum distance between the fracture lengths is increased from 97 feet in the baseline case to 129 feet. However, when the permeability is increased to 100 Darcies, this distance reaches 234 feet. Reducing the permeability to 100 mD also does not improve the response. The maximum distance in this case is 161 feet. Scenario VII alters the volume fraction of diverting agent and exhibits similar behavior to Scenario VI. Reducing the volume fraction limits the diversion in a similar manner as increasing the permeability. It should be noted that the volume of diverting agent is limited by the size of the perforations and therefore large adjustments in this parameter are not possible.

Scenario VIII illustrates the point that the optimum parameters are interrelated. If the permeability of the diverting agent changes then so too should the volume fraction in order to optimize the treatment. While a reduction in permeability to 100 miliDarcies in Scenario VI did not result in an improvement, it did improve the response in Scenario VII because the volume fraction of the diverting agent was reduced as well. This scenario underscores the point that the parameters involved in a refracturing treatment should not be selected in isolation, but rather considered within the design of the entire treatment.

In Scenario IX the pumping rate of the injected fluid is adjusted. Aside from the expected change in absolute fracture lengths, little impact is seen when the rate is increased from 56 bpm to 69 bpm. However, the overall pattern of the system is impacted when the rate is decreased to 28 bpm. More diversion occurs in this case because the reduction in flow rate also reduces the frictional forces. With smaller frictional forces, the

pressure drop due to the diverting agent plays a larger relative role and causes more diversion. In Scenario X, the fracture propagation pressure is altered. As in the first model, the fractures with lower fracture propagation pressure receive a large majority of the injected fluid. In addition, the diverting agent also successfully diverts flow in this case. Application of the diverting agent results in the growth of the fractures that would otherwise not grow, and consequently provides a much more equal stimulation of the wellbore along its length.

FUTURE WORK

A variety of areas in this model should be further developed in the future. First, limited information is available on the mechanisms of diverting agent bridge formation and disassociation. Testing with diverting agents should be done to further refine the physics of formation and disassociation used in this model. Second, in the model where the plug forms in the perforation tunnel, a mechanism should be included to allow for flow of proppant after the pumping of diverting agent. Possible solutions include the opening of additional channels with high pressures or the plugging of only a fraction of the perforations that flow into a fracture.

The model would also be enhanced if it incorporated interference between fractures. Currently, the model assumes that fractures are spaced sufficiently far away so that there is no interference during the treatment. Furthermore, fracture propagation is assumed to occur in the same direction as the original fractures. If the model incorporated information about the in-situ stress state at the time of the refracturing treatment, it would be possible to address the potential of fracture reorientation. Last, UTWID assumes that transverse fractures in horizontal wells have a constant height, even at the wellbore. The width of the diverting agent cake is currently calculated by assuming it takes up the full

height of the fracture, and therefore also relies upon a constant height fracture at the wellbore. A modification to allow for a more realistic geometry of the diverting agent cake in the near wellbore region would result in more accurate pressure drop calculations.

References

Allison, D., Curry, S., and Todd, B. 2011. Restimulation of Wells using Biodegradable Particulates as Temporary Diverting Agents. Presented at the Canadian Unconventional Resources Conference held in Calgary, Alberta, Canada, 15-17 November 2011. SPE 149221.

Alramahi, B. and Sundberg, M. 2012. Proppant Embedment and Conductivity of Hydraulic Fractures in Shales. Presented at the 46th US Rock Mechanics / Geomechanics Symposium held in Chicago, Illinois U.S.A., 24-27 June 2012. ARMA 12-291

Baihly, J., Altman, R., Malpani, R., and Luo, F. 2010. Shale Gas Production Decline Trend Comparison Over Time and Basins. Presented at the SPE Annual Technical Conference and Exhibition held in Florence, Italy, 19-22 September 2010. SPE 135555

Barba, R. 2009. A Novel Approach to Identifying Refracturing Candidates and Executing Refracture Treatments in Multiple Zone Reservoirs. Presented at the 2009 SPE Annual Technical Conference and Exhibition held in New Orleans, Louisiana, USA, 4-7 October 2009. SPE 125008

Besler, M., Steele, J., Egan, T., and Wagner J. 2007. Improving Well Productivity and Profitability in the Bakken – A Summary of Our Experiences Drilling, Stimulating, and Operating Horizontal Wells. Presented at the 2007 SPE Annual Technical Conference and Exhibition held in Anaheim, California, U.S.A., 11-14 November 2007. SPE 110679

Besler, M. 2008. Re-fracturing: Is Too Little Prevention Requiring the Cure? Presented at the 2008 Williston Basin Petroleum Conference, Minot ND, April 27-29.

Carey, J. 2012. Surprise Side Effect Of Shale Gas Boom: A Plunge In U.S. Greenhouse Gas Emissions. *Forbes* (in press; published online 7 December 2012) http://www.forbes.com/sites/energysource/2012/12/07/surprise-side-effect-of-shale-gas-boom-a-plunge-in-u-s-greenhouse-gas-emissions/

Conway, M., McMechan, D., McGowen, J., Brown, D., Chisholm, P., and Venditto, J. 1985. Expanding Recoverable Reserves Through Refracturing. Presented at the 60th Annual Technical Conference and Exhibition of the Society of Petroleum Engineers held in Las Vegas, NV, September 22-25, 1985. SPE 14376

Craig, D. and Brown, T. 1999. Estimating Pore Pressure and Permeability in Massively Stacked Lenticular Reservoirs Using Diagnostic Fracture-Injection Tests. Presented at the 1999 SPE Annual Technical Conference and Exhibition held in Houston, Texas, 3-6 October 1999. SPE 56600.

Craig, M., Wendte, S., and Buchwalter, J. 2012. Barnett Shale Horizontal Restimulations: A Case Study of 13 Wells. Presented at the Americas Unconventional Resources Conference held in Pittsburgh, Pennsylvania, USA 5-7 June 2012. SPE 154669

Daniels, J., Waters, G., LeCalvez, J., Lassek, J., and Bentley, D. 2007. Contacting More of the Barnett Shale Through an Integration of Real-Time Microseismic Monitoring, Petrophysics and Hydraulic Fracture Design. Presented at the 2007 SPE Annual Technical Conference and Exhibition held in Anaheim California, U.S.A., 12-14 October 2007. SPE 110562

Duenckel, R., Conway, M., Eldred, B., and Vincent, M. 2011. Proppant Diagenesis - Integrated Analyses Provide New Insights Into Origin, Occurrence, and Implications for Proppant Performance. Presented at the SPE Hydraulic Fracturing Technology Conference and Exhibition, The Woodlands, Texas, U.S.A., 24-26 January 2011. SPE 139875.

EIA. 2013a. Technically Recoverable Shale Oil and Shale Gas Resources: An Assessment of 137 Shale Formations in 41 Countries Outside the United States. U.S. DOE, Energy Information Administration, Washington, DC (June 2013).

EIA. 2013b. Monthly Energy Review. U.S. DOE, Energy Information Administration, Washington, DC (July 2013)

EIA. 2013c. How much carbon dioxide (CO2) is produced per kilowatt-hour when generating electricity with fossil fuels?, http://www.eia.gov/tools/faqs/faq.cfm?id=74&t=11 (accessed 10 August 2013).

EIA. 2013d. Henry Hub Gulf Coast Natural Gas Spot Price, http://www.eia.gov/dnav/ng/hist/rngwhhdm.htm (accessed 13 August 2013).

Elbel, J. and Mack, M. 1993. Refracturing: Observations and Theories. Presented at the Production Operations Symposium held in Oklahoma city, OK, U.S.A., March 21-23, 1993. SPE 25464

Fisher, K., Robinson, B., and Voneiff, G. 1995. A Comprehensive Study of the Analysis and Economic Benefits of Radioactive Tracer Engineered Stimulation Procedures. Presented at the SPE Annual Technical Conference and Exhibition held in Dallas, U.S.A., 22-25 October, 1995. SPE 30794

Gidley, J., Holditch, S., Nierode, D., and Veatch, R. 1989. *Recent Advances in Hydraulic Fracturing*, Vol. 12. Richardson, Texas: Monograph Series, SPE.

Green, D., and Seanard, K. 2006. Hydraulic Fracturing of Miocene and Oligocene Sandstones in the Taranaki Basin, New Zealand. Presented at the 2006 SPE Asia Pacific Oil & Gas Conference and Exhibition held in Adelaide, Australia, 11-13 September 2006. SPE 101121

Greiser, B., Wiemers, T., and Hill, B. 1999. Fluid Frictional Diversion Technique for Sequential Multistage Horizontal Stimulation. Presented at the 1999 SPE Rocky Mountain Regional Meeting held in Gillette, Wyoming, May 15-18. SPE 55615

Gringarten, A., Ramey, H., and Raghavan, R. 1972. Unstead-State Pressure Distributions Created by a Well With a Single Infinite-Conductivity Vertical Fracture. Presented at the SPE-AIME 47th Annual Fall Meeting held in San Antonio, Texas, U.S.A., Oct. 8-11, 1972. SPE 4051.

Halliburton. BioVert NWB Biodegradable Diverting Agent. Online, http://www.halliburton.com/public/pe/contents/Data_Sheets/web/H/H08003.pdf (downloaded 21 June 2013).

Khalid, S., Faurschou, K., Gorchynski, T., Zhao, X., and Marechal, F. 2010. Mapping Key Reservoir Properties Along Horizontal Shale Gas Wells. Presented at the Canadian Unconventional Resources & International Petroleum Conference held in Calgary, Alberta, Canada, 19-21 October 2010. SPE 137413

Kurz, B., Schmidt, D., and Cortese, P. 2013. Investigation of Improved Conductivity and Proppant Applications in the Bakken Formations. Presented at the SPE Hydraulic Fracturing Technology Conference held in The Woodlands, Texas, U.S.A., 4-6 February 2013. SPE 163849

Lagrone, K., and Rasmussen, J. 1963. A New Development in Completion Methods - The Limited Entry Technique. Presented at the SPE Rocky Mountain Regional Meeting held in Denver, CO, May 27-28, 1963. SPE 530

Lantz, T. and Greene, D. 2007. Refracture Treatments Proving Successful in Horizontal Bakken Wells: Richland Count, Montana. Presented at the 2007 SPE Rocky Mountain Oil & Gas Technology Symposium held in Denver, Colorado, U.S.A., 16-18 April 2007. SPE 108117

Lonnes, S., Nygaard, K., Sorem, W., Hall, T., and Tolman, R. 2005. Advanced Multizone Stimulation Technology. Presented at the SPE Annual Technical Conference and Exhibition held in Dallas, Texas, U.S.A., 9-12 October 2005. SPE 95778

McDaniel, B. 1986. Conductivity Testing of Proppants at High Temperature and Stress. Presented at the 56th California Regional Meeting of the Society of Petroleum Engineers held in Oakland, CA, April 2-4, 1986. SPE 15067

Mohaghegh, S., Popa, A., Gaskari, R., Ameri, S., and Wolhart, S. 2002. Identification of Successful Practicies in Hydraulic Fracturing Using Intelligent Data Mining Tools; Application to the Codell Formation in the DJ-Basin. Presented at the SPE Annual Technical Conference and Exhibition held in San Antonio, Texas, 29 September-2 October 2002. SPE 77597

Mohaghegh, S., Reeves, S., and Hill, D. 2000. Development of an Intelligent Systems Approach or Restimulation Candidate Selection. Presented at the 2000 SPE/CERI Gas Technology Symposium held in Calgary, Alberta Canada, 3-5 April 2000. SPE 59767

Montgomery, C. and Steanson, R. 1985. Proppant Selection: The Key to Successful Fracture Stimulation. *Journal of Petroleum Technology* **37** (12). SPE 12616-PA. http://www.onepetro.org/mslib/app/Preview.do?paperNumber=00012616&societyCode=SPE

Moore, L. and Ramakrishnan, H. 2006. Restimulation: Candidate Selection Methodologies and Treatment Optimization. Presented at the 2006 SPE Annual Technical Conference and Exhibition held in San Antonio, Texas, U.S.A., 24-27 September 2006. SPE 102681

Nordgren, R. 1970. Propagation of a Vertical Hydraulic Fracture. Presented at the SPE 45th Annual Fall Meeting, held in Houston, Oct. 4-7, 1970. SPE 3009

Perkins, T. and Gonzalez, J. 1985. The Effect of Thermoelastic Stresses on Injection Well Fracturing. *SPE Journal* **25** (1): 78-88. SPE 11332-PA. http://www.onepetro.org/mslib/app/Preview.do?paperNumber=00011332&societyCode=SPE

Perkins, T. and Kern, L. 1961. Widths of Hydraulic Fractures. Presented at the 36th Annual Fall Meeting of SPE, Oct. 8-11, 1961 in Dallas, Texas, U.S.A. SPE 89

Potapenko, D., Tinkham, S., Lecerf, B., Fredd, C., Samuelson, M., Gillard, M., Le Calvez, J., and Daniels, J. 2009. Barnett Shale Refracture Stimulations Using a Novel Diversion Technique. Presented at the 2009 SPE Hydraulic Fracturing Technology Conference held in The Woodlands, Texas, USA, 19-21 January 2009. SPE 119636

Rayson, N. and Weaver, J. 2012. Improved Understanding of Proppant-Formation Interactions for Sustaining Fracture Conductivity. Presented at the SPE Saudi Arabia Section Technical Symposium and Exhibition held in Al-Khobar, Saudi Arabia 2012. SPE 160885

Reeves, S. and Wolhart, S. 2001. Study Looks at Tight-Gas Restimulation Candidate Wells. *Oil and Gas Journal* **99** (11). http://www.ogj.com/articles/print/volume-99/issue-41/drilling-production/study-looks-at-tight-gas-restimulation-candidate-wells.html

Reeves, S., Bastian, P., Spivey, J., Flumerfelt, R., Mohaghegh, S., and Koperna, G. 2000. Benchmarking of Restimulation Candidate Selection Techniques in Layered, Tight Gas Sand Formations Using Reservoir Simulation. Presented at the 2000 SPE Annual Technical Conference and Exhibition held in Dallas, Texas, 1-4 October 2000. SPE 63096

Reeves, S., Hill, D., Tiner, R., Bastian, P., Conway, M., and Mohaghegh, S. 1999. Restimulation of Tight Gas Sand Wells in the Rocky Mountain Region. Presented at the 1999 SPE Rocky Mountain Regional Meeting held in Gillette, Wyoming, 15-18 May 1999. SPE 55627

Roussel, N. and Sharma, M. 2010. Role of Stress Reorientation in the Success of Refracture Treatments in Tight Gas Sands. Presented at the SPE Annual Technical Conference and Exhibition held in Florence, Italy, 19-22 September 2010. SPE 134491

Roussel, N. and Sharma, M. 2011. Selecting Candidate Wells for Refracturing Using Production Data. Presented at the SPE Annual Technical Conference and Exhibition, Denver, Colorado, 30 October-2 November 2011. SPE 146103

Sallee, W. and Rugg, F. 1953. Artificial Formation Fracturing in Southern Oklahoma and North-Central Texas. Bulletin of the American Association of Petroleum Geologists **37** (11): 2539-2550.

Sencenbaugh, R., Lytle, D., Birmingham, T., Simmons, J., and Shaefer, M. 2001. Restimulating Tight Gas Sand: Case Study of the Codell Formation. Presented at the Rocky Mountain Petroleum Technology Conference, Keystone, CO, May 21-23. SPE 71045.

Shaefer, M. 2006. Awakening an Old Field - A Case Study of a Refracturing Program in the Greater Green River Basin. Presented at the 2006 SPE Annual Technical Conference and Exhibition, San Antonio, Texas, U.S.A., 24-27 September 2006. SPE 101026.

Shelley, R. 1999. Artificial Neural Networks Identify Restimulation Candidates in the Red Oak Field. Presented at the 1999 SPE Mid-Continent Operations Symposium held in Oklahoma City, March 28-31. SPE 52190.

Sinha, S., and Ramakrishnan, H. 2011. A Novel Screening Method for Selection of Horizontal Refracturing Candidates in Shale Gas Reservoirs. Presented at the SPE North American Unconventional Gas Conference and Exhibition held in The Woodlands, Texas, USA, 14-16 June 2011. SPE 144032

Suri, A., Sharma, M., and Peters, E. 2010. Estimates of Fracture Lengths and Injection Profile in an Injection Well by History Matching Bottom Hole Pressures. Presented at the SPE Western Regional Meeting held in Anaheim, California, U.S.A., 27-29 May 2010. SPE 132524

Terracina, J., Turner, J., Collins, D., and Spillars, S. 2010. Proppant Selection and Its Effect on the Results of Fracturing Treatments Performed in Shale Formations. Presented at the SPE Annual Technical Conference and Exhibition held in Florence, Italy, 19-22 September 2010. SPE 135502.

The University of Texas. 2009. Guide to Using UTWID 7.1. Austin, Texas.

Valko, P. and Economides, M.J. 1995. *Hydraulic Fracture Mechanics*. John Wiley & Sons Inc.

Vincent, M. 2010a. Refracs - Why Do They Work, and Why Do They Fail In 100 Published Field Studies?. Presented at the SPE Annual Technical Conference and Exhibition held in Florence, Italy, 19-22 September 2010. SPE 134330.

Vincent, M.C. 2010b. Restimulation of Unconventional Reservoirs: when are Refracs Beneficial? Presented at the Canadian Unconventional Resources and International Petroleum Conference held in Calgary, Alberta, Canada, 19-21 October 2010. SPE 136757

Wang, S., Luo, X., and Hurt, R. 2013. What We Learned from a Study of Re-fracturing in Barnett shale: An Investigation of Completion/Fracturing, and Production of Re-fractured Wells. Presented at the International Petroleum Technology Conference held in Beijing, China, 26-28 March 2013. IPTC 17081

Wang, X., Liu, G., Wang, D., and Economides, J. 2011. The Use of Sealing Ball Staged Fracturing. Presented at the SPE Hydraulic Fracturing Technology Conference and Exhibition held in The Woodlands, Texas, USA, 24-26 January 2011. SPE 140529

Waters, G., Ramakrishnan, H., Daniels, J., and Bentley, D. 2009. Utilization of Real Time Microseismic Monitoring and Hydraulic Fracture Diversion Technology in the Completion of Barnett Shale Horizontal Wells. Presented at the 2009 Offshore Technology Conference held in Houston, Texas, USA, 4-7 May 2009. OTC 20268

Wright, C. and Conant, R. 1995. Hydraulic Fracture Reorientation in Primary and Secondary Recovery from Low-Permeability Reservoirs. Presented at the SPE Annual Technical Conference & Exhibition held in Dallas, Texas, U.S.A., 22-25 October, 1995. SPE 30484

Wright, C., Stewart, D., Emanuele, M., and Wright, W. 1994. Reorientation of Propped Refracture Treatments in the Lost Hills Field. Presented at the SPE Western Regional Meeting, 23-25 March 1994, Long Beach, California, USA. SPE 27896.